

# Line Luminosities of Galactic and Magellanic Cloud Wolf-Rayet stars

Paul A. Crowther<sup>1</sup>\*, G. Rate<sup>1</sup>, Joachim M. Bestenlehner<sup>1</sup>

*1. Department of Physics and Astronomy, University of Sheffield, Sheffield, S3 7RH, UK*

Accepted 2022 July 5. Received 2022 July 5; in original form 2022 April 8

## ABSTRACT

We provide line luminosities and spectroscopic templates of prominent optical emission lines of 133 Galactic Wolf-Rayet stars by exploiting *Gaia* DR3 parallaxes and optical spectrophotometry, and provide comparisons with 112 counterparts in the Magellanic Clouds. Average line luminosities of the broad blue ( $\text{He II } \lambda\lambda 4686, \text{C III } \lambda\lambda 4647, 51, \text{N III } \lambda\lambda 4634, 41, \text{N V } \lambda\lambda 4603, 20$ ) and yellow ( $\text{C IV } \lambda\lambda 5801, 12$ ) emission features for WN, WN/C, WC and WO stars have application in characterising the Wolf-Rayet populations of star-forming regions of distant, unresolved galaxies. Early-type WN stars reveal lower line luminosities in more metal poor environments, but the situation is less clear for late-type WN stars. LMC WC4–5 line luminosities are higher than their Milky Way counterparts, with line luminosities of Magellanic Cloud WO stars higher than Galactic stars. We highlight other prominent optical emission lines,  $\text{N IV } \lambda\lambda 3478, 85$  for WN and WN/C stars,  $\text{O IV } \lambda\lambda 3403, 13$  for WC and WO stars and  $\text{O VI } \lambda\lambda 3811, 34$  for WO stars. We apply our calibrations to representative metal-poor and metal-rich WR galaxies, IC 4870 and NGC 3049, respectively, with spectral templates also applied based on a realistic mix of subtypes. Finally, the global blue and  $\text{C IV } \lambda\lambda 5801, 12$  line luminosities of the Large (Small) Magellanic Clouds are  $2.6 \times 10^{38} \text{ erg s}^{-1}$  ( $9 \times 10^{36} \text{ erg s}^{-1}$ ) and  $8.8 \times 10^{37} \text{ erg s}^{-1}$  ( $4 \times 10^{36} \text{ erg s}^{-1}$ ), respectively, with the cumulative WR line luminosity of the Milky Way estimated to be an order of magnitude higher than the LMC.

**Key words:** stars: massive – stars: Wolf-Rayet – galaxies: stellar content

## 1 INTRODUCTION

Wolf-Rayet (WR) stars, the evolved descendants of (very) high mass stars, exhibit broad optical emission lines owing to their dense stellar winds (Crowther 2007). There are three flavours of WR stars known, nitrogen-sequence (WN) stars dominated by helium and nitrogen features, carbon-sequence (WC) stars with prominent carbon and helium lines, and rare oxygen-sequence (WO) stars with dominant oxygen and carbon features<sup>1</sup>. Their unusual spectroscopic signatures permit their use as tracers of star-formation in galaxies (Allen et al. 1976; Kunth & Sargent 1981). Indeed, a subset of starburst galaxies have been coined Wolf-Rayet galaxies owing to the presence of broad  $\text{He II } \lambda 4686$  emission from WN stars, and occasionally  $\text{C IV } \lambda 5808$  emission from WC stars (Vacca & Conti 1992). The advent of highly multiplexed instrumentation (e.g. SDSS) plus large-field integral field spectroscopic capabilities (e.g. MUSE) has identified large numbers of WR stars in external galaxies (Brinchmann et al. 2008; Miralles-Caballero et al. 2016; Monreal-Ibero et al. 2017; Gómez-González et al. 2021; Senchyna et al. 2021).

Population synthesis models have incorporated WR stars via either empirical calibrations (Schaerer & Vacca 1998) or synthetic spectra (Smith et al. 2002; Eldridge et al. 2017). The former approach has relied heavily on calibrations of WR stars in the metal-poor Magellanic Clouds (Smith et al. 1990a; Crowther & Hadfield 2006) while the lat-

ter depend on predictions from single or binary evolutionary models and suitable prescriptions for theoretical wind densities at a range of metallicities. Various mass-loss prescriptions are available, and differ between very massive stars exhibiting WR spectral morphologies (Bestenlehner 2020) and classical WR stars (Nugis & Lamers 2000; Sander et al. 2020) although these are generally untested for a broad range of metallicities. By way of example, Eldridge et al. (2017) utilise the grid of PoWR (Gräfener et al. 2002) model atmospheres<sup>2</sup> for spectral synthesis, yet predictions are highly dependent on the choice of WR models.

Empirical calibrations have been produced for WR stars in the Magellanic Clouds, but uncertain distances to Milky Way WR stars has severely hindered calibrations at high metallicity to date. The advent of reliable Galactic WR distances from *Gaia* (Rate & Crowther 2020) has opened up the possibility of solar metallicity calibrations and spectral templates. In this study we exploit *Gaia* DR3 parallaxes and archival spectrophotometry of large numbers of Galactic WR stars to provide calibrations at (near) solar composition, with which to complement synthetic spectroscopy, and revisit Magellanic Cloud calibrations in view of new discoveries and higher quality observations since Crowther & Hadfield (2006).

This paper is structured as follows. Section 2 discusses the observational datasets employed to construct WR line luminosities, Section 3 compares Milky Way WR line luminosities with Magellanic Cloud counterparts and includes templates for each environment, Section 4

\* paul.crowther@sheffield.ac.uk

<sup>1</sup> The Wolf-Rayet phenomenon is common to evolved massive stars (classical WN, WC, WO), very massive main sequence stars (H-rich WN, Of/WN) and a subset of central stars of Planetary Nebulae ([WC], [WN])

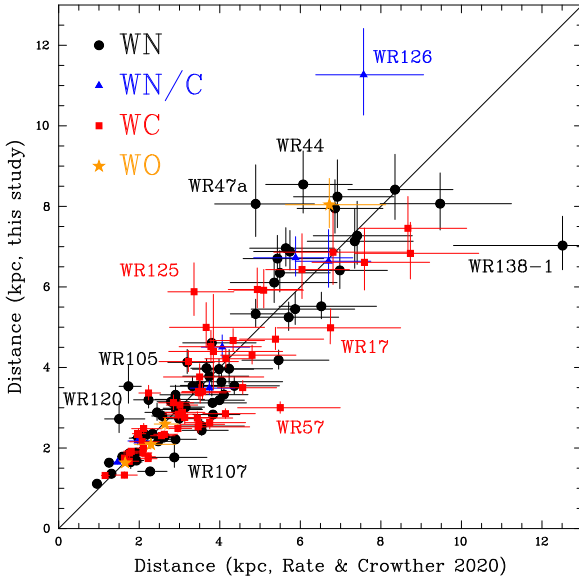
<sup>2</sup> <https://www.astro.physik.uni-potsdam.de/PoWR/>

**Table 1.** Source of optical spectrophotometry of Galactic and Magellanic Cloud WR stars for this study, including representative spectral resolutions at  $\lambda=5000\text{\AA}$ .

ID	Telescope	Instrument	Epoch	Sp. Res ( $\text{\AA}$ )	Wavelength Coverage ( $\text{\AA}$ )	Flux Calib.	Ref	Notes
AD	ANU 2.3m	DBS	Dec 1997	5	3200–11000	10%	2	Southern WR stars, 6070–6400 $\text{\AA}$ detector gap.
AR	AAT	RGO	Mar 1992–Dec 1994	2	3680–6000	10%	1	LMC/SMC WN and WN/C stars.
CS	CTIO 1.5m	SIT	Nov 1981–Feb 1985	10	3400–7270	10%	16	Southern Milky Way WR stars. Variable $\lambda_{\max}$ .
HF	HST	FOS	Jan 1996–Jan 1997	3	3230–6820	10%	4–6	LMC WN stars. G400 only ( $\lambda_{\max}=4780\text{\AA}$ ) except for R136.
HS	HST	STIS	Mar 2014–Sep 2016	10	2900–10250	10%	17	AB5 (HD 5980).
II91	INT	IDS	Sep 1991	2	3320–7300	20%	7	Northern Milky Way WN and WN/C stars. Variable $\lambda_{\min/\max}$ .
II96	INT	IDS	Jul 1996	3	3620–6810	10%	8	Northern Milky Way WN stars.
II13	INT	IDS	Sep 2013	5	3800–9350	20%	9	Northern Milky Way WR stars.
KI	KPNO 0.91m	IRS	Oct 1980–Feb 1983	9	3450–6900	10%	10	Northern Milky Way WR stars.
MM	Magellan	MagE	Sep 2014–Dec 2020	1.2	3170–9440	10%	13, 14	LMC WR stars.
SC	Mt Stromlo 1.9m	Coudé	Dec 1995	1	4700–6700	20%	1	LMC late-type WN stars.
WI94	WHT	ISIS	Jun 1994	3	4450–6030	10%	11	Northern Milky Way WN and WN/C stars.
WI02	WHT	ISIS	Aug 2002	3.5	3400–9500	10%	12	Northern Milky Way WC stars.
VM	VLT	MUSE	Aug 2014	3	4600–9350	10%	15	LMC WN stars. Calibration via BAT99–100 (HST/FOS).
VU	VLT	UVES	Jan 2002–Jan 2003	0.1	3200–10240	10%	18, 19	Southern Milky Way WR stars.
VX	VLT	XShooter	Nov 2011–Aug 2013	0.8	3100–24700	10%	20, 21	Southern Milky Way and LMC WR stars.

1: Crowther &amp; Smith (1997); 2: Crowther et al. (2002); 3: Crowther &amp; Hadfield (2006); 4: de Koter et al. (1997); 5: Massey &amp; Hunter (1998);

6: Walborn et al. (1999); 7: Crowther et al. (1995a); 8: Crowther (1997); 9: This study; 10: Massey (1984); 11: Crowther et al. (1995c);

12: Crowther et al. (2006b); 13: Neugent et al. (2017); 14: Aadland et al. (2022b); 15: Castro et al. (2018); 16: Torres-Dodgen & Massey (1988);  
17: Hillier et al. (2019); 18: Bagnulo et al. (2003); 19: Borisov et al. (2022); 20: Tramper et al. (2015); 21: Rubin-Diez et al. (in prep.);

**Figure 1.** Comparison between Galactic WR distances (in kpc) following a common Bayesian methodology of Rate & Crowther (2020) using either *Gaia* DR2 parallaxes incorporating global zero point corrections of Lindegren et al. (2018), versus DR3 parallaxes incorporating local zero point corrections of Lindegren et al. (2021) and Maíz Apellániz (2022). The key distinguishes between WN (black circles), WN/C (blue triangles), WC (red squares) and WO (orange stars) subtypes. In general, DR3 plus revised zero points provides improved uncertainties on distances, with some outliers labelled.

applies calibrations and templates to representative WR galaxies at low and high metallicity, with conclusions drawn in Section 5.

## 2 OBSERVATIONS

Our primary objective is to provide line luminosities of prominent optical emission lines in Milky Way WR stars, requiring (i) spectrophotometric datasets; (ii) interstellar extinctions drawn from spectroscopic studies; (iii) distances from *Gaia* DR3 parallaxes.

### 2.1 Milky Way WR stars

A subset of flux calibrated spectroscopic datasets involved observations through large apertures, while others involved relatively flux calibrated datasets adjusted to literature photometry, primarily narrow-band *ubvr* photometry of Massey (1984) or Torres-Dodgen & Massey (1988). In instances of discrepant photometric measurements, inspection of large aperture low resolution (LORES) LWR or LWP (1850–3350 $\text{\AA}$ ) spectrophotometry from IUE<sup>3</sup> provided the primary reference. We also utilise IUE SWP (1150–1980 $\text{\AA}$ ) spectrophotometry, where available.

Our primary optical spectroscopic datasets are summarised in Table 1, with typical spectral resolutions of 1–5 $\text{\AA}$ , although some historical datasets were obtained at low spectral resolution. In view of the (typically) broad WR emission lines, this doesn't adversely impact on line flux measurements, but FWHM of narrow lined stars (typically WN8–11) are impacted, so all quoted FWHM are corrected for instrumental broadening (typical uncertainties are  $\pm 100 \text{ km s}^{-1}$ ). All datasets have been previously discussed with the exception of INT IDS spectroscopy from 16–17 Sep 2013 (PI Ross Lowe), involving observations of WR138-1<sup>4</sup>, WR140 and WR149 with the 235 mm camera, R300V grating and EEV10 detector. Relative flux calibration was achieved using standard star BD+25° 4655.

<sup>3</sup> INES datasets obtained from <http://sdc.cab.inta-csic.es/ines/>

<sup>4</sup> Gvaramadze et al. (2009) discovered WR138a, which was subsequently reclassified as WN9 by Flagey et al. (2014) and its WR catalogue number was revised to WR138-1 following Ross Lowe & Crowther (2015).

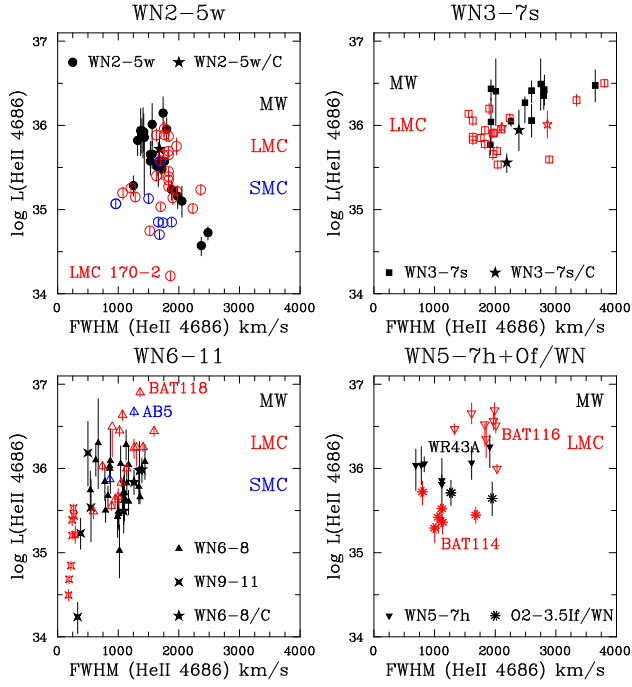


**Figure 2.** He II  $\lambda 4686$  line luminosities of WN2-5w (top left), WN3-7s (top right), WN6-8 (bottom left) and WN5-7h+Of/WN (bottom right) stars in the Milky Way (black, filled), LMC (red, open) and SMC (blue, open) versus FWHM ( $\text{km s}^{-1}$ ). Weak and strong-lined early-type WN stars are indicated as circles and squares, respectively, WN/C stars as stars, WN6-8 as triangles, WN9-11 as crosses, H-rich main sequence WN5-7h stars as inverted triangles and Of/WN stars as asterisks.

Flux calibrated UVES POP datasets (Bagnulo et al. 2003; Borisov et al. 2022) are included if the key C IV  $\lambda\lambda 5801,12$  line, missing due to the UVES detector gap, is available from other sources. In some instances spectroscopy extends to or beyond  $1\mu\text{m}$  (e.g. ANU 2.3m/DBS, VLT/XShooter) which are supplemented by additional near-IR spectrophotometry (e.g. IRTF/SpeX, Crowther et al. 2006a). For inclusion in the present sample we require He II  $\lambda 4686$  for WN and Of/WN stars, C IV  $\lambda\lambda 5801,12$  for WC stars, and O IV  $\lambda\lambda 3811,34$  for WO stars, thereby excluding heavily reddened stars, such as the rich WR population in Westerlund 1 (Crowther et al. 2006a). We also omit WR+WR binaries involving differing subtypes (e.g. WR70–16, Callingham et al. 2020).

Line fluxes were measured using the multiple gaussian fitting routines ELF within the Starlink DIPSO spectroscopic package (Howarth et al. 2004). Spectral coverage varies by instrument/telescope, but usually includes  $\lambda 4000\text{--}7000$ , so may exclude some violet (e.g. O IV  $\lambda\lambda 3403,13$ , N IV  $\lambda\lambda 3478,85$ ) or red (e.g. N IV  $\lambda\lambda 7103,29$ , C III  $\lambda\lambda 9701,19$  diagnostics). We adopt uncertainties of 10% for the majority of line flux measurements, 20% for Mt Stromlo 1.9m/Coudé and INT/IDS spectroscopy from 1991 and 2013. Comparisons between He II  $\lambda 4686$  line fluxes and literature results for WN stars from Leitherer et al. (2019) reveal  $\log F_{\text{HeII}4686} - F_{\text{HeII}4686}^{\text{L19}} = 0.00 \pm 0.10$  for 35 stars in common, while comparisons between C IV  $\lambda\lambda 5801,12$  line fluxes and literature results for WC stars from Smith et al. (1990b) reveal  $\log F_{\text{CIV}5801,12} - F_{\text{CIV}5801,12}^{\text{S90b}} = 0.00 \pm 0.11$  for 48 stars in common.

In the era of reliable Galactic distances courtesy of *Gaia*, interstellar extinctions are of critical importance for line luminosity determinations. Here we adopt  $E_{\text{B-V}}$  and  $R_V$  values from contemporary spectroscopic studies (Hamann et al. 2006; Sander et al. 2012). For

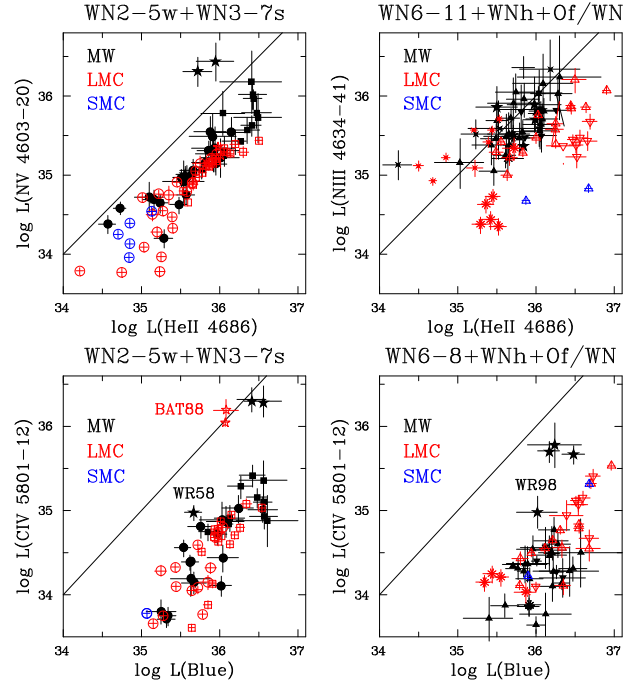


**Figure 3.** (Upper panels): He II  $\lambda 4686$  versus N V  $\lambda\lambda 4603,20$ +N III  $\lambda\lambda 4634,41$  line luminosities of WN, Of/WN and WN/C stars in the Milky Way (black), LMC (red) and SMC (blue). C III  $\lambda 4647,51$  also contributes for WN/C subtypes, N III  $\lambda\lambda 4634,41$  for WN6-7s subtypes and N II  $\lambda\lambda 460,43$  for WN10–11 subtypes; (Lower panels): Blue (He II  $\lambda 4686$ , N V  $\lambda\lambda 4603,20$ , N III  $\lambda\lambda 4634,41$ , C III  $\lambda 4647,51$ ) versus C IV  $\lambda\lambda 5801,12$  line luminosities. C IV  $\lambda\lambda 5801,12$  is an order of magnitude stronger in WN/C stars than WN stars. The solid line indicates equal line luminosities. Symbols as in Figure 2 (WN9-11 are omitted from lower panels since C IV  $\lambda\lambda 5801,12$  is weak/absent).

stars (usually WR+O binaries) lacking modern extinction determinations, we follow the approach adopted by Crowther & Hadfield (2006) involving the relationship between the He II  $\lambda 4686$  equivalent width ( $W_{\text{HeII} 4686}$ ) and intrinsic colour of WN stars, or adopt  $(b-v)_0 = -0.30$  mag, plus  $E_{\text{B-V}} = 1.21 \times E_{b-v}$  and  $R_V = 3.1$ . In order to determine intrinsic fluxes we adopt the Milky Way extinction law of Seaton (1979), parameterised by Howarth (1983), which provided the default law for the majority of Galactic WN and WC stars studied by Hamann et al. (2006) and Sander et al. (2012), respectively<sup>5</sup>. For error calculations we assume  $A_V$  magnitudes are reliable to 10% throughout. By way of example, we measure  $W_{\text{HeII} 4686} = 19\text{\AA}$  for WR138-1, which implies  $(b-v)_0 \sim -0.31$  mag (Crowther & Hadfield 2006, their fig. 1), so  $E_{b-v} = 1.87$  mag, based on  $b-v = 1.56$  mag from our INT/IDS spectroscopy, resulting in  $A_V = 7.0 \pm 0.7$  mag (versus  $A_V = 7.4$  mag from Gvaramadze et al. 2009).

Distances to Galactic WR stars follow from *Gaia* DR3 parallaxes (Gaia Collaboration et al. 2021), using star-specific zero point corrections from Lindegren et al. (2021) updated by Mafz Apellániz (2022), and the Bayesian methods set out in Rate & Crowther (2020). Inferred distances are generally in good agreement with Bailer-Jones et al. (2021). A comparison between distances obtained from Rate & Crowther (2020) based on DR2 parallaxes and the global zero point correction of Lindegren et al. (2018) versus DR3 parallaxes and updated zero-point corrections is presented in Fig. 1. In general,

<sup>5</sup> Contemporary extinction laws are available (e.g. Fitzpatrick et al. 2019)

DR3 plus star-specific zero point corrections provides significantly improved uncertainties on WR distances. Sources with DR3 warning flags (e.g. WR2, WR31, WR66, WR104, WR115) are excluded, while we include H-rich WN stars within NGC 3603 (WR43) for which we adopt the distance of  $7.27^{+0.38}_{-0.35}$  kpc determined by [Drew et al. \(2021\)](#). Average distances to Galactic WN and WN/C stars in our sample are  $4.0 \pm 2.2$  kpc while average distances to WC and WO stars are  $3.5 \pm 1.7$  kpc. For Galactic stars, *Gaia* DR3 distance uncertainties are typically  $\leq 10\%$ , so extinctions usually dominate uncertainties in line luminosities.

We group WN stars into five categories, strong-lined ("WN3–7s") weak-lined, early-type ("WN2–5w") stars, weak-lined late-type ("WN6–8") or very late-type ("WN9–11"), and (main sequence) very massive H-rich stars ("WN5–7h") stars, and additionally include transition Of/WN stars ("O2–3.5If/WN"). The division between strong and weak-lined stars was set at  $W_{\text{HeII}} \lambda 5412 = 40\text{\AA}$  ([Koesterke et al. 1991](#)). We follow this approach with the exception of BAT99-5 which is assigned as a weak-lined star despite  $W_{\text{HeII}} \lambda 5412 = 41 \pm 1$   $\text{\AA}$ . Weak/strong lined categories are preferred to narrow/broad-lined ([Smith et al. 1996](#)) whose threshold is  $\text{FWHM}(\text{He II } \lambda 4686) = 30\text{\AA}$  (corresponding to  $\sim 1900 \text{ km s}^{-1}$ ), since a subset of broad-lined stars possess a very weak emission line spectrum (e.g. WR46, [Crowther et al. 1995b](#)), although the majority of strong-lined stars also possess broad lines, and ([Smith et al. 1996](#)) included  $W_\lambda(\text{He II } \lambda 5412) = 40\text{\AA}$  as one of their criteria for broad-lined WN stars. The majority of strong-lined stars have WN3–4 subtypes, although examples in the Milky Way extend as late as WN6 (WR134, WR136) or WN7 (WR91). LMC 170–2 (WN3/O3, [Neugent et al. 2017](#)) is included as a WN2–5w star, although H $\beta$  absorption would usually favour an O-type classification in preference to either WN or Of/WN ([Crowther & Walborn 2011](#)). In order to discriminate between classical WN and main-sequence WN5–7h stars, we consider spectral morphologies as well as association with young star-forming regions (e.g. Carina Nebula, NGC 3603). WC stars are categorised as early-type ("WC4–5"), mid-type ("WC6–7") or late-type ("WC8–9").

Line luminosities of individual Galactic WN, WN/C, WC and WO stars are presented in Tables A1–A4 in the Appendix. For WN and WN/C stars, aside from the blends at  $\lambda 4100$  and  $\lambda 4630$ , we have endeavoured to exclude the contribution of He I  $\lambda 7065$  and He II  $\lambda 7177$  from the N IV  $\lambda\lambda 7103, 29$  multiplet. For early-type WC and WO stars, C IV  $\lambda 4658$  (6–5),  $\lambda 4686$  (8–6),  $\lambda 4689$  (11–7) will also contribute to the C III  $\lambda\lambda 4647, 51$ +He II  $\lambda 4686$  blend. Uncertainties in absolute luminosities involve a combination of absolute flux calibration, distance and extinction, with the latter dominating uncertainties for the majority of Galactic WR stars. Uncertainties on stellar luminosities from literature results account for distance and extinction, but exclude systematic uncertainties resulting from individual studies which varies between studies (typically 0.1–0.2 dex).

In general, WR stars within unresolved star-forming regions are detected via blue ( $\lambda 4686$ ) or yellow ( $\lambda 5808$ ) bumps. Binaries comprise a significant subset of our sample, but WR fluxes/luminosities are not generally impacted with a few exceptions. Strong absorption lines of OB companions impacts measurements of features in the proximity of (usually) upper Balmer lines, while a few systems are host to multiple WR stars in which case calibrations adopt equal contribution from each component, which is a reasonable approximation for systems with mass ratios of order unity (e.g. WR43A, [Schnurr et al. 2008](#)). Excess line emission is also observed in colliding wind systems, usually witnessed in C III  $\lambda 5696$  in WC+O binaries ([Luehrs 1997](#)).

## 2.2 Magellanic Cloud WR stars

We supplement Galactic WR datasets with Magellanic Cloud counterparts, updated from [Crowther & Hadfield \(2006\)](#) to include additional datasets (e.g. [Tramper et al. 2015](#); [Neugent et al. 2017](#); [Adland et al. 2022b](#)). Observations of SMC WN2–5w stars suffer from poor S/N, so we also calibrate higher quality datasets from [Foellmi et al. \(2003\)](#). We also make use of archival ultraviolet IUE or HST spectrophotometry, the latter involving FOS ([Crowther et al. 2002](#)), STIS ([Crowther et al. 2016](#); [Adland et al. 2022b](#)) and COS ([Adland et al. 2022b](#)) instruments. VLT/Xshooter and ANU 2.3m/DBS spectrophotometry extend to the near-IR, with Magellan FIRE datasets also utilised for LMC WC and WO stars ([Adland et al. 2022b](#)). Again, we assume typical uncertainties of 10% for line flux measurements obtained from spectrophotometric datasets (e.g. [Crowther & Hadfield 2006](#)).

Comparisons between He II  $\lambda 4686$  line fluxes and literature results for LMC WN stars from [Leitherer et al. \(2019\)](#) reveal  $\log F_{\text{HeII}4686} - F_{\text{HeII}4686}^{\text{L19}} = +0.02 \pm 0.05$  for 30 stars in common, while comparisons between C IV  $\lambda 5808$  line fluxes and literature results for LMC WC stars from [Smith et al. \(1990a\)](#) reveal  $\log F_{\text{CIV}5801,12} - F_{\text{CIV}5801,12}^{\text{S90a}} = -0.07 \pm 0.09$  for 10 stars in common. Several Magellanic Cloud systems are host to multiple WN+WN stars, including BAT99-116 (Mk 34, [Tehrani et al. 2019](#)), and BAT99-118 (R144, [Shenar et al. 2021](#)), so we adopt equal line contributions from each component since mass ratios are close to unity, which should be a reasonable assumption with the potential exception of AB5 (HD 5980, [Koenigsberger et al. 2014](#)). Since AB5 is known to be spectroscopically variable ([Koenigsberger et al. 2022](#)), we have selected the HST/STIS dataset from 2016 (phase 0.36) instead of 2014 (phase 0.0) ([Hillier et al. 2019](#)). R140a is omitted since it involves a mix of WN and WC populations which are difficult to deblend ([Castro et al. 2018](#)).

Revised interstellar extinctions are again drawn from spectroscopic studies where available (e.g. [Hainich et al. 2014](#)), or  $(b - v)_0 = -0.30$  mag otherwise, plus  $E_{B-V} = 1.21 E_{b-v}$  and  $R_V = 3.1$ . Again, we assume that literature  $A_V$  values are reliable to 10%. For reference, the average difference between values of  $E_{B-V}$  adopted here for LMC WC+O binaries is  $-0.03 \pm 0.13$  mag with respect to [Bartzakos et al. \(2001\)](#). The LMC distance of 49.6 kpc adopted from [Pietrzyński et al. \(2019\)](#) and a SMC distance of 61.2 kpc obtained from the 0.458 mag difference in distance moduli between the Magellanic Clouds ([Graczyk et al. 2014](#)). We assume an uncertainty of 2% for individual distances within the Magellanic Clouds. We adopt the LMC extinction law of [Howarth \(1983\)](#) for both Clouds, in common with the studies of Magellanic Cloud WR stars by [Hainich et al. \(2014\)](#) and [Hainich et al. \(2015\)](#), noting that alternative prescriptions are available ([Gordon et al. 2003](#); [Maíz Apellániz et al. 2014](#)).

Line luminosities of individual Magellanic Cloud WN, Of/WN, WN/WC, WC and WO stars are included in Tables A1–A4 in the Appendix. The largest source of uncertainty in line luminosities of Magellanic Cloud stars is usually flux calibration since distances are well established and extinctions are generally low, with a few exceptions (e.g. VFTS 682, Rubin-Diez et al. in prep). Since Rubin-Diez et al. adopt the 30 Dor extinction law of [Maíz Apellániz et al. \(2014\)](#) for the heavily reddened star VFTS 682 (WN5–7h) we are able to quantify differences in line intensities following [Howarth \(1983\)](#). We typically obtain line intensities within 10–20%, higher intensities for violet lines following [Howarth \(1983\)](#), and higher intensities for red lines following [Maíz Apellániz et al. \(2014\)](#). Uncertainties on stellar luminosities from literature results account for distance

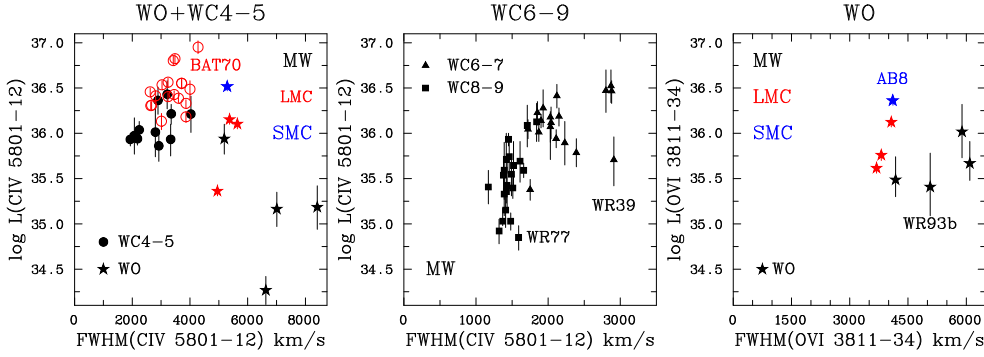


**Figure 4.** (left): C IV  $\lambda\lambda 5808$  line luminosities of WO (stars) and WC4–5 (circles) stars in the Milky Way, LMC and SMC versus FWHM ( $\text{km s}^{-1}$ ); (centre): C IV  $\lambda\lambda 5801,12$  line luminosities of Milky Way WC6–7 (black triangles) and WC8–9 (black squares) versus FWHM ( $\text{km s}^{-1}$ ); (right): O VI  $\lambda\lambda 3811,34$  line luminosities of WO stars in the Milky Way, LMC and SMC versus FWHM ( $\text{km s}^{-1}$ ).

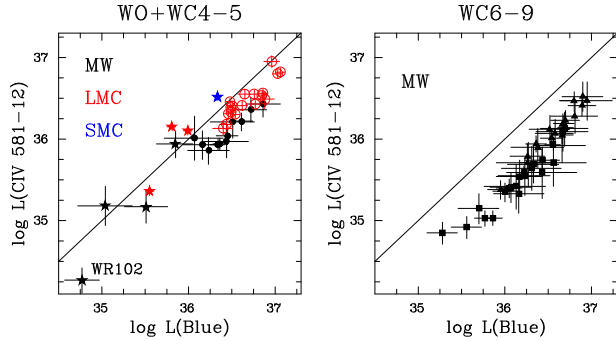


**Figure 5.** Blue (C III  $\lambda\lambda 4647,51$ , C IV  $\lambda 4658$ , He II  $\lambda 4686$ ) versus yellow (C IV  $\lambda\lambda 5801,12$ ) line luminosities of WC and WO stars in the Milky Way (black), LMC (red) and SMC (blue). Symbols as in Figure 4. The solid line indicates equal blue and yellow luminosities.

and extinction, but exclude systematic uncertainties resulting from individual studies (variable, albeit typically 0.1–0.2 dex).

### 3 RESULTS

#### 3.1 WN, Of/WN and WN/C stars

In Fig. 2 we compare He II  $\lambda 4686$  FWHM and line luminosities for Milky Way and Magellanic Cloud WN and Of/WN stars. Galactic strong-lined WN stars exhibit the highest line luminosities and largest FWHM  $\lambda 4686$ . LMC strong-lined WN stars overlap with Galactic counterparts, but typically have lower luminosities and FWHM. Weak-lined WN2–5 stars in the Milky Way span a broad range of line luminosities, ranging from  $\log(L_{4686}/\text{erg s}^{-1}) = 36.1 \pm 0.2$  (WR141) to  $34.6 \pm 0.1$  (WR3), with similar results obtained for LMC stars, except that LMC 170–2 (Neugent et al. 2017) has a very low luminosity of  $\log(L_{4686}/\text{erg s}^{-1}) = 34.2$ , and is morphologically similar to WR3 and WR46 in the Milky Way (Crowther et al. 1995b). SMC WN2–5w stars possess uniformly low  $\lambda 4686$  line luminosities, spanning  $\log(L_{4686}/\text{erg s}^{-1}) = 35.6$  (AB3) to 34.7 (AB11), which has previously been highlighted by Crowther & Hadfield (2006). Sander et al. (2020) have investigated wind driving of WR stars, and establish a dependence on metallicity (Fe-group elements) and Eddington parameter  $\Gamma_e$  ( $\propto L/M$ ) so strong-lined WN stars likely differ in their wind properties from weak-lined WN stars owing to higher luminosity-to-mass ratios. He II  $\lambda 4686$  properties of Galactic and LMC WN/C stars are similar to normal WN stars in these galaxies.

Galactic weak-lined WN6–8 stars possess relatively low FWHM  $\lambda 4686$ , albeit a wide range of line luminosities, spanning  $\log(L_{4686}/\text{erg s}^{-1}) = 36.3 \pm 0.5$  (WR147) to  $35.0 \pm 0.3$  (WR107). LMC

weak-lined WN6–8 stars extend the Galactic sequence to higher luminosities, including R144 (BAT99–118), which is host to a multiple WN+WN system (Shenar et al. 2021) and R145 (BAT99–119) which is also a binary system (Shenar et al. 2019). There are too few SMC late-type WN stars to draw robust conclusions, although the high luminosity SMC system AB 5 (HD 5980) is also multiple (Koenigsberger et al. 2014, 2022). Milky Way and LMC WN9–11 stars possess very low FWHM and line luminosities, with the notable exception of WR105 (WN9) whose  $\lambda 4686$  line luminosity is comparable to WN6–8 stars. H-rich main sequence WN6–7h stars in the Milky Way form a relatively homogenous group, overlapping with weak-lined classical WN stars in He II  $\lambda 4686$  properties, and includes the WN+WN binary system WR43A. LMC counterparts extend to higher luminosity, broader lines (WN5h) stars, including the WN5h+WN5h binary Mk 34 (BAT99–116, Tehrani et al. 2019) with Of/WN stars, such as Mk 35 (BAT99–114, Crowther & Walborn 2011), possessing lower line luminosities.

Fig. 3 (upper panels) compares He II  $\lambda 4686$  and N V  $\lambda\lambda 4603,20+N$  III  $\lambda\lambda 4634,41$  line luminosities of WN, Of/WN and WN/C stars. For early subtypes N V  $\lambda\lambda 4603,20/\text{He II } \lambda 4686 \sim 0.2$ –0.3 in all environments, with the exception of Galactic WN/C stars which also exhibit a contribution from C III  $\lambda\lambda 4647,51$ . In contrast, for late subtypes N III  $\lambda\lambda 4634,41/\text{He II } \lambda 4686 \sim 0.8$  in the Milky Way,  $\sim 0.2$  in the LMC and  $\leq 0.1$  in the SMC, with the exception of WN9–11 stars for which N II  $\lambda\lambda 4601,43+N$  III  $\lambda\lambda 4634,41/\text{He II } \lambda 4686 \geq 1$ . Fig. 3 (lower panels) compares the blue (He II  $\lambda 4686$ , N V  $\lambda\lambda 4603,20$ , N III  $\lambda\lambda 4634,41$ , C III  $\lambda\lambda 4647,51$ ) and C IV  $\lambda\lambda 5801,12$  line luminosities of WN, Of/WN and WN/C stars. For Galactic early-type WN stars the line luminosity of C IV  $\lambda\lambda 5801,12$  is an order of magnitude weaker than the blue feature, with late-type WN stars somewhat weaker still (and usually resolved into individual components). A broadly similar dependence is obtained for Magellanic Cloud counterparts, with C IV  $\lambda\lambda 5801,12$  undetected in a subset of WN stars from all environments. In contrast, C IV  $\lambda\lambda 5801,12$  luminosities of WN/C stars exceed normal WN stars by an order of magnitude, and are more typical of WC stars. The least extreme examples of WN/C stars in our sample are WR58 and WR98 (Conti & Massey 1989).

Tables 2–3 provide calibrations of He II  $\lambda 4686$  line luminosities for WN2–8 (N=140), WN9–11 (N=12), Of/WN (N=8) and WN/C (N=9) stars, respectively, together with other prominent optical emission lines. This highlights features that may be detectable in high S/N observations of WR galaxies, notably the  $\lambda 4100$  complex in WN stars which is largely unaffected by nebular emission, in contrast with H $\alpha$ , H $\beta$ , He I  $\lambda 5876$ . Although H $\beta$  is omitted here,  $L_{\text{H}\alpha}/L_{\text{H}\beta} = 1.9 \pm 0.8$  for 141 Milky Way and Magellanic Cloud WN and WN/C stars.

**Table 2.** WN and Of/WN line luminosity calibrations for Milky Way, LMC and SMC stars, including He II  $\lambda\lambda 4686$  FWHM in  $\text{km s}^{-1}$ . The complex at  $\lambda 4100$  involves N III  $\lambda\lambda 4097, 4103$ , Si IV  $\lambda\lambda 4088, 4116$ , He II  $\lambda 4100 + \text{H}\delta$ , while the feature at  $\lambda 4630$  involves N V  $\lambda\lambda 4603, 20$ , N III  $\lambda\lambda 4634, 41$  (or N II  $\lambda\lambda 4601, 43$  for very late WN subtypes). Line luminosities have been adjusted for systems host to WN+WN binaries (marked with  $\diamond$ ), namely WR43A, BAT99-116, BAT99-118 and AB5.

Category	N	HeII 4686 FWHM	$L_{\text{HeII} 4686}$ $10^{35} \text{ erg s}^{-1}$	$L_{\text{NIV} 3478, 85}$ $10^{-3} L_{\text{Bol}}$	$L_{\text{NIV} 4058}$ $L_{\text{HeII} 4686}$	$L_{4100}$ $L_{\text{HeII} 4686}$	$L_{4630}$ $L_{\text{HeII} 4686}$	$L_{\text{HeII} 5412}$ $L_{\text{HeII} 4686}$	$L_{\text{CIV} 5801, 12}$ $L_{\text{HeII} 4686}$	$L_{\text{HeI} 5876}$ $L_{\text{HeII} 4686}$	$L_{\text{H}\alpha}$ $L_{\text{HeII} 4686}$	$L_{\text{NIV} 7103, 29}$ $L_{\text{HeII} 4686}$		
Milky Way ( $Z_\odot$ )														
WN2–5w	22	1680±310	4.9± 3.7	0.37±0.23	0.68±0.21	0.26±0.14	0.27±0.14	0.29±0.15	0.12±0.03	0.06±0.05	0.03±0.02	0.20±0.08	0.21±0.15	
WN3–7s	12	2480±510	20.3± 8.9	1.25±0.40	0.49±0.14	—	0.40±0.25	—	0.27±0.16	0.13±0.02	0.07±0.03	0.05±0.03	0.15±0.04	0.16±0.04
WN6–8	25	990±240	7.4± 5.0	0.44±0.20	0.30±0.16	0.18±0.09	0.65±0.28	0.86±0.44	0.11±0.04	0.03±0.02	0.32±0.31	0.51±0.43	0.12±0.10	
WN9–11	4	440±100	5.1± 6.9	0.13±0.11	...	0.00±0.00	6.2±10.2	3.1±3.2	0.03±0.03	0.01±0.01	9.7±18.0	45±87	0.01±0.0	
WN5–7h	7 $\diamond$	1260±510	11.0± 3.8	0.15±0.04	0.37±0.39	0.18±0.07	0.54±0.23	0.58±0.32	0.06±0.01	0.03±0.02	0.05±0.02	0.64±0.13	0.09±0.01	
Of/WN	2	1610±470	4.8±0.5	0.05±0.01	0.16±0.08	0.25±0.09	0.26±0.24	0.48±0.16	0.06	0.01	0.00	0.58	...	
LMC (0.4Z $\odot$ )														
WN2–5w	24	1750±280	3.3± 2.6	0.21±0.14	0.79±0.19	0.10±0.11	0.13±0.12	0.19±0.12	0.11±0.03	0.04±0.03	0.00±0.01	0.22±0.06	0.08±0.04	
WN3–7s	18	2170±600	10.1± 6.9	0.70±0.24	0.50±0.23	—	0.12±0.04	—	0.16±0.03	0.13±0.01	0.05±0.03	0.01±0.02	0.16±0.03	0.07±0.03
WN6–8	13 $\diamond$	1080±270	17.8±14.0	0.39±0.16	0.20±0.08	0.17±0.03	0.33±0.14	0.34±0.19	0.09±0.03	0.03±0.02	0.09±0.06	0.41±0.24	0.06±0.01	
WN9–11	8	240± 40	1.6±1.1	0.09±0.07	...	0.01±0.02	1.50±0.93	1.9±1.1	0.05±0.09	0.00±0.00	1.8±1.5	6.5±5.1	...	
WN5–7h	8 $\diamond$	1830±250	30.2±13.6	0.24±0.12	0.44±0.14	0.18±0.05	0.18±0.09	0.07±0.03	0.09±0.02	0.03±0.01	0.01±0.01	0.34±0.08	0.11±0.04	
Of/WN	6	1130±300	3.7±1.9	0.05±0.02	0.30	0.22	0.00	0.18±0.12	0.02±0.02	0.04±0.04	0.00±0.00	0.59±0.13	0.11±0.05	
SMC (0.2Z $\odot$ )														
WN2–5w	9	1630±280	1.7± 1.3	0.05±0.03	0.58	0.04±0.08	0.00±0.01	0.19±0.13	0.06±0.02	0.01±0.02	0.00±0.00	0.25±0.14	0.22	
WN6–8	2 $\diamond$	1060±280	15.5±11.4	0.35±0.06	0.23±0.07	0.09±0.07	0.10±0.03	0.04±0.03	0.10±0.00	0.03±0.02	0.03±0.02	0.23±0.02	0.06±0.01	
All WN2–8	140 $\diamond$	1570±610	9.7±10.1	0.42±0.37	0.48±0.27	0.14±0.11	0.26±0.25	0.34±0.33	0.10±0.04	0.04±0.03	0.08±0.17	0.30±0.23	0.12±0.14	
All WN9–11	12	300±120	2.8±4.1	0.10±0.07	...	0.01±0.01	3.1 ±5.9	2.3±1.9	0.02±0.02	0.00±0.01	4.4±10.3	20±52	0.01±0.00	
All Of/WN	8	1250±380	3.5±1.3	0.05±0.02	0.21±0.10	0.24±0.07	0.18±0.23	0.26±0.19	0.03±0.02	0.03±0.03	0.00±0.00	0.59±0.12	0.11±0.05	

**Table 3.** WN/C line luminosity calibrations for Milky Way and LMC stars, including He II  $\lambda\lambda 4686$  FWHM in  $\text{km s}^{-1}$ . The complex at  $\lambda 4100$  involves N III  $\lambda\lambda 4097, 4103$ , Si IV  $\lambda\lambda 4088, 4116$ , He II  $\lambda 4100 + \text{H}\delta$ , while the feature at  $\lambda 4603–51$  involves N V  $\lambda\lambda 4603, 20$ , N III  $\lambda\lambda 4634, 41$  and C III  $\lambda\lambda 4647, 51$ .

Category	N	HeII 4686 FWHM	$L_{\text{HeII} 4686}$ $10^{35} \text{ erg s}^{-1}$	$L_{\text{NIV} 3478–85}$ $10^{-3} L_{\text{Bol}}$	$L_{\text{NIV} 4058}$ $L_{\text{HeII} 4686}$	$L_{4100}$ $L_{\text{HeII} 4686}$	$L_{4603, 51}$ $L_{\text{HeII} 4686}$	$L_{\text{HeII} 5412}$ $L_{\text{HeII} 4686}$	$L_{\text{CIII} 5696}$ $L_{\text{HeII} 4686}$	$L_{\text{CIV} 5801, 12}$ $L_{\text{HeII} 4686}$	$L_{\text{H}\alpha}$ $L_{\text{HeII} 4686}$	$L_{\text{NIV} 7103, 29}$ $L_{\text{HeII} 4686}$	
3 Milky Way ( $Z_\odot$ ) and 2 LMC (0.4Z $\odot$ )													
WNE/C	5	2240±430	7.5±2.9	0.47±0.30	0.64±0.04	0.14±0.12	0.26±0.19	1.54±1.82	0.18±0.08	0.01±0.02	1.38±1.39	0.21±0.08	0.19±0.20
Milky Way ( $Z_\odot$ )													
WNL/C	4	1270±130	7.3±3.1	0.36±0.17	0.82	0.91	0.87	1.75±1.32	0.15±0.05	0.06±0.08	0.53±0.17	0.18±0.09	0.20
All WN/C	9	1810±600	7.4±2.8	0.43±0.25	0.68±0.10	0.27±0.33	0.36±0.30	1.63±1.53	0.17±0.06	0.03±0.06	1.26±1.21	0.20±0.08	0.19±0.14

**Table 4.** WC line luminosity calibrations for Milky Way and LMC stars, including C IV  $\lambda\lambda 5801, 12$  FWHM in  $\text{km s}^{-1}$ . The blue feature involves C III  $\lambda\lambda 4647, 51$ , C IV  $\lambda 4658$  and He II  $\lambda 4686$ , while the feature at  $\lambda 6559, 81$  involves He II  $\lambda 6560$  and C II  $\lambda\lambda 6559, 81$ .

Category	N	CIV 5801,12 FWHM	$L_{\text{CIV} 5801,12}$ $10^{35} \text{ erg s}^{-1}$	$L_{\text{OIV} 3403, 13}$ $10^{-3} L_{\text{Bol}}$	$L_{\text{CIV} 5801, 12}$ $L_{\text{CIV} 5801, 12}$	$L_{\text{Blue}}$ $L_{\text{CIV} 5801, 12}$	$L_{\text{CIII} 5696}$ $L_{\text{CIV} 5801, 12}$	$L_{\text{HeI} 5876}$ $L_{\text{CIV} 5801, 12}$	$L_{\text{6559, 81}}$ $L_{\text{CIV} 5801, 12}$	$L_{\text{CIII} 6727, 73}$ $L_{\text{CIV} 5801, 12}$	$L_{\text{CIV} 7725}$ $L_{\text{CIV} 5801, 12}$	$L_{\text{CIII} 9701, 19}$ $L_{\text{CIV} 5801, 12}$
Milky Way ( $Z_\odot$ )												
WC4–5	11	2790±630	13.3± 6.6	1.43±0.44	0.55±0.25	2.30±0.51	0.02±0.03	0.08±0.01	0.07±0.03	0.11±0.03	0.09±0.02	0.13±0.07
WC6–7	18	2180±400	15.3± 9.0	0.89±0.43	0.77±0.24	3.11±0.50	0.35±0.24	0.16±0.11	0.16±0.06	0.17±0.03	0.11±0.01	0.28±0.06
WC8–9	21	1480±140	4.1± 3.5	0.41±0.20	1.32±0.92	4.82±1.19	3.21±1.01	0.56±0.26	1.12±0.48	0.60±0.27	0.11±0.04	0.99±0.28
LMC (0.4Z $\odot$ )												
WC4–5	18	3370±490	34.1±19.8	2.19±0.27	0.55±0.26	1.63±0.40	0.02±0.03	0.02±0.03	0.05±0.01	0.06±0.02	0.06±0.01	0.06±0.03
All WC	68	2380±850	16.4±16.2	0.98±0.68	0.79±0.53	3.12±1.48	1.09±1.54	0.26±0.28	0.45±0.56	0.26±0.27	0.08±0.03	0.34±0.38

### 3.2 WC and WO stars

In Fig. 4 (left and centre panels) we compare the FWHM and line luminosities of C IV  $\lambda\lambda 5801, 12$  for Milky Way and Magellanic Cloud WO and WC stars. WO stars possess exceptionally high FWHM though span a wide range of C IV  $\lambda\lambda 5801, 12$  line luminosities,

ranging from  $\log(L_{\text{CIV} 5801, 12}/\text{erg s}^{-1}) = 36.52 \pm 0.05$  (AB8, SMC) to  $34.25 \pm 0.15$  (WR102, Milky Way). In contrast, LMC WC4–5 stars possess uniformly high luminosities, with the WC4+O binary BAT99-70 possessing the highest luminosity C IV  $\lambda\lambda 5801, 12$ . Galactic counterparts overlap with LMC stars, though extend to lower luminosities. Galactic WC6–7 stars overlap with WC4–5 subtypes,

**Table 5.** WO line luminosity calibrations for Milky Way, LMC and SMC stars, including C IV  $\lambda\lambda 5808$  FWHM in  $\text{km s}^{-1}$ . The blue feature involves C IV  $\lambda 4658$  and He II  $\lambda 4686$ .

Subtype	N	CIV 5801,12 FWHM	$L_{\text{CIV}} 5801,12$ $10^{35} \text{ erg s}^{-1} 10^{-3} L_{\text{Bol}}$	$\frac{L_{\text{OIV}} 3403,13}{L_{\text{CIV}} 5801,12}$	$\frac{L_{\text{OVI}} 3811,34}{L_{\text{CIV}} 5801,12}$	$\frac{L_{\text{Blue}}}{L_{\text{CIV}} 5801,12}$	$\frac{L_{\text{OV}} 5572,607}{L_{\text{CIV}} 5801,12}$	$\frac{L_{\text{HeII}} 6560}{L_{\text{CIV}} 5801,12}$	$\frac{L_{\text{CIV}} 7725}{L_{\text{CIV}} 5801,12}$	
Milky Way ( $Z_\odot$ )										
WO2–4	4	6800±1300	3.0±3.9	0.25±0.20	1.8±0.8	8.6±12.2	1.7±1.2	0.5±0.6	0.22±0.16	0.45±0.47
LMC (0.4 $Z_\odot$ )										
WO3–4	3	5300±300	9.7±6.5	1.18±0.84	1.9±2.0	2.2±3.1	0.9±0.6	0.16±0.14	0.08±0.08	0.14±0.13
SMC (0.2 $Z_\odot$ )										
WO4	1	5300	32.9	0.59	1.0	0.7	0.65	0.16	0.04	0.19
All WO	8	6100±1200	9±11	0.70±0.69	1.7±1.3	5.2±8.5	1.3±1.0	0.3±0.4	0.13±0.13	0.30±0.36

although these extend to lower luminosities, unusually so for WR39. Galactic WC8–9 stars exhibit a narrow range of FWHM but a broad range of line luminosities, ranging from  $\log(L_{\text{CIV}} 5801,12/\text{erg s}^{-1}) = 36.1\pm0.2$  (WR60) to  $34.85\pm0.15$  (WR77). Smith et al. (1990b) have previously studied Galactic WC stars in clusters and associations to suggest uniform C IV  $\lambda\lambda 5801\text{--}12$  fluxes for Galactic WC5–7 stars, with lower line fluxes for WC8–9 stars. Fig. 4 (right panel) compares O VI  $\lambda\lambda 3811,34$  FWHM and line luminosities of Milky Way and Magellanic Cloud WO stars, revealing uniformly high FWHM, though an order of magnitude spread in line luminosity from  $\log(L_{\text{OVI}} 3811,34/\text{erg s}^{-1}) = 36.35\pm0.05$  (AB8) to  $35.4\pm0.3$  (WR93b).

Fig. 5 compares blue (C III  $\lambda\lambda 4647,51$ , C IV  $\lambda 4658$ , He II  $\lambda 4686$ ) to yellow (C IV  $\lambda\lambda 5801,12$ ) line luminosities of WC and WO stars. For Galactic WC4–5 stars the blue and yellow features are well correlated, with the former exceeding C IV  $\lambda\lambda 5801,12$  by a factor of 2–3, while these features are more comparable in strength in LMC WC4–5 and WO stars. Blue and yellow features are also tightly correlated for WC6–9 stars, with the former exceeding C IV  $\lambda\lambda 5801,12$  by a factor of 3 (WC6–7) to 5 (WC8–9).

Tables 4–5 provide calibrations of C IV  $\lambda\lambda 5801,12$  line luminosities for WC (N=68) and WO (N=8) stars, respectively. Other strong WC features include C III  $\lambda\lambda 4647,51$ ,  $\lambda 5696$ , the latter having occasionally been reported in WR galaxies (e.g. Schaefer et al. 1999), with O IV  $\lambda\lambda 3403,13$  also prominent in WC and WO stars.

### 3.3 Calibrations

In order to analyse distant, unresolved star-forming regions host to WR stars we shall primarily focus on the broad blue bump, involving a blend of N V  $\lambda\lambda 4603,20$ , N III  $\lambda\lambda 4634,41$ , C III  $\lambda\lambda 4647,51$ , He II  $\lambda 4686$ , plus the yellow C IV  $\lambda\lambda 5801,12$  bump. Although C IV  $\lambda\lambda 5801,12$  is present in the majority of WN stars, it is typically much weaker than the blue bump (Fig. 3), with upper limits measured for many weak-lined WN stars. WN/C stars possess high C IV  $\lambda\lambda 5801,12$  line luminosities, with an average value of  $\log(L_{\text{CIV}} 5801,12/\text{erg s}^{-1}) = 36.0$ , although one would not expect prominent C IV emission from such stars in an unresolved stellar population since they only comprise a small fraction of the overall WR population. The strength of the bumps are tightly correlated for WC stars, confirming results from Smith et al. (1990b), with  $L_{\text{Blue}}/L_{\text{CIV}} 5801,12 = 1.9\pm0.6$  for WC4–5 stars,  $3.0\pm0.4$  for WC6–7 stars and  $4.8\pm1.2$  for WC8–9 stars. In contrast, these features are poorly correlated in WO stars.

Previous optical calibrations have been obtained by Smith et al. (1990a) for LMC WC stars, Schaefer & Vacca (1998) for Milky Way and LMC WR stars, and Crowther & Hadfield (2006) for Magellanic Cloud WN stars, which have also been adapted for other metallicities

(López-Sánchez & Esteban 2010). In Table 6 we compare our current results with previous calibrations. Overall we reinforce the decrease in line luminosity of early-type WN stars with metallicity established by Crowther & Hadfield (2006) by the addition of Milky Way stars, plus higher line luminosities of WC4–5 stars in the LMC with respect to the Milky Way. However, we find no clear metallicity dependence for late-type WN or WO stars (hindered by low number of SMC stars), with significantly improved statistics for Galactic WC6–7 and WC8–9 stars with respect to Smith et al. (1990b) and Schaefer & Vacca (1998). The lack of strong metallicity dependence for some subtypes is somewhat surprising, recalling Sander et al. (2020). However, the lower (luminosity) threshold to the formation of WR stars increases at lower metallicity (Shenar et al. 2020, their figure 3) so reduced wind strengths at low metallicity are countered by a shift to higher stellar luminosities on average.

Schaerer & Vacca (1998) have previously adopted  $L_{\text{HeII}} 4686 = 6.5 \times 10^{35} \text{ erg s}^{-1}$  and  $2.5 \times 10^{35} \text{ erg s}^{-1}$  for (LMC) Of/WN and Of stars, respectively. We obtain  $L_{\text{HeII}} 4686 = (3.5 \pm 1.3) \times 10^{35} \text{ erg s}^{-1}$  for Of/WN stars (Table 2), whereas  $L_{\text{HeII}} 4686 \leq 10^{35} \text{ erg s}^{-1}$  is more typical of Magellanic Cloud Of supergiants. For example,  $L_{\text{HeII}} 4686 = 8 \times 10^{34} \text{ erg s}^{-1}$  for the O2 supergiant Mk 42 (BAT99-105) based on our MUSE dataset and the interstellar extinction from Hainich et al. (2014). Definitive results await analysis of VLT/Xshooter flux calibrated spectroscopy of Magellanic Cloud OB stars obtained via the X-Shooting ULLYSES initiative (Vink et al., submitted).

Beyond the usual blue and yellow WR bumps, we include line luminosities for prominent violet features, O IV  $\lambda\lambda 3811,34$ , N IV  $\lambda\lambda 3478,85$  and O IV  $\lambda\lambda 3811,34$ , noting that the latter is challenging to measure in WC stars due to line blends with other features, primarily the  $\lambda 3700$  complex of O III–IV and C IV on its blue wing. Although these are weaker than the standard WR diagnostics, they may be detectable in suitable host galaxies, especially those below the Balmer jump. The absence of O VI  $\lambda\lambda 3811,34$  from WO stars in integrated populations is not wholly unexpected in view of the low line luminosity with respect to C IV  $\lambda\lambda 5801,12$  in WC4–5 stars (Table 6) and location adjacent to stellar absorption lines (e.g. H9 at  $\lambda 3835$ , Sidoli et al. 2006). Longward of the visible range, N IV  $\lambda\lambda 3710,39$  and He II  $\lambda 10124$  are the strongest emission lines in WNE and WNE/C stars, with  $L_{\text{HeII}} 10124/L_{\text{HeII}} 4686 = 0.13\pm0.02$  while He I  $\lambda 10830$  is the strongest feature in WN6–8 (WN9–11) stars with  $L_{\text{HeI}} 10830/L_{\text{HeII}} 4686 = 0.7\pm0.6$  ( $0.9\pm0.8$ ). C IV  $\lambda 7725$  and C III  $\lambda\lambda 4970,19$  are the strongest red features in WC4–5 stars, albeit an order of magnitude weaker than C IV  $\lambda\lambda 5801,12$ , the former also prominent in WO stars. C III  $\lambda\lambda 4970,19$  is prominent in late WC subtypes, with  $L_{\text{CIII}} 4970\text{--}19/L_{\text{CIV}} 5801\text{--}12 = 0.3\pm0.1$  and  $1.0\pm0.3$  for WC6–7 and WC8–9 stars, respectively. C II  $\lambda 7231,37$  is promi-

**Table 6.** Comparison to literature calibrations of violet ( $\text{O IV } \lambda\lambda 3403,11$ ,  $\text{N IV } \lambda\lambda 3478,85$ ,  $\text{O VI } \lambda\lambda 3811,34$ ), blue ( $\text{He II } \lambda 4686$ ,  $\text{C III } \lambda\lambda 4647,51$ ,  $\text{N III-V } \lambda\lambda 4603,41$ ), yellow ( $\text{C III } \lambda 5696$ ,  $\text{C IV } \lambda\lambda 5801,12$ ) and red ( $\text{N IV } \lambda\lambda 7103,29$ ,  $\text{C III } \lambda\lambda 9701,19$ ) WR line luminosities. Wind features associated with strong nebular emission ( $\text{H}\alpha, \beta$ ) are excluded.

	$L_{\text{OIV}} 3403,13$	N	$L_{\text{NIV}} 3478,85$	N	$L_{\text{OVI}} 3811,34$	N	$L_{\text{Blue}}$	N	$L_{\text{CIII}} 5696$	N	$L_{\text{CIV}} 5801,12$	N	$L_{\text{NIV}} 7103,29$	N	$L_{\text{CIII}} 9701,19$	N	Sample	Ref	
WN3–7s																			
...	9.5±5.7	10	...		26±12	12	...		1.3±0.7	11	3.3±1.7	8	...			MW	3		
...	5.4±3.7	15	...		12±7	18	...		0.5±0.4	18	0.7±0.5	16	...			LMC	3		
WN2–5w																			
...	...	...	...		5±3	26	...		0.4±0.1	5	...	...	...			MW+LMC†	1		
...	3.8±2.7	13	0.1‡	1	6±5	23	...		0.3±0.3	19	1.0±0.7	11	...			MW	3		
...	3.0±1.8	12	...		4±3	24	...		0.2±0.2	23	0.3±0.3	20	...			LMC	3		
...	2.1	1	...		2±1	9	...		0.01±0.02	7	0.3	1	...			SMC	3		
WN6–8																			
...	...	...	...		21±18	19	...		1.0±0.6	10	...	...	...			MW+LMC‡	1		
...	2.2±1.4	12	...		13±8	25	...		0.2±0.1	24	0.9±1.0	6	...			MW	3		
...	2.8±2.6	8	...		26±25	15	...		0.6±0.6	13	1.3±0.1	4	...			LMC	3		
...	3.2±1.6	2	...		10±3	2	...		0.6±0.6	2	0.9±0.6	2	...			SMC	3		
WN9–11																			
...	...	...	...		7±10	12	...		0.01±0.01	4	0.03±0.02	2	...			MW+LMC	3		
WN5–7h+Of/WN																			
...	3.1±3.8	8	...		14±7	9	...		0.2±0.1	6	...	...	...			MW	3		
...	11.8±7.1	8	...		20±18	14	...		0.7±0.7	13	1.9±1.6	8	...			LMC	3		
WN/C																			
...	4.9±1.6	4	...		18±10	9	0.1±0.2	3	9.5±7.8	9	1.4±0.8	3	...			MW+LMC	3		
WC4–5																			
...	...	...	...		50	5	...		32	5	...	...	...			LMC	2		
...	...	...	...		49±17	32	0.7±0.4	20	28±12	20	...	...	...			MW+LMC	1		
6±4	8	...	0.9±0.5	9	31±18	11	0.2±0.3	11	13±7	11	...	...	1.5±1.1	4	MW	3			
16±7	7	...	2.0±1.6	15	53±29	17	0.5±0.8	17	34±20	17	...	...	2.1±1.2	7	LMC	3			
WC6–7																			
...	...	...	...		37±11	25	5.5±4.1	25	12±5	7	...	...	...			MW	1		
9±5	12	...	1.1±0.7	15	45±23	18	5.6±6.9	18	15±9	18	...	...	4.7±2.1	7	MW	3			
WC8–9																			
...	...	...	...		10±2	24	7.3±1.4	25	2.9±2.5	5	...	...	...			MW	1		
9±7	7	...	...		19±14	21	11±8	21	4.1±3.5	21	...	...	2.7±1.6	5	MW	3			
WO																			
19±14	3	...	15±9	3	8±3	3	...		11±2	3	...	...	...			MC+IC1613	1		
9±10	8	...	8±7	8	7±7	8	...		9±11	8	...	...	...			MW+MC	3		

1: Schaefer & Vacca (1998); 2: Smith et al. (1990a); 3: This work

‡: O VI is observed in WR46 (Crowther et al. 1995b) with  $L_{\text{OVI}} 3811,34 / L_{\text{HeII}} 4686 = 0.17$ ; †: WN2–4 weak and strong lined; ‡: WN6–9 weak and strong lined.

net in WC8–9 subtypes, with He I  $\lambda 10830$  also very strong with  $L_{\text{HeI}} 10830 / L_{\text{CIV}} 5801–12 = 0.5±0.4$ .

In the vacuum ultraviolet attention has usually been focused on He II  $\lambda 1640$  ( $n=3–2$ ) since it is prominent in most WR subtypes, and its line luminosity exceeds He II  $\lambda 4686$  ( $n=4–3$ ) by an order of magnitude (Crowther & Hadfield 2006, their fig. 3). Schaefer & Vacca (1998) obtained  $L_{1640} / L_{4686} = 7.8$  for Milky Way and LMC WN stars, supported by the comprehensive study of Leitherer et al. (2019), while Crowther & Hadfield (2006) obtained  $L_{4686} / L_{1640} = 10$  from LMC WN stars and theoretical models. Based on our adopted extinctions and  $\lambda 1640$  line fluxes measured from low resolution IUE/SWP spectroscopy we obtain  $L_{4686} / L_{1640} = 12±4$  for Galactic, and Magellanic Cloud WN and WN/C stars. N IV  $\lambda\lambda 1238,42$  is also strong in early WN stars, although this line and C IV  $\lambda\lambda 1548,51$  are present in early O stars (Crowther et al. 2016). N IV  $\lambda 1486$  and N IV  $\lambda 1718$  are

also prominent in early WN stars, with emission line luminosities 20–30% of He II  $\lambda 1640$ . In late WN stars He II  $\lambda 1640$  is less dominant, in part due to the forest of iron lines in its vicinity (Crowther et al. 1995a, their fig. 2), especially Fe IV  $\lambda 1633$ , with C IV  $\lambda\lambda 1548,51$ , Si IV  $\lambda\lambda 1393,1402$  and N IV  $\lambda 1718$  P Cygni profiles also prominent. In the near-UV, the strongest WN emission line is He II  $\lambda 3203$  ( $n=5–3$ ) with  $L_{3203} / L_{4686} = 0.7±0.2$  for Milky Way and Magellanic Cloud WN stars.

The strongest far-ultraviolet feature in WC4–7 stars is C IV  $\lambda\lambda 1548,51$  (Crowther & Hadfield 2006, their fig. 5), with He II  $\lambda 1640$ , C III]  $\lambda 1909$ , O IV  $\lambda\lambda 1338,43$ , O IV]  $\lambda\lambda 1397,1407$  and C III  $\lambda 1247$  also prominent. For LMC and Milky Way WC4–5 stars,  $L_{\text{CIV}} 1548,51 / L_{\text{CIV}} 5801,12 = 8±2$  and  $L_{\text{HeII}} 1640 / L_{\text{CIV}} 5801,12 = 5±2$ , somewhat higher than the ratios of 6.0 and 2.6 obtained by Crowther & Hadfield (2006) for single LMC WC4–5 stars in-

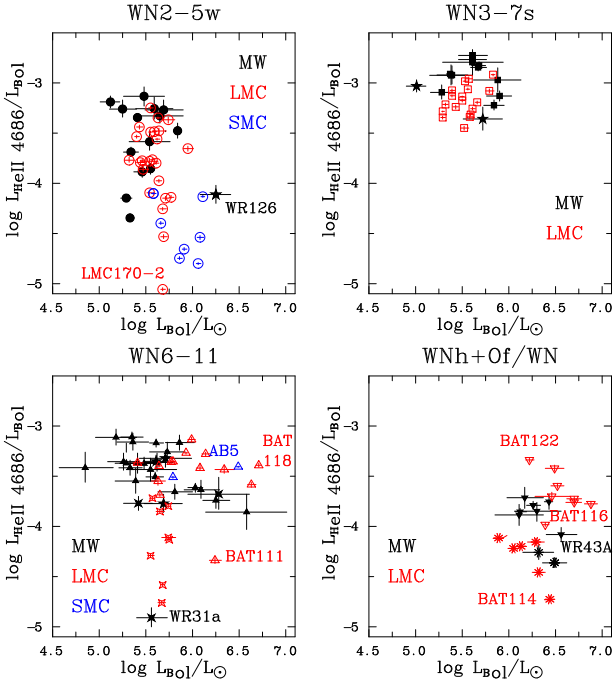


**Figure 6.** Bolometric luminosity versus ratio of He II  $\lambda 4686$  line to bolometric luminosity for weak-lined WN2–5 (top left), strong lined WN3–7 (top right), weak lined WN6–11 (bottom left) and WNh+Of/WN (bottom right) stars in the Milky Way (black), LMC (red) and SMC (blue). Symbols as in Figure 2.

dicating the sensitivity to extinction determinations and sample size. C IV  $\lambda\lambda 1548, 51$  remains the strongest far-UV line in WC6–7 stars, with C III]  $\lambda 1909$  the strongest far-UV emission line in WC8–9 stars. We obtain  $L_{\text{CIII]} 1909}/L_{\text{CIV} 5801,12} = 4 \pm 2, 7 \pm 4, 23 \pm 8$  for Galactic WC4–5, WC6–7 and WC8–9 stars, respectively. In the near-UV, the strongest WC emission line is C III  $\lambda 2297$ , followed by C IV  $\lambda 2530$  in early WC stars.  $L_{\text{CIII} 2297}/L_{\text{CIV} 5801,12} = 5 \pm 2, 6 \pm 4, 23 \pm 10$  for Galactic WC4–5, WC6–7 and WC8–9 stars, respectively.

#### 3.4 Line to bolometric luminosity ratio

In view of the range of properties of WR stars within different environments, one can compare the ratios of line to bolometric luminosities for WR stars whose physical properties have been determined from spectroscopic analysis. Results are primarily drawn from Hamann et al. (2019) and Sander et al. (2019) for Galactic WR stars, Hainich et al. (2014), Shenar et al. (2019), Aadland et al. (2022a), and Aadland et al. (2022b) for LMC WR stars, plus Hainich et al. (2015) and Shenar et al. (2016) for SMC WR stars. These are supplemented by studies of WO stars (Tramper et al. 2015) and very massive WNh and Of/WN stars in dense clusters (Crowther et al. 2010; Brands et al. 2022).

In Figure 6 we compare bolometric luminosities to the ratio of He II  $\lambda 4686$  line to bolometric luminosity for Milky Way, LMC and SMC WN, WN/C and Of/WN stars, with average values provided in Table 2. This reinforces the difference in line strength of He II  $\lambda 4686$  between strong and weak-lined WN stars in view of their comparable bolometric luminosities, since  $\log L_{\text{HeII} 4686}/L_{\text{Bol}} = -3.0^{+0.1}_{-0.3}$  for strong-lined WN stars, whereas  $\log L_{\text{HeII} 4686}/L_{\text{Bol}} = -3.6^{+0.2}_{-0.9}$  for weak-lined WN2–5 stars, with the lowest ratio for LMC 170–2 (Neugent et al. 2017). The metallicity dependence for weak-lined early-type WN stars is also apparent (compare Milky Way and SMC stars).

The situation is less clear for weak-lined WN6–8 stars, since Milky Way and Magellanic Cloud stars are broadly similar in their ratios of line to bolometric luminosities,  $\log L_{\text{HeII} 4686}/L_{\text{Bol}} = -3.4^{+0.2}_{-0.2}$ . WN9–11 stars universally exhibit very low ratios (e.g. WR31a, Smith et al. 1994) with  $\log L_{\text{HeII} 4686}/L_{\text{Bol}} = -4.0^{+0.3}_{-0.5}$ . Figure 6 also reveals a low line to bolometric luminosity ratio for BAT99–111 (R136b) which has previously been classified O4 If/WN8 (Crowther et al. 2016) although WN8 is preferred on the basis of its H $\beta$  morphology from MUSE/NFM observations (Crowther & Walborn 2011; Castro et al. 2021). Bolometric luminosities of WN5–7h stars are high in both galaxies, with  $\log L/L_{\text{Bol}} = 6.3 \pm 0.2$  and  $6.5 \pm 0.2$  for the Milky Way and LMC respectively, with typical ratios of  $\log L_{\text{HeII} 4686}/L_{\text{Bol}} = -3.7^{+0.2}_{-0.3}$ , and ratios of line to bolometric luminosities for Of/WN stars somewhat lower still,  $\log L_{\text{HeII} 4686}/L_{\text{Bol}} = -4.3^{+0.2}_{-0.2}$ .

Figure 7 compares bolometric luminosities to the ratio of C IV  $\lambda\lambda 5801,12$  line to bolometric luminosity for Milky Way and Magellanic Cloud WC and WO stars, and bolometric luminosities to the ratio of O VI  $\lambda\lambda 3811,34$  line to bolometric luminosity for WO stars. Galactic WC4–5 stars reveal significantly higher ratios than WC8–9 stars, with intermediate ratios for most WC6–7 stars (WR39 is an notable outlier), and very high ratios for LMC WC4–5 stars. WO stars show a broad range of C IV  $\lambda\lambda 5801,12$  line ratios, some in common with WC4–5 stars (BAT99–123 and LH 41–1042) with others revealing far lower ratios (e.g. WR102 in Milky Way, LMC195–1 in LMC). Line ratios of O VI  $\lambda\lambda 3811,34$  to bolometric luminosity for WO stars suggest a weak metallicity dependence, with higher ratios for Milky Way stars than those in Magellanic Clouds.

#### 3.5 Templates

In addition to calibrations, we have produced WR emission line templates for each environment, although this is hindered by the variation in spectral coverage of individual datasets (Table 1), so stars with limited spectral coverage are generally excluded. We have degraded composite spectra to a resolution of 10Å, and produced continuum-subtracted templates based on single WR stars and all (single and binary) WR stars, since the latter are often contaminated by (Balmer) absorption lines from companion OB stars. Templates incorporate velocity corrections of 284 km s $^{-1}$  and 162 km s $^{-1}$  for the LMC and SMC, respectively (Tully et al. 2016). Templates generally correct for atmospheric telluric effects, but no adjustment for interstellar atomic features (Ca II H&K, Na I D) lines or diffuse interstellar bands (e.g.  $\lambda 4430$ ) is made.

Fig. B1 presents templates for Galactic, LMC and SMC early-type WN stars from single and combined (single and binary) samples, separated into weak and strong lined subsets. Aside from He II  $\lambda 4686$ , the strongest feature in metal-rich early-type WN stars is N IV  $\lambda\lambda 3478, 85$  followed by He II  $\lambda 5412, \lambda 6560$  and the complex involving N IV  $\lambda 4058$ , He II  $\lambda 4100$ , Si IV  $\lambda\lambda 4088, 4116$  and N III  $\lambda\lambda 4097, 4103$ . C IV  $\lambda\lambda 5801,12$  is present, though relatively weak, in Galactic and LMC early-type WN stars.

Fig. B2 presents templates for Galactic, LMC and SMC late-type WN stars, separated into classical (WN6–8) and main-sequence H-rich (WN5–7h) subsets. The scarcity of LMC main-sequence WN stars required the use of 30 Doradus MUSE datasets (Castro et al. 2018) which exclude the spectral region shortward of  $\lambda 4600$ . He II  $\lambda 4686$  aside, the strongest stellar features in WN6–8 stars include N IV  $\lambda\lambda 3478, 85$ , the  $\lambda 4100$  complex, N III  $\lambda\lambda 4634, 41$ , plus H $\alpha$ , H $\beta$  and He I  $\lambda 5876$  in the Milky Way. The change in N III  $\lambda\lambda 4634, 41$ /He II  $\lambda 4686$  ratio from high to low metallicity is apparent. H-rich main sequence WN5–7h stars resemble WN6–8 stars aside from the relative

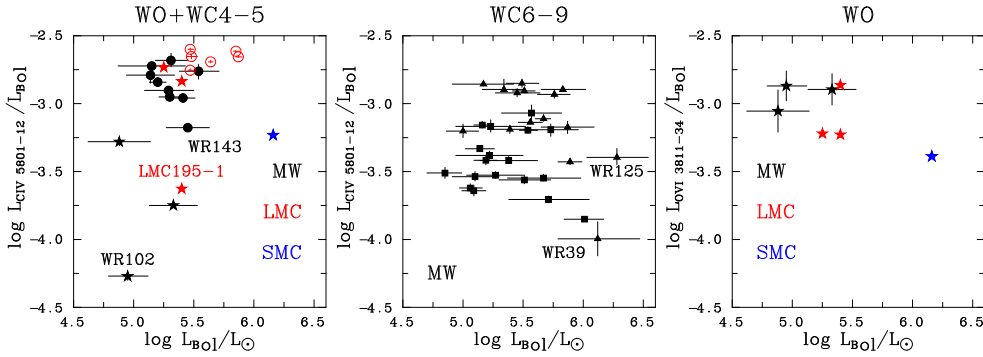


**Figure 7.** (left) Bolometric luminosity versus ratio of C IV  $\lambda\lambda 5801,12$  line to bolometric luminosity for WO and WC4–5 stars; (centre) Bolometric luminosity versus ratio of C IV  $\lambda\lambda 5801,12$  line to bolometric luminosity for WC6–7 (triangles) and WC8–9 (squares) stars; (right) Bolometric luminosity versus ratio of O VI  $\lambda\lambda 3811,34$  line to bolometric luminosity for WO stars. Symbols as in Figure 4

strength of N IV  $\lambda 4058$ , weakness of N III  $\lambda\lambda 4634,41$ , plus He I lines and higher  $\lambda 4686$  FWHM (Fig. 2).

Fig. B3 presents templates for Of/WN and WN9–11 stars in the Milky Way and LMC. Of/WN stars reveal weak, narrow He II  $\lambda 4686$  emission, plus N IV  $\lambda 4058$  and H $\alpha$ , with the upper Balmer series in absorption. WN9–11 stars also exhibit weak, narrow weak He II  $\lambda 4686$  emission, with either the N III  $\lambda\lambda 4634,41$  triplet or N II  $\lambda\lambda 4601,43$  multiplet prominent and strong Balmer and He I emission lines. Guseva et al. (2000) have highlighted N III  $\lambda\lambda 4512,48$  and Si III  $\lambda\lambda 4554,76$  from late WN stars in WR galaxies. Such features are present in late WN stars, albeit with the  $\lambda 4100$  complex and N III  $\lambda\lambda 4634,41$ /N II  $\lambda 4601,43$  more prominent.

Fig. B4 presents templates for Galactic and LMC WN/C stars, separated into early and late-type categories. Early subtypes are dominated by C IV  $\lambda\lambda 5801,12$  plus the blend of C III  $\lambda\lambda 4647,51$  and He II  $\lambda 4686$ , while the latter dominates late WN/C subtypes. C III  $\lambda 5696$  is present, albeit weakly in late WN/C templates. We combine Galactic and LMC WN/C stars to construct templates, noting that some exhibit strong C III  $\lambda 4647,51$  (e.g. WR26, WR126), while this feature is absent in others (e.g. WR58, BAT99-36, BAT99-88) such that spectroscopy of C IV  $\lambda 5801,12$  is essential in discriminating between WN and WN/C stars.

Fig. B5 presents templates for Galactic WC4–5, WC6–7 and WC8–9 stars from single and combined (single plus binary) samples. C III  $\lambda\lambda 4647,51$  (plus He II  $\lambda 4686$ ) dominates the blue WR bump for all subtypes, while the transition from C IV  $\lambda 5801,12$  to C III  $\lambda 5696$  in the yellow from early to late subtypes is apparent, with O IV  $\lambda\lambda 3403,13$  prominent in WC4–7 stars. At late subtypes, C II  $\lambda\lambda 6559,81, \lambda\lambda 7231,7$  are particularly strong in the red. The forest of blue features in WC8–9 stars primarily involve C II–III (Crowther et al. 2006b).

The upper panel of Fig. B6 presents templates of LMC WC4–5 emission lines. Aside from C III  $\lambda 4647–51$ +He II  $\lambda 4686$  and C IV  $\lambda\lambda 5801,12$ , O IV  $\lambda\lambda 3403,13$  is also prominent, in common with Milky Way counterparts. The lower panel presents templates of our combined WO sample, incorporating Milky Way, LMC and SMC stars, highlighting the defining O VI  $\lambda\lambda 3811,34$  feature, together with prominent O IV  $\lambda\lambda 3403,13$ , C IV  $\lambda 4658$ +He II  $\lambda 4686$  and C IV  $\lambda 5801,12$ . Comparing WO and LMC WC4–5 stars, the average O VI  $\lambda\lambda 3811,34$  line luminosity is factor of  $\sim 4$  stronger in the former group, while C III  $\lambda 4647,51$ +C IV  $\lambda 4658$ +He II  $\lambda 4686$  and C IV  $\lambda 5801,12$  are 4–8 times weaker (Table 6).

### 3.6 Cumulative WR line luminosities

Armed with line luminosities for a large subset of (optically detected) WR stars in the Milky Way and Magellanic Clouds we can also consider their cumulative blue and yellow line luminosities, and

contributions from different WR populations. Our sample includes all known WR stars in the SMC, 66% of the WR population in the LMC (Neugent et al. 2018)<sup>6</sup>, though only  $\sim 7\%$  of the estimated Milky Way population ( $N=1900\pm 250$ , Rosslowe & Crowther 2015). 18% of the LMC population are carbon or oxygen sequence WR stars, whereas these comprise 21% of our sample. In the Milky Way carbon and oxygen sequence stars represent 42% of the known population, in close agreement with our dataset<sup>7</sup>.

Table 7 summarises cumulative blue and yellow WR line luminosities from our current dataset in the Milky Way, LMC and SMC. As expected, WC and WO stars dominate the integrated C IV  $\lambda\lambda 5801,12$  line luminosity in all environments, but also contribute significantly to the blue feature: 58% in the Galaxy, 49% in the LMC and 23% in the SMC, for the samples included. AB5 (HD 5980) alone contributes half of the integrated blue WR bump of the SMC. If we utilise our LMC calibrations for the remainder of the known WR population, we estimate total blue and yellow line luminosities of  $2.6\times 10^{38}$  erg s $^{-1}$  (51% from WN, Of/WN and WN/C stars, 49% from WC and WO stars) and  $8.8\times 10^{37}$  erg s $^{-1}$  (8% from WN, Of/WN and WN/C stars, 92% from WC and WO stars), respectively. The fractional contributions from WN and WC stars are not affected because the overwhelming majority of omitted nitrogen-sequence stars possess weak lines (weak-lined WNE, WN10–11, Of/WN and LMC 170–2 type).

Accounting for line luminosities of all known WR stars in the Milky Way, we obtain cumulative blue and C IV  $\lambda 5801,12$  line luminosities of  $1.2\times 10^{39}$  erg s $^{-1}$  and  $2.7\times 10^{38}$  erg s $^{-1}$ , respectively. If these are representative of the total ( $\sim 1900$ ) the blue ( $3.6\times 10^{39}$  erg s $^{-1}$ ) and yellow ( $7.7\times 10^{38}$  erg s $^{-1}$ ) sum is an order of magnitude higher than the LMC. This is reasonable, given their relative star-formation rates of  $1.9 M_\odot \text{yr}^{-1}$  (Chomiuk & Povich 2011) and  $0.25 M_\odot \text{yr}^{-1}$  (Kennicutt et al. 2008), respectively, and environmental differences in WR line luminosities.

The fractional contribution to the cumulative WR bumps are further highlighted in Fig. 8 which provides the integrated line spectrum of 102 Galactic stars (upper panel), 80 LMC stars (middle panel) and 10 SMC stars (lower panel). The integrated Milky Way template highlights that strong lined and late-type WN stars are the primary contributors to He II  $\lambda 4686$ , WC4–7, WC8–9 and late-type WN subtypes dominating the  $\lambda 4650$  feature, and WC4–7 and WC8–9 subtypes dominating C IV  $\lambda 5801,12$  and C III  $\lambda 5696$  respectively. Sim-

<sup>6</sup> The global WR population of the LMC is 153, following Neugent et al. (2018) after including the WN8 star BAT99-111 (R136b), excluding two Of stars (Mk 42, LH 99-3), and noting that their catalogue entry 125 is Mk 37 rather than Mk 30 (also listed as entry 129).

<sup>7</sup> 275 WC or WO stars from a total of 667 stars according to v1.25 of the Galactic WR catalogue <https://pacrowther.staff.shef.ac.uk/WRcat>

**Table 7.** Cumulative blue and yellow line luminosities for our sample of WR systems in the Milky Way, LMC and SMC, with completeness fractions of ~7%, 66% and 100% (Rosslowe & Crowther 2015; Neugent et al. 2018). Systems involved WN+WN binaries (WR43A, BAT99-116, BAT199-118, AB5) are reflected in + statistics. WC and WO stars dominate the C IV  $\lambda\lambda 5801,12$  feature, and also contribute the majority of the integrated blue feature in Milky Way and LMC. AB5 (HD 5980) alone contributes half of the integrated blue WR bump of the SMC. We estimate total LMC (Milky Way) blue and yellow line luminosities of  $2.6 \times 10^{38}$  erg s $^{-1}$  ( $3.6 \times 10^{39}$  erg s $^{-1}$ ) and  $8.8 \times 10^{37}$  erg s $^{-1}$  ( $7.7 \times 10^{38}$  erg s $^{-1}$ ), respectively.

Galaxy	Milky Way			LMC			SMC			Milky Way			LMC			SMC					
	N	$\Sigma L$	erg s $^{-1}$	%	N	$\Sigma L$	erg s $^{-1}$	%	N	$\Sigma L$	erg s $^{-1}$	%	N	$\Sigma L$	erg s $^{-1}$	%	N	$\Sigma L$	erg s $^{-1}$	%	
Subtype	—— Blue bump (N III-v $\lambda\lambda 4603,41$ , C III $\lambda\lambda 4647,51$ , He II $\lambda 4686$ ) ——										—— Yellow bump (C IV $\lambda\lambda 5801,12$ ) ——										
WN3–7s	12	$3.1 \times 10^{37}$	12		18	$2.1 \times 10^{37}$	10		.	...	...		12	$1.4 \times 10^{36}$	2	18	$0.9 \times 10^{36}$	1	.	...	...
WN2–5w	22	$1.4 \times 10^{37}$	5		24	$0.9 \times 10^{37}$	5		9	$1.7 \times 10^{36}$	18		19	$0.6 \times 10^{36}$	1	22	$0.3 \times 10^{36}$	0	7	$0.1 \times 10^{35}$	0
WN6–11	29	$3.9 \times 10^{37}$	15		21+1	$4.2 \times 10^{37}$	21		2+1	$5.6 \times 10^{36}$	59		25	$0.5 \times 10^{36}$	1	15+1	$1.0 \times 10^{36}$	1	2+1	$2.2 \times 10^{35}$	6
WN5–7h*	9+1	$1.3 \times 10^{37}$	5		14+1	$3.0 \times 10^{37}$	15		.	...	...		6+1	$0.1 \times 10^{36}$	0	13+1	$1.0 \times 10^{36}$	1	.	...	...
WN/C	7	$1.4 \times 10^{37}$	5		2	$0.2 \times 10^{37}$	1		.	...	...		7	$5.9 \times 10^{36}$	10	2	$2.7 \times 10^{36}$	4	.	...	...
WC4–5	11	$3.4 \times 10^{37}$	13		18	$9.7 \times 10^{37}$	48		.	...	...		11	$14.7 \times 10^{36}$	24	17	$61.5 \times 10^{36}$	88	.	...	...
WC6–9	39	$12.0 \times 10^{37}$	45		.	...	...		.	...	...		39	$36.1 \times 10^{36}$	59	.	...	...	.	...	...
WO	4	$0.1 \times 10^{37}$	0		3	$0.2 \times 10^{37}$	1		1	$2.2 \times 10^{36}$	23		4	$1.2 \times 10^{36}$	2	3	$2.9 \times 10^{36}$	4	1	$32.9 \times 10^{35}$	93
Total	133+1	$26.7 \times 10^{37}$	100		100+2	$20.4 \times 10^{37}$	100		12+1	$9.5 \times 10^{36}$	100		123+1	$60.4 \times 10^{36}$	100	91+2	$70.2 \times 10^{36}$	100	10+1	$35.2 \times 10^{35}$	100

\* incl. Of/WN stars.

ilar results are obtained for the LMC, aside from the lack of WC6–9 stars, while the cumulative SMC bumps are dominated by late-type WN stars (primarily AB5) and the WO star AB8. Fig. 8 is reminiscent of WR bumps observed in star-forming galaxies (Vacca & Conti 1992; Schaerer et al. 1999; Brinchmann et al. 2008; Senchyna et al. 2021), but serves as a caution to approximating Wolf-Rayet populations by restricted WC and WN flavours, which additional (violet or red) WR diagnostics would help discriminate.

#### 4 APPLICATIONS

We now undertake analysis of two WR galaxies with our revised line luminosity calibration, selected at low and high metallicities. Historically, two methods have been employed to quantify the number of WR stars from optical emission line bumps, gaussian fits to emission lines calibrated with reference line luminosities or template fitting. The former approach is more straightforward, but discards line profile information and may result in unphysical solutions through independent solutions to blue and red bumps. The latter approach incorporates line profile information but may involve templates ill suited to the host galaxy metallicity. Here we apply both approaches to our selected WR galaxies.

##### 4.1 NGC 3049 (Mrk 710)

Our high metallicity target, NGC 3049 is a barred spiral at a distance of 19.3 Mpc (Tully et al. 2013) which was identified as a WR galaxy by Kunth & Schild (1986). WR populations of NGC 3049 have been studied using ESO 2.2m/EFOSC2 (Schaerer et al. 1999) and HST/STIS (González Delgado et al. 2002), and exhibits broad emission at N III  $\lambda\lambda 4634,41$ /C III  $\lambda\lambda 4647,51$ , He II  $\lambda 4686$ , C III  $\lambda 5696$  and C IV  $\lambda\lambda 5801,12$ . NGC 3049 is unusual in the  $\lambda 4634,41$  feature being comparable in strength to He II  $\lambda 4686$  (see Schmutz & Vacca 1999). Fig. 9 (left panels) presents de-reddened, velocity corrected WR bumps including gaussian fits to stellar and nebular emission lines. Table 8 provides a summary of nebular and stellar line luminosities in NGC 3049, remeasured from EFOSC observations which provides a spectral coverage of 4370–6550Å at a resolving power of  $R \sim 750$  (Schaerer et al. 1999). The spectroscopic L(H $\beta$ ) corresponds

**Table 8.** Line luminosities of selected nebular and stellar emission lines in NGC 3049 (Schaerer et al. 1999) based on  $c(\text{H}\beta)=0.22$ , a distance of 19.3 Mpc and Milky Way calibrations from this study. Results in parenthesis are from Galactic template fits.

Line	FWHM km s $^{-1}$	$F_\lambda$ $10^{-15}$ erg s $^{-1}$ cm $^{-2}$	$I_\lambda$ $10^{-15}$ erg s $^{-1}$ cm $^{-2}$	$L_\lambda$ $10^{37}$ erg s $^{-1}$	N(WR)
C III $\lambda\lambda 4647,51$	$3300 \pm 800$	$26.2 \pm 5.8$	$45.2 \pm 9.9$	$202 \pm 44$	
[Fe III] $\lambda 4658$	...	$1.3 \pm 1.1$	$2.3 \pm 2.1$	$10 \pm 9$	
He II $\lambda 4686$	$2200 \pm 600$	$13.0 \pm 4.9$	$21.9 \pm 8.2$	$98 \pm 37$	1300 WN6–8
H $\beta$	...	$98.9 \pm 1.2$	$169 \pm 2$	$755 \pm 9$	(750 WN2–8)
[O III] $\lambda 4959$	...	$11.8 \pm 0.5$	$19.8 \pm 0.9$	$88 \pm 4$	
[O III] $\lambda 5007$	...	$36.2 \pm 0.7$	$60.6 \pm 1.1$	$271 \pm 5$	
C III $\lambda 5696$	$2100 \pm 500$	$1.9 \pm 0.5$	$2.7 \pm 0.7$	$12 \pm 3$	
[N II] $\lambda 5755$	...	$0.9 \pm 0.2$	$1.3 \pm 0.3$	$6 \pm 1$	
C IV $\lambda\lambda 5801,12$	$2700 \pm 300$	$6.5 \pm 0.7$	$9.6 \pm 1.0$	$43 \pm 5$	380 WC6–7
He I $\lambda 5876$	...	$11.9 \pm 0.2$	$18.1 \pm 0.3$	$81 \pm 1$	(260 WC4–7)

to an ionizing output of  $Q_H = 1.6 \times 10^{52}$  ph s $^{-1}$ , comparable to 30 Doradus in the LMC, although the integrated output is likely to be considerably higher.

Strong line calibrations indicate NGC 3049 is supersolar ( $\log \text{O/H} + 12 \geq 8.9$ , Guseva et al. 2000) so we apply Galactic calibrations to estimate its WR populations. The C IV  $\lambda\lambda 5801,12$  to C III  $\lambda 5696$  ratio suggest a dominant WC6–7 subclass, requiring 380 WC stars. The contribution from WC6–7 stars to the He II  $\lambda 4686$  is considered to be negligible, so we adopt a WN6–8 population of  $\sim 1300$ .

Fig. 9 (right panels) present continuum subtracted line luminosities of blue and yellow WR bumps in NGC 3049, together with emission line templates for Milky Way WN (red) and WC (blue) stars, plus their sum (pink). For the yellow bump we prefer a reduced WC4–7 content of 260 stars in order to reproduce the C IV  $\lambda\lambda 5801,12$  and C III  $\lambda 5696$  emission line, whose FWHM is well reproduced (we adopt a similar mix of WC4–5 and WC6–7 stars to the Milky Way sample i.e. 1:3). For the blue bump, N V  $\lambda 4634–20$  is not apparent, but we adhere to a mix of WNEw:WN3–7s:WN6–8 stars corresponding to the Milky Way (1:1:3), requiring  $\sim 750$  stars to reproduce the He II  $\lambda 4686$  line, accounting for the contribution of WC stars to this

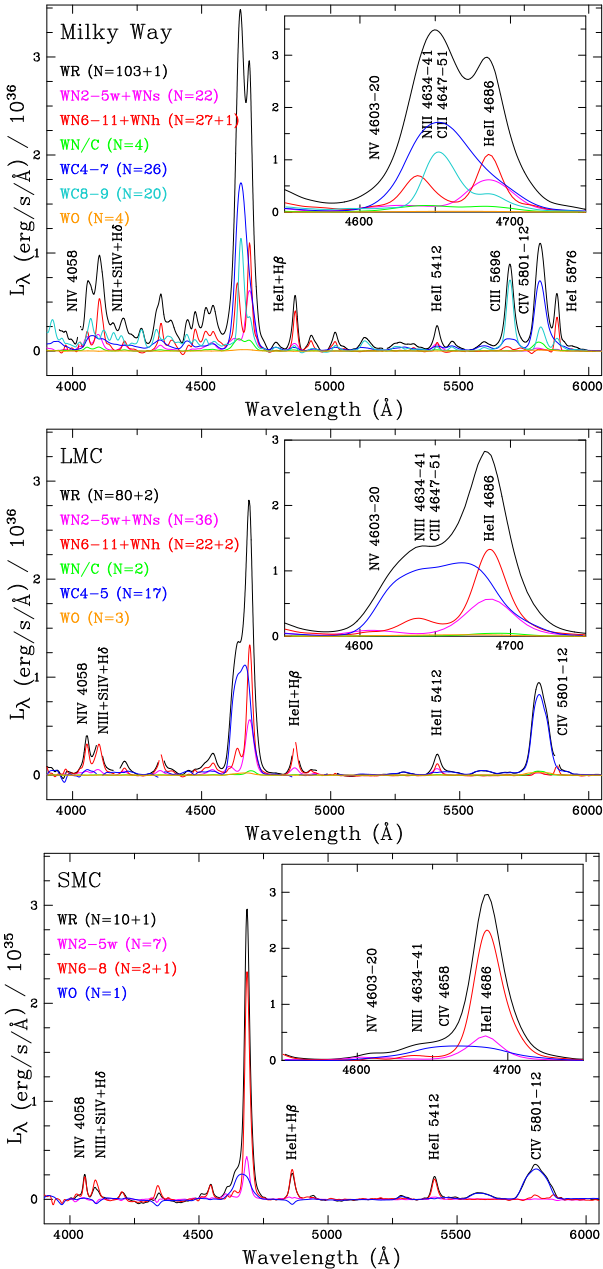


**Figure 8.** (Top): Cumulative  $\lambda\lambda 3950$ – $6050$  emission line spectrum of 103+1 Milky Way WR stars (black) together, plus inset for the blue WR bump, including contributions from WN2–5w+WN3–7s ( $N=22$ ), WN6–11+WNh ( $N=27+1$ ), WN/C ( $N=4$ ), WC4–7 ( $N=26$ ), WC8–9 ( $N=20$ ) and WO ( $N=4$ ) stars, indicating the primary contributors to the blue and yellow WR bumps. The global Milky Way WR line luminosity is estimated to be a factor of  $\sim 13$  times higher than presented here based on the known WR subtype distribution; (Middle): As above, for 80+2 LMC WR stars (black), highlighting contributions from WN2–5w+WN3–7s ( $N=36$ ), WNL+WNh ( $N=22+2$ ), WN/C ( $N=2$ ), WC4–5 ( $N=17$ ) and WO ( $N=3$ ) stars. The global LMC WR line luminosity is estimated to be  $\sim 25\%$  higher than presented here, accounting for incompleteness; (bottom): As above for 10+1 SMC WR stars (black), highlighting contributions from WNE ( $N=7$ ), WNL ( $N=2+1$ ) and WO ( $N=1$ ) stars. The global SMC WR line luminosity is estimated to be a few percent higher than presented here, owing to the omission of two WN2–5w stars.

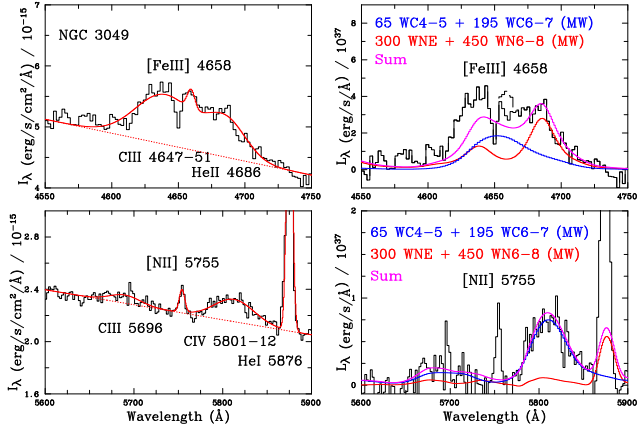


**Figure 9.** Left panels: De-reddened, velocity corrected, blue and yellow WR bumps in NGC 3049 from Schaerer et al. (1999), including gaussian fits (red) to broad (C III  $\lambda\lambda 4647,51$ , He II  $\lambda 4686$ , C III  $\lambda 5696$ , C IV  $\lambda\lambda 5801,12$ ) and nebular ([Fe III]  $\lambda 4658$ , [N II]  $\lambda 5755$ , He I  $\lambda 5876$ ) lines, with the continuum indicated as dotted lines.  $\sim 1300$  WN6–8 and  $\sim 380$  WC6–7 stars are estimated from Galactic calibrations, adopting a distance of 19.3 Mpc. Right panels: Continuum subtracted luminosities of blue and yellow WR bumps in NGC 3049 (black, nebular [Fe III] component indicated in dashed lines) plus composite template fits adopting 750 Milky Way WN stars (red, distributed 1:1:3 between WN2–5w:WN3–7s:WN6–8 stars as observed in the Milky Way), 260 Milky Way WC4–7 stars (blue, distributed between WC4–5 and WC6–7 stars as observed in the Milky Way) plus their sum (pink). Nebular [N II]  $\lambda 5755$  and He I  $\lambda 5876$  are not reproduced by the stellar WR templates. The poor match to the  $\lambda 4640$ – $4650$  blend may arise from the use of solar metallicity WN6–8 stars (NGC 3049 is considered to be supersolar).

region. The combination of N III  $\lambda\lambda 4634,41$  (from WN6–8 stars) and C III  $\lambda\lambda 4647,51$  (from WC4–7 stars) reproduce the majority of the blue bump reasonably well. The residual mismatch likely arises from stronger N III/He II is observed to scale with metallicity (recall Fig. 3) and NGC 3049 is likely supersolar. C III  $\lambda 5696$  is reasonably well matched, and includes modest contributions from WN6–8 stars via N IV  $\lambda 5737$ /Si III  $\lambda 5740$  and the N II  $\lambda 5680$  multiplet (note also nebular [N II]  $\lambda 5755$ ). The use of empirical templates requires fewer WR stars, owing to the contribution of WN stars to the yellow bump, and WC stars to the blue bump, which are usually not accounted for, and suggests a WN to WC ratio of  $\sim 3$ .

## 4.2 IC 4870 (ESO 105–IG 011)

Our low metallicity target IC 4870 is a nearby barred irregular galaxy at a distance of 8.5 Mpc (Tully et al. 2013) which was identified as a WR galaxy by Joguet et al. (2001). Spectroscopy reported by Joguet et al. (2001) focus on the blue WR bump, so we have utilised archival NTT/EMMI spectroscopy from May 1999 (PA = 0,  $T_{\text{exp}} = 600$  s). Grism #5 and a 1 arcsec slit provided a spectral coverage of 3975–6685 Å at a resolving power of  $R = 1000$ – $1300$ . The brightest knot reveals a strong emission line spectrum, including broad C III  $\lambda 4647$ – $51$ /C IV  $\lambda 4658$ , He II  $\lambda 4686$  and C IV  $\lambda\lambda 5801,12$ , plus extended nebular emission. After standard reduction techniques, including flux calibration, we obtained  $c(\text{H}\beta)=0.19$  from the observed flux ratio  $F(\text{H}\alpha)/F(\text{H}\beta) = 3.37$ . Since the spectral coverage does not extend to [O II]  $\lambda 3727$ , we are unable to determine a direct oxygen abundance, but strong line calibrations (N2, O3N2, Pettini & Pagel 2004) indicate IC 4870 is metal-poor ( $\log \text{O/H} + 12 \sim 7.9$ , or  $1/6 Z_\odot$ ), which is supported by the high electron temperature of  $T_e = 13.7$  kK obtained from [O III]  $\lambda 4363/5007$ .

**Table 9.** Line luminosities of selected emission lines in IC 4870 from gaussian fits, based on  $c(\text{H}\beta)=0.18$ , a distance of 8.5 Mpc and calibrations from this study. Separate nebular (n) and broad (b) entries are provided for He II  $\lambda\lambda 4686$ . Calibrations are from SMC (WN6–8) and LMC (WC4–5) samples, while results shown in parenthesis arise from LMC (WC) and SMC (WN) template fits.

Line	FWHM km s <sup>-1</sup>	$F_\lambda$ $10^{-15}$ erg s <sup>-1</sup> cm <sup>-2</sup>	$I_\lambda$ $10^{-15}$ erg s <sup>-1</sup> cm <sup>-2</sup>	$L_\lambda$ $10^{37}$ erg s <sup>-1</sup>	N(WR)
H $\delta$	...	13.5±0.2	22.5±0.4	19.5±0.3	
H $\gamma$	...	23.2±0.2	37.8±0.4	32.8±0.3	
[O III] $\lambda\lambda 4363$	...	4.5±0.2	7.2±0.3	6.3±0.3	
He I $\lambda\lambda 4471$	...	2.1±0.2	3.4±0.3	2.9±0.3	
C III $\lambda\lambda 4647,51$	5700±2200	7.0±3.2	10.8±4.8	9.0±4.0	
He II $\lambda\lambda 4686$ (b)	1300±300	5.4±0.9	8.5±1.4	7.3±1.2	47 WN6–8
He II $\lambda\lambda 4686$ (n)	...	0.8±0.4	1.3±0.6	1.1±0.5	(120 WN2–8)
[Ar IV] $\lambda\lambda 4711$	...	1.0±0.3	1.5±0.5	1.4±0.3	
H $\beta$	...	51.0±0.3	78.6±0.5	68.1±0.4	
[O III] $\lambda\lambda 4959$	...	114 ±2	174 ±4	151 ±3	
[O III] $\lambda\lambda 5007$	...	339 ±3	515 ±4	446 ±3	
C IV $\lambda\lambda 5801,12$	4300±200	7.3±0.5	10.3±0.7	8.9±0.6	26 WC4–5
He I $\lambda\lambda 5876$	...	6.6±0.1	9.3±0.1	8.1±0.1	(22 WC4–5)
H $\alpha$	...	172 ±1	231 ±2	200 ±2	
[N II] $\lambda\lambda 6584$	...	2.7±1.1	3.6±1.5	3.1±1.3	

Fig. 10 (left panels) presents de-reddened, velocity corrected WR bumps including gaussian fits to stellar and nebular emission lines. Fluxes of selected nebular and stellar emission lines in IC 4870 measured from fits are presented in Table 9. He II  $\lambda\lambda 4686$  comprises both stellar (86%) and nebular (14%) components, with a nebular He II  $\lambda\lambda 4686$ /H $\beta$  intensity ratio of 2%. Indeed, Jouquet et al. (2001) attribute 16% of the He II  $\lambda\lambda 4686$  to nebular origin in their higher resolution 1.5m ESO Boller & Chivens spectroscopy of IC 4870 ( $R = 2100$  at  $\lambda\lambda 4686$ ). The spectroscopic H $\alpha$  luminosity corresponds to an ionizing output of  $Q_H = 1.5 \times 10^{51} \text{ ph s}^{-1}$ , typical of nearby giant H II regions (e.g. NGC 595 in M33), although the integrated ionizing output is likely to be significantly larger. The yellow C IV  $\lambda\lambda 5801,12$  feature is very broad, exceeding the average value of LMC WC4–5 stars (Table 4).

Ideally one would apply SMC-metallicity calibrations to IC 4870, but since WC stars are not observed in the SMC we revert to LMC calibrations, allowing us to estimate a population of ∼26 WC4–5 stars in IC 4870 from the yellow bump. FWHM(He II  $\lambda\lambda 4686$ ) is intermediate between early and late WN subtypes (Table 2), so we apply a SMC WN6–8 (WN2–5w) calibration to estimate a population of 47 (440) stars, excluding the nebular component. At SMC metallicity, N III  $\lambda\lambda 4634,41$ /He II  $\lambda\lambda 4686 \sim 0.04$ , so accounting for this modest contribution to the broad C III  $\lambda\lambda 4647,51$  feature, we can estimate the number of WC4–5 stars from this diagnostic, again based on LMC calibrations. We estimate a slightly lower population of 19 WC4–5 stars from the blue bump.

Fig. 10 (right panels) present continuum subtracted line luminosities of blue and yellow WR bumps in IC 4870, together with emission line templates for WN and WC stars, plus their sums (pink). For the yellow WR bump, 22 (LMC) WC4–5 stars provide a satisfactory match to the broad C IV  $\lambda\lambda 5801,12$  emission line, with negligible contribution from WN stars. For the blue bump, a mix of early and late WN stars are more plausible than a purely early or late WN population, recalling the WNE:WNL ratio is 2 (LMC) to 3 (SMC) in local metal-poor galaxies. Consequently we adopt a ratio of 3:1 for the WN2–5w:WN6–8 population in IC 4870, with both comprising

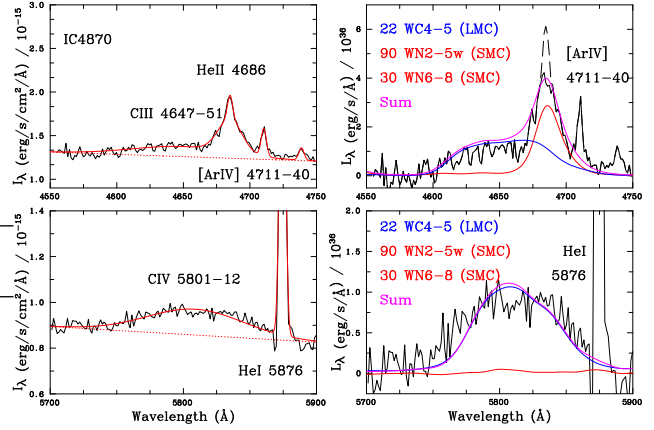


**Figure 10.** Left panels: De-reddened, velocity corrected, blue and yellow WR bumps in IC 4870 (black), including gaussian fits (red) to broad (C III  $\lambda\lambda 4647,51$ , He II  $\lambda\lambda 4686$ , C IV  $\lambda\lambda 5801,12$ ) and nebular ([Ar IV]  $\lambda\lambda 4711,40$ , He I  $\lambda\lambda 5876$ ) lines, with the continuum indicated as dotted lines. ∼47 SMC WN6–8 and 26 LMC WC4–5 stars are estimated from calibrations, adopting a distance of 8.5 Mpc. Right panels: Continuum subtracted luminosities of blue and yellow WR bumps in IC 4870 (black, nebular He II  $\lambda\lambda 4686$  component indicated in dashed lines) plus template fits adopting 120 SMC WN stars (red), 22 LMC WC4–5 stars (blue) plus their sum (pink).

SMC templates. We require a total of 120 WN stars to reproduce the non-nebular He II  $\lambda\lambda 4686$  feature, accounting for the contribution of 22 WC4–5 stars, which also provide a satisfactory fit to C III  $\lambda\lambda 4647,51$ +C IV  $\lambda\lambda 4658$ .

Although there is no direct evidence supporting the presence of WN2–5w stars in IC 4870, they are capable of producing the observed nebular He II  $\lambda\lambda 4686$  emission, in contrast to WN6–8 or WC4–5 stars (Crowther & Hadfield 2006). The measured nebular He II  $\lambda\lambda 4686$  luminosity (Table 9) corresponds to an ionizing budget of  $Q(\text{He}^+) = 1.3 \times 10^{49} \text{ photon s}^{-1}$ , an order of magnitude higher than individual nebular He III  $\lambda\lambda 4686$  producing H II regions in Local Group galaxies (Garnett et al. 1991). Adopting  $Q(\text{He}^+)$  ionizing photons of SMC WN2–5w stars from Hainich et al. (2015), only ∼10 stars are required to produce sufficient ionizing photons in order to reproduce the observed nebular emission. Consequently only ∼10% of the inferred population would need to be located within H II regions to match observations. This more realistic WN population inferred for this metal poor galaxy produces a WN:WC ratio of ∼5.5:1, which is more plausible than 2:1 if solely WN6–8 and WC4–5 calibrations are adopted (Table 9). The modest He II  $\lambda\lambda 4686$  line luminosity of metal-poor WN2–5w stars would severely hinder their direct detection, so the spectroscopic absence of WR bumps in nebular  $\lambda\lambda 4686$  emitting galaxies does not necessarily exclude them from being responsible for the observed nebular emission (Schaerer 1996; Shirazi & Brinchmann 2012), although several alternative candidates exist (Götberg et al. 2019; Schaerer et al. 2019; Oskinova & Schaerer 2022).

## 5 OUTLOOK AND CONCLUSIONS

We report calibrations of line luminosities of optical emission lines of Galactic WR stars, greatly expanding on previous studies owing to the availability of *Gaia* DR3 parallaxes, and provide revised line luminosities for Magellanic Cloud counterparts, updated from previous calibrations (Smith et al. 1990a; Schaerer & Vacca 1998; Crowther & Hadfield 2006).

Overall we confirm previous results for a reduction in He II  $\lambda\lambda 4686$  line luminosity for early-type WN stars at low metallicity, providing separate calibrations for strong-lined and weak-lined stars. Sander et al. (2020) have investigated wind driving of WR stars, and establish a dependence on metallicity (Fe-group elements) and Edington parameter  $\Gamma_e$  ( $\propto L/M$ ) so strong-lined stars likely differ from weak-lined stars in their wind properties owing to their higher luminosity-to-mass ratios.

The situation is less clear for late-type WN stars since average line luminosities of LMC stars are higher than Galactic counterparts and one of the two late WN stars in the SMC is the complex multiple system HD 5980, whose primary potentially dominates the line emission (Hillier et al. 2019). This does not necessarily argue against a metallicity dependence of wind strengths since the lower (luminosity) threshold to the formation of WR stars increases at lower metallicity (Shenar et al. 2020), so reduced wind strengths at low metallicity are countered by a shift to higher stellar luminosities on average. We find very massive main-sequence stars in the Milky Way and LMC possess similar He II  $\lambda\lambda 4686$  line luminosities to classical late WN stars, albeit with broader lines plus weaker N III  $\lambda\lambda 4634,41$  and He I  $\lambda\lambda 5876$  lines. C IV  $\lambda\lambda 5801,12$  is an order of magnitude weaker than the blue bump in early WN stars, and is weaker still in late subtypes, though has comparable strength in WN/C subtypes.

LMC WC4–5 stars possess higher C IV  $\lambda\lambda 5801,12$  line luminosities than Galactic counterparts, while we provide the first calibration of line luminosities for WC6–7 and WC8–9 stars based on large samples. C III  $\lambda\lambda 4647,51$ +He II  $\lambda\lambda 4686$  is strong for all WC subtypes, with C III  $\lambda\lambda 5696$  is the dominant emission line in the yellow region for WC9 stars. The blue WC bump is well correlated with C IV  $\lambda\lambda 5801,12$  in all subtypes. We also provide line luminosities of O VI  $\lambda\lambda 3811,34$  in WO stars, plus other prominent lines (O IV  $\lambda\lambda 3403,13$ , C IV  $\lambda\lambda 4658$ +He II  $\lambda\lambda 4686$ , C IV  $\lambda\lambda 5801,12$ ). We also utilise spectroscopic studies to quantify the line to bolometric luminosity ratios for each spectral type, which ranges from  $L_{\text{HeII} 4686}/L_{\text{Bol}} = 3 \times 10^{-5}$  for SMC WNEW stars, to  $L_{\text{CIV} 5801,12}/L_{\text{Bol}} = 2 \times 10^{-3}$  for LMC WC4–5 stars.

Figures 2 and 4 emphasise the diversity in line luminosities within our various WR categories, so average properties should be used with caution. For example, Littlefield et al. (2012) have presented optical line fluxes of WR142–1 (WN6w) from Hobby–Eberly Telescope (HET) observations. Applying their derived extinction ( $A_V = 8.1^{+0.6}_{-0.7}$  mag) and the average He II  $\lambda\lambda 4686$  line luminosity of Galactic WN6–8 stars (Table 2) implies a distance of  $2.1^{+0.6}_{-0.9}$  kpc, whereas the *Gaia* DR3 distance to WR142–1 is  $1.58 \pm 0.05$  kpc.

Flux calibrated spectroscopy also permits us to produce templates for single and composite (single and binary) subtypes at each metallicity. We construct cumulative emission line luminosities for the Milky Way (~7% completeness), LMC (66% complete) and SMC (100% complete), with global blue WR line luminosities of  $\approx 3.7 \times 10^{39}$  erg s $^{-1}$ ,  $2.6 \times 10^{38}$  erg s $^{-1}$  and  $9.5 \times 10^{37}$  erg s $^{-1}$ , respectively. We also apply our templates to representative metal-poor (IC 4870) and metal-rich (NGC 3049) galaxies that exhibit strong WR bumps at optical wavelengths. Reasonable consistency is achieved, although templates are preferred since they exploit line profile information and incorporate contributions from WN stars to the yellow WR bump, and contributions from WC stars to the blue WR bump.

The prospect for additional empirical WR line luminosities is promising at high metallicity, thanks to large numbers of detections in M31 (Neugent & Massey 2019), while the situation is less satisfactory at low metallicity. IC10 has a relatively high star-formation rate, although it suffers from high foreground extinction and its metallicity

is close to that of the LMC (Tehrani et al. 2017). Other nearby dwarf galaxies suffer from very low star formation rates (Crowther 2019, their fig.11), so only a handful of WR stars are known in NGC 6822 and IC 1613 (Armandroff & Massey 1991). Consequently there is little alternative to the use of theoretical spectra below SMC metallicity, providing these are carefully calibrated against empirical results.

## ACKNOWLEDGEMENTS

PAC and JMB are supported by the Science and Technology Facilities Council research grant ST/V000853/1 (PI. V. Dhillon). Thanks to Bill Vacca for sharing his IRTF/SpeX dataset, Frank Tramper for providing his VLT/Xshooter spectra of WO stars, Nidia Morrell for sharing her Magellan/MagE spectrum of LMC 170–2, Paco Najarro for providing his VLT/Xshooter spectrum of VFTS 682, Gloria Koenigsberger for providing her HST/STIS spectra of HD 5980, and Daniel Schaefer for providing his flux calibrated ESO 2.2m EFOSC2 spectrum of NGC 3049.

This research has made extensive use of NASA’s Astrophysics Data System Bibliographic Services, and the SIMBAD database, operated at CDS, Strasbourg, France, plus the European Space Agency (ESA) *Gaia* archive whose website is <https://archives.esac.esa.int/gaia> and the ESO Science Archive Facility (IC 4870 was observed under programme 59.A-9004). The INES System has been developed by the ESA IUE Project at VILSPA. Data and access software are distributed and maintained by INTA through the INES Principal Centre at LAEFF. The Starlink software (Currie et al. 2014) is currently supported by the East Asian Observatory.

For the purpose of open access, the author has applied a Creative Commons Attribution (CC BY) license to any Author Accepted Manuscript version arising.

## DATA AVAILABILITY

Template continuum subtracted emission line spectra of Milky Way and Magellanic Cloud WR stars will be publicly available in a Zenodo collection upon publication (ascii format, wavelength units of Å, monochromatic luminosity units of erg s $^{-1}$  Å $^{-1}$ ) at [10.5281/zenodo.7573775](https://zenodo.10.5281/zenodo.7573775), separately for single and single+binary WN2–5w, WN3–7s, WN6–8, WN9–11, WN5–7h+Of/WN (main sequence), WN/C, WC4–5, WC6–7, WC8–9, WO stars.

## REFERENCES

- Aadland E., Massey P., Hillier D. J., Morrell N., 2022a, *ApJ*, **924**, 44
- Aadland E., Massey P., Hillier D. J., Morrell N. I., Neugent K. F., Eldridge J. J., 2022b, *ApJ*, **931**, 157
- Allen D. A., Wright A. E., Goss W. M., 1976, *MNRAS*, **177**, 91
- Armandroff T. E., Massey P., 1991, *AJ*, **102**, 927
- Bagnulo S., Jehin E., Ledoux C., Cabanac R., Melo C., Gilmozzi R., ESO Paranal Science Operations Team 2003, *The Messenger*, **114**, 10
- Bailer-Jones C. A. L., Rybizki J., Fouesneau M., Demleitner M., Andrae R., 2021, *AJ*, **161**, 147
- Bartzakos P., Moffat A. F. J., Niemela V. S., 2001, *MNRAS*, **324**, 18
- Bestenlehner J. M., 2020, *MNRAS*, **493**, 3938
- Bohannan B., Crowther P. A., 1999, *ApJ*, **511**, 374
- Borisov S., et al., 2022, arXiv e-prints, [p. arXiv:2211.09130](https://arxiv.org/abs/2211.09130)
- Brands S. A., et al., 2022, *A&A*, **663**, A36
- Brinchmann J., Kunth D., Durret F., 2008, *A&A*, **485**, 657
- Callingham J. R., Crowther P. A., Williams P. M., Tuthill P. G., Han Y., Pope B. J. S., Marcote B., 2020, *MNRAS*, **495**, 3323

- Castro N., Crowther P. A., Evans C. J., Mackey J., Castro-Rodriguez N., Vink J. S., Melnick J., Selman F., 2018, *A&A*, **614**, A147
- Castro N., et al., 2021, *The Messenger*, **182**, 50
- Chomiuk L., Povich M. S., 2011, *AJ*, **142**, 197
- Conti P. S., Massey P., 1989, *ApJ*, **337**, 251
- Crowther P. A., 1997, *MNRAS*, **290**, L59
- Crowther P. A., 2007, *ARA&A*, **45**, 177
- Crowther P. A., 2019, *Galaxies*, **7**, 88
- Crowther P. A., Hadfield L. J., 2006, *A&A*, **449**, 711
- Crowther P. A., Smith L. J., 1997, *A&A*, **320**, 500
- Crowther P. A., Walborn N. R., 2011, *MNRAS*, **416**, 1311
- Crowther P. A., Smith L. J., Hillier D. J., Schmutz W., 1995a, *A&A*, **293**, 427
- Crowther P. A., Smith L. J., Hillier D. J., 1995b, *A&A*, **302**, 457
- Crowther P. A., Smith L. J., Willis A. J., 1995c, *A&A*, **304**, 269
- Crowther P. A., Dessart L., Hillier D. J., Abbott J. B., Fullerton A. W., 2002, *A&A*, **392**, 653
- Crowther P. A., Hadfield L. J., Clark J. S., Negueruela I., Vacca W. D., 2006a, *MNRAS*, **372**, 1407
- Crowther P. A., Morris P. W., Smith J. D., 2006b, *ApJ*, **636**, 1033
- Crowther P. A., Schnurr O., Hirschi R., Yusof N., Parker R. J., Goodwin S. P., Kassim H. A., 2010, *MNRAS*, **408**, 731
- Crowther P. A., et al., 2016, *MNRAS*, **458**, 624
- Currie M. J., Berry D. S., Jenness T., Gibb A. G., Bell G. S., Draper P. W., 2014, in Manset N., Forshay P., eds, Astronomical Society of the Pacific Conference Series Vol. 485, Astronomical Data Analysis Software and Systems XXIII. p. 391
- de Kotter A., Heap S. R., Hubeny I., 1997, *ApJ*, **477**, 792
- Drew J. E., Monguió M., Wright N. J., 2021, *MNRAS*, **508**, 4952
- Eldridge J. J., Stanway E. R., Xiao L., McClelland L. A. S., Taylor G., Ng M., Greis S. M. L., Bray J. C., 2017, *Publ. Astron. Soc. Australia*, **34**, e058
- Fitzpatrick E. L., Massa D., Gordon K. D., Bohlén R., Clayton G. C., 2019, *ApJ*, **886**, 108
- Flagey N., Noriega-Crespo A., Petric A., Geballe T. R., 2014, *AJ*, **148**, 34
- Foellmi C., Moffat A. F. J., Guerrero M. A., 2003, *MNRAS*, **338**, 360
- Gaia Collaboration et al., 2021, *A&A*, **649**, A1
- Garnett D. R., Kennicutt Robert C. J., Chu Y.-H., Skillman E. D., 1991, *ApJ*, **373**, 458
- Gómez-González V. M. A., Mayya Y. D., Toalá J. A., Arthur S. J., Zaragoza-Cardiell J., Guerrero M. A., 2021, *MNRAS*, **500**, 2076
- González Delgado R. M., Leitherer C., Stasińska G., Heckman T. M., 2002, *ApJ*, **580**, 824
- Gordon K. D., Clayton G. C., Misselt K. A., Landolt A. U., Wolff M. J., 2003, *ApJ*, **594**, 279
- Götberg Y., de Mink S. E., Groh J. H., Leitherer C., Norman C., 2019, *A&A*, **629**, A134
- Graczyk D., et al., 2014, *ApJ*, **780**, 59
- Gräfener G., Koesterke L., Hamann W. R., 2002, *A&A*, **387**, 244
- Guseva N. G., Izotov Y. I., Thuan T. X., 2000, *ApJ*, **531**, 776
- Gvaramadze V. V., et al., 2009, *MNRAS*, **400**, 524
- Hainich R., et al., 2014, *A&A*, **565**, A27
- Hainich R., Pasemann D., Todt H., Shenar T., Sander A., Hamann W. R., 2015, *A&A*, **581**, A21
- Hamann W. R., Gräfener G., Liermann A., 2006, *A&A*, **457**, 1015
- Hamann W. R., et al., 2019, *A&A*, **625**, A57
- Hillier D. J., Koenigsberger G., Nazé Y., Morrell N., Barbá R. H., Gamen R., 2019, *MNRAS*, **486**, 725
- Howarth I. D., 1983, *MNRAS*, **203**, 301
- Howarth I. D., Murray J., Mills D., Berry D. S., 2004, Starlink User Note, **50**
- Joguet B., Kunth D., Melnick J., Terlevich R., Terlevich E., 2001, *A&A*, **380**, 19
- Kennicutt Robert C. J., Lee J. C., Funes J. G., J. S., Sakai S., Akiyama S., 2008, *ApJS*, **178**, 247
- Koenigsberger G., Morrell N., Hillier D. J., Gamen R., Schneider F. R. N., González-Jiménez N., Langer N., Barbá R., 2014, *AJ*, **148**, 62
- Koenigsberger G., Morrell N., Hillier D. J., Schmutz W., Gamen R., Arias J. I., Barbá R., Ferrero G., 2022, *Rev. Mex. Astron. Astrofis.*, **58**, 403
- Koesterke L., Hamann W. R., Schmutz W., Wessolowski U., 1991, *A&A*, **248**, 166
- Kunth D., Sargent W. L. W., 1981, *A&A*, **101**, L5
- Kunth D., Schild H., 1986, *A&A*, **169**, 71
- Leitherer C., Lee J. C., Faisst A., 2019, *AJ*, **158**, 192
- Lindgren L., et al., 2018, *A&A*, **616**, A2
- Lindgren L., et al., 2021, *A&A*, **649**, A4
- Littlefield C., Garnavich P., Marion G. H. H., Vinkó J., McClelland C., Rettig T., Wheeler J. C., 2012, *AJ*, **143**, 136
- López-Sánchez Á. R., Esteban C., 2010, *A&A*, **516**, A104
- Luehrs S., 1997, *PASP*, **109**, 504
- Maíz Apellániz J., 2022, *A&A*, **657**, A130
- Maíz Apellániz J., et al., 2014, *A&A*, **564**, A63
- Massey P., 1984, *ApJ*, **281**, 789
- Massey P., Hunter D. A., 1998, *ApJ*, **493**, 180
- Miralles-Caballero D., et al., 2016, *A&A*, **592**, A105
- Monreal-Ibero A., Walsh J. R., Iglesias-Páramo J., Sandin C., Relaño M., Pérez-Montero E., Vilchez J., 2017, *A&A*, **603**, A130
- Neugent K., Massey P., 2019, *Galaxies*, **7**, 74
- Neugent K. F., Massey P., Hillier D. J., Morrell N., 2017, *ApJ*, **841**, 20
- Neugent K. F., Massey P., Morrell N., 2018, *ApJ*, **863**, 181
- Nugis T., Lamers H. J. G. L. M., 2000, *A&A*, **360**, 227
- Oskinova L. M., Schaerer D., 2022, *A&A*, **661**, A67
- Pettini M., Pagel B. E. J., 2004, *MNRAS*, **348**, L59
- Pietrzyński G., et al., 2019, *Nature*, **567**, 200
- Rate G., Crowther P. A., 2020, *MNRAS*, **493**, 1512
- Rosslowe C. K., Crowther P. A., 2015, *MNRAS*, **447**, 2322
- Sander A., Hamann W. R., Todt H., 2012, *A&A*, **540**, A144
- Sander A. A. C., Hamann W. R., Todt H., Hainich R., Shenar T., Ramachandran V., Oskinova L. M., 2019, *A&A*, **621**, A92
- Sander A. A. C., Vink J. S., Hamann W. R., 2020, *MNRAS*, **491**, 4406
- Schaerer D., 1996, *ApJ*, **467**, L17
- Schaerer D., Vacca W. D., 1998, *ApJ*, **497**, 618
- Schaerer D., Contini T., Kunth D., 1999, *A&A*, **341**, 399
- Schaerer D., Fragos T., Izotov Y. I., 2019, *A&A*, **622**, L10
- Schmutz W., 1997, *A&A*, **321**, 268
- Schmutz W., Vacca W. D., 1999, *New Astron.*, **4**, 197
- Schnurr O., Casoli J., Chené A. N., Moffat A. F. J., St-Louis N., 2008, *MNRAS*, **389**, L38
- Seaton M. J., 1979, *MNRAS*, **187**, 73
- Senchyna P., Stark D. P., Charlot S., Chevallard J., Bruzual G., Vidal-García A., 2021, *MNRAS*, **503**, 6112
- Shenar T., et al., 2016, *A&A*, **591**, A22
- Shenar T., et al., 2019, *A&A*, **627**, A151
- Shenar T., Gilkis A., Vink J. S., Sana H., Sander A. A. C., 2020, *A&A*, **634**, A79
- Shenar T., et al., 2021, *A&A*, **650**, A147
- Shirazi M., Brinchmann J., 2012, *MNRAS*, **421**, 1043
- Sidoli F., Smith L. J., Crowther P. A., 2006, *MNRAS*, **370**, 799
- Smith L. F., Shara M. M., Moffat A. F. J., 1990a, *ApJ*, **348**, 471
- Smith L. F., Shara M. M., Moffat A. F. J., 1990b, *ApJ*, **358**, 229
- Smith L. J., Crowther P. A., Prinja R. K., 1994, *A&A*, **281**, 833
- Smith L. F., Shara M. M., Moffat A. F. J., 1996, *MNRAS*, **281**, 163
- Smith L. J., Norris R. P. F., Crowther P. A., 2002, *MNRAS*, **337**, 1309
- Tehrani K., Crowther P. A., Archer I., 2017, *MNRAS*, **472**, 4618
- Tehrani K. A., Crowther P. A., Bestenlehner J. M., Littlefair S. P., Pollock A. M. T., Parker R. J., Schnurr O., 2019, *MNRAS*, **484**, 2692
- Torres-Dodgen A. V., Massey P., 1988, *AJ*, **96**, 1076
- Tramper F., et al., 2015, *A&A*, **581**, A110
- Tully R. B., et al., 2013, *AJ*, **146**, 86
- Tully R. B., Courtois H. M., Sorce J. G., 2016, *AJ*, **152**, 50
- Vacca W. D., Conti P. S., 1992, *ApJ*, **401**, 543
- Walborn N. R., Drissen L., Parker J. W., Saha A., MacKenty J. W., White R. L., 1999, *AJ*, **118**, 1684

## APPENDIX A: LINE LUMINOSITIES OF GALACTIC AND MAGELLANIC CLOUD WR STARS

Line luminosities of individual Galactic and Magellanic Cloud WN+Of/WN, WN/WC, WC and WO stars are provided in Tables A1-A4, sorted by catalogue number (WR for Milky Way, BAT for LMC, AB for SMC). Optical datasets refer to Table 1, Galactic distances are from *Gaia* DR3 parallaxes (Gaia Collaboration et al. 2021), using zero point corrections from Lindegren et al. (2021) updated by Maíz Apellániz (2022), and the Bayesian methods set out in Rate & Crowther (2020), while Magellanic Cloud distances are from Pietrzyński et al. (2019) and Graczyk et al. (2014). References are provided for  $A_V$  (mag) and stellar luminosities ( $L_\odot$ ), with the latter adjusted to our adopted distances. Observed line fluxes, line luminosities and FWHM of He II  $\lambda 4686$  (for WN, WN/C, Of/WN stars) or C IV  $\lambda\lambda 5801,12$  are provided in  $\text{erg s}^{-1} \text{cm}^{-2}$ ,  $\text{erg s}^{-1}$  and  $\text{km s}^{-1}$ , the latter corrected for instrumental broadening. The He II  $\lambda 4686$  or C IV  $\lambda\lambda 5801,12$  line luminosity (in  $10^{-3} L_{\text{Bol}}$ ) is restricted to stars with a measured stellar luminosity, with other optical line luminosities provided with respect to He II  $\lambda 4686$  or C IV  $\lambda\lambda 5801,12$  (· · · refers to a lack of data). For WN and WN/C stars, aside from the blends at  $\lambda 4100$  and  $\lambda 4630$ , we have endeavoured to exclude the contribution of He I  $\lambda 7065$  and He II  $\lambda 7177$  to the N IV  $\lambda\lambda 7103,29$  multiplet. For early-type WC and WO stars, C IV  $\lambda 4658$  (6-5),  $\lambda 4686$  (8-6),  $\lambda 4689$  (11-7) will also contribute to the C III  $\lambda\lambda 4647,51$ +He II  $\lambda 4686$  blend.

**Table A1.** Luminosities of prominent optical emission lines of Galactic (WR), LMC (BAT99) and SMC (AB) WN stars, categorised as weak-lined early-type (WN2–5w), strong-lined (WN3–7s), late-type (WN6–8), very late-type (WN9–11) or (main sequence) very massive H-rich (WN5–7h) stars. He II  $\lambda$ 4686 FWHM are also provided in  $\text{km s}^{-1}$  ( $\pm 100 \text{ km s}^{-1}$ ). The feature at  $\lambda$ 4100 involves N III  $\lambda\lambda$ 4097,4103, Si IV  $\lambda\lambda$ 4088,4116, He II  $\lambda$ 4100+H $\delta$ , while the feature at  $\lambda$ 4630 involves N V  $\lambda\lambda$ 4603,20, N III  $\lambda\lambda$ 4634,41. Stars included in spectral templates are indicated in bold (the remainder are excluded owing to limited spectral coverage).

Star	Category	Data	<i>d</i>	$A_V$	log	Ref	$\log F_{\text{HeII} 4686}$	HeII 4686	$L_{\text{HeII} 4686}$	$L_{\text{NIV} 3478,85}$	$L_{\text{NIV} 4058}$	$L_{4100}$	$L_{4630}$	$L_{\text{HeII} 5412}$	$L_{\text{CIV} 5801,12}$	$L_{\text{HeI} 5876}$	$L_{\text{H}\alpha}$	$L_{\text{NIV} 7103,29}$		
		ID	kpc	mag	$L_{\text{Bol}}/L_\odot$		$\text{erg s}^{-1} \text{cm}^{-2}$	FWHM	$10^{35} \text{ erg s}^{-1}$	$10^{-3} L_{\text{Bol}}$	$L_{\text{HeII} 4686}$	$L_{\text{HeII} 4686}$	$L_{\text{HeII} 4686}$	$L_{\text{HeII} 4686}$	$L_{\text{HeII} 4686}$	$L_{\text{HeII} 4686}$	$L_{\text{HeII} 4686}$	$L_{\text{HeII} 4686}$		
<b>WR1</b>	WN3–7s	II91	$3.0 \pm 0.1$	$2.5 \pm 0.3$	$5.84^{+0.11}_{-0.11}$	a	$-10.06^{+0.08}_{-0.10}$	2500	$15.9^{+6.1}_{-5.1}$	$0.60 \pm 0.07$	$0.28^{+0.03}_{-0.02}$	—	$-0.21^{+0.01}_{-0.00}$	—	0.17	$0.16^{+0.01}_{-0.01}$	$0.12^{+0.01}_{-0.01}$	0.04	$0.21^{+0.02}_{-0.02}$	$0.21^{+0.02}_{-0.03}$
<b>WR3</b>	WN2–5w	II91	$2.2 \pm 0.1$	$1.4^{+0.2}_{-0.1}$	$5.33^{+0.07}_{-0.07}$	a	$-10.89^{+0.08}_{-0.10}$	2400	$0.4^{+0.1}_{-0.1}$	$0.05^{+0.00}_{-0.01}$	...	...	...	...	0.65	$0.16^{+0.01}_{-0.00}$	0.02	0.00	$0.24^{+0.01}_{-0.01}$	...
<b>WR6</b>	WN3–7s	VU	$1.4 \pm 0.1$	$0.4^{+0.1}_{-0.0}$	$5.37^{+0.05}_{-0.04}$	a	$-8.55^{+0.04}_{-0.05}$	2300	$11.2^{+1.4}_{-1.4}$	$1.23^{+0.26}_{-0.05}$	$0.60^{+0.01}_{-0.01}$	—	$-0.28$	—	0.16	0.13	#0.06	0.03	0.14	$0.15^{+0.00}_{-0.01}$
WR7	WN3–7s	AR	$4.0 \pm 0.4$	$2.0 \pm 0.2$	$5.28^{+0.12}_{-0.12}$	a	$-10.48^{+0.04}_{-0.04}$	1900	$5.9^{+1.7}_{-1.4}$	$0.81^{+0.14}_{-0.12}$	$0.50^{+0.03}_{-0.03}$	0.02	$0.07^{+0.01}_{-0.00}$	0.20	$0.15^{+0.01}_{-0.00}$	$0.09^{+0.01}_{-0.00}$	0.02	$0.18^{+0.01}_{-0.02}$	$\pm 0.07^{+0.01}_{-0.00}$	
<b>WR10</b>	WN2–5w	CS	$4.2 \pm 0.2$	$2.2 \pm 0.2$	$5.55^{+0.10}_{-0.10}$	a	$-11.10^{+0.04}_{-0.04}$	1300	$1.9^{+0.6}_{-6.6}$	$0.14^{+0.02}_{-0.02}$	$0.63^{+0.05}_{-0.03}$	$0.62^{+0.03}_{-0.02}$	$0.38^{+0.01}_{-0.01}$	0.08	$0.08^{+0.01}_{-0.00}$	0.03	0.00	0.27 <sup>+0.02</sup>	...	
<b>WR12</b>	WN6–8	CS	$5.2^{+0.4}_{-0.3}$	$3.6^{+0.3}_{-0.4}$	$5.86^{+0.16}_{-0.15}$	a	$-10.94^{+0.05}_{-0.04}$	1100	$19.1^{+9.4}_{-6.6}$	$0.68^{+0.13}_{-0.10}$	$0.18^{+0.02}_{-0.01}$	$0.22^{+0.01}_{-0.01}$	$0.58^{+0.03}_{-0.03}$	$0.56^{+0.01}_{-0.00}$	$0.09^{+0.01}_{-0.00}$	0.01	$0.18^{+0.02}_{-0.01}$	$0.50^{+0.06}_{-0.05}$	...	
<b>WR16</b>	WN6–8	CS	$2.3 \pm 0.1$	$2.3^{+0.2}_{-0.3}$	$5.60^{+0.09}_{-0.10}$	a	$-10.21^{+0.05}_{-0.04}$	600	$4.7^{+1.4}_{-1.2}$	$0.31^{+0.04}_{-0.03}$	...	0.10	$0.83^{+0.03}_{-0.02}$	$1.11^{+0.01}_{-0.00}$	$0.08^{+0.00}_{-0.01}$	0.01	$0.33^{+0.02}_{-0.02}$	$0.65^{+0.05}_{-0.05}$	...	
WR18	WN3–7s	AR	$3.1 \pm 0.1$	$3.3^{+0.3}_{-0.4}$	$5.90^{+0.13}_{-0.14}$	a	$-10.27^{+0.04}_{-0.04}$	2800	$22.6^{+10.0}_{-7.2}$	$0.74^{+0.09}_{-0.08}$	...	—	$-0.28^{+0.01}_{-0.01}$	—	$0.16^{+0.01}_{-0.00}$	$0.12^{+0.00}_{-0.00}$	0.02	$0.15^{+0.02}_{-0.01}$	$0.17^{+0.03}_{-0.02}$	
<b>WR20</b>	WN2–5w	CS	$6.4^{+0.5}_{-0.4}$	$4.8 \pm 0.5$	$5.69^{+0.21}_{-0.20}$	a	$-12.03^{+0.04}_{-0.04}$	1600	$10.3^{+7.5}_{-4.5}$	$0.54^{+0.14}_{-0.11}$	$0.64^{+0.10}_{-0.08}$	$0.24^{+0.02}_{-0.02}$	$0.29^{+0.02}_{-0.02}$	0.16	$0.12^{+0.01}_{-0.01}$	$0.07^{+0.01}_{-0.01}$	0.02	$0.10^{+0.02}_{-0.02}$	$0.15^{+0.04}_{-0.03}$	
<b>WR21</b>	WN2–5w+O	CS	$3.2 \pm 0.1$	$2.1 \pm 0.2$	...	b	$-10.56^{+0.05}_{-0.04}$	1800	$3.7^{+1.1}_{-0.9}$	...	$0.61^{+0.03}_{-0.04}$	$0.09^{+0.01}_{-0.00}$	$0.12^{+0.01}_{-0.00}$	0.15	$0.08^{+0.00}_{-0.01}$	$0.07^{+0.00}_{-0.01}$	0.00	$0.15^{+0.02}_{-0.01}$	$0.28^{+0.03}_{-0.03}$	
<b>WR22</b>	WN5–7h+O	VU	$2.4^{+0.1}_{-0.2}$	$1.6 \pm 0.2$	$6.26^{+0.08}_{-0.07}$	a	$-9.52^{+0.04}_{-0.05}$	800	$11.4^{+2.5}_{-2.2}$	$0.16^{+0.02}_{-0.01}$	$0.03^{+0.01}_{-0.00}$	0.13	$0.55^{+0.01}_{-0.01}$	0.61	$0.05^{+0.01}_{-0.00}$	#0.02	0.05	$0.59^{+0.03}_{-0.03}$	$0.09^{+0.00}_{-0.01}$	
<b>WR24</b>	WN5–7h	VU	$2.4^{+0.2}_{-0.1}$	$0.9 \pm 0.1$	$6.12^{+0.07}_{-0.05}$	a	$-9.44^{+0.05}_{-0.04}$	1100	$7.2^{+1.1}_{-1.1}$	$0.14^{+0.01}_{-0.01}$	0.09	0.20	0.34	0.41	$0.06^{+0.01}_{-0.01}$	#0.04 <sup>+0.00</sup> <sub>-0.01</sub>	0.00	$0.49^{+0.02}_{-0.01}$	0.10	
<b>WR25</b>	Of/WN+O	CS	$2.3 \pm 0.1$	$3.0 \pm 0.3$	$6.49^{+0.13}_{-0.13}$	a,c	$-10.47^{+0.04}_{-0.05}$	1300	$5.1^{+2.0}_{-1.5}$	$0.04^{+0.01}_{-0.00}$	$0.10^{+0.01}_{-0.01}$	$0.31^{+0.01}_{-0.01}$	$0.43^{+0.01}_{-0.01}$	0.60	$0.06^{+0.01}_{-0.00}$	0.01	0.00	$0.58^{+0.05}_{-0.04}$	...	
<b>WR28</b>	WN6–8+O	CS	$6.9 \pm 0.5$	$4.5^{+0.5}_{-0.4}$	$6.09^{+0.20}_{-0.18}$	a	$-11.91^{+0.04}_{-0.04}$	1200	$11.1^{+7.4}_{-4.6}$	$0.23^{+0.06}_{-0.04}$	$0.29^{+0.04}_{-0.04}$	$0.21^{+0.02}_{-0.01}$	$0.39^{+0.03}_{-0.02}$	0.33	$0.09^{+0.01}_{-0.01}$	$0.03^{+0.00}_{-0.01}$	0.02	$0.26^{+0.05}_{-0.05}$	...	
<b>WR29</b>	WN6–8+O	CS	$7.0 \pm 0.5$	$3.6 \pm 0.4$	...	b	$-12.06^{+0.04}_{-0.04}$	1000	$2.9^{+1.4}_{-1.0}$	...	$0.15^{+0.01}_{-0.02}$	$0.19^{+0.01}_{-0.01}$	$0.37^{+0.02}_{-0.02}$	0.39	$0.08^{+0.00}_{-0.01}$	$0.03^{+0.00}_{-0.01}$	0.04	$0.27^{+0.04}_{-0.04}$	...	
<b>WR31a</b>	WN9–11	AR	$7.1^{+0.8}_{-0.6}$	$3.5^{+0.4}_{-0.3}$	$5.56^{+0.17}_{-0.16}$	d	$-13.28^{+0.05}_{-0.04}$	300	$0.2^{+0.1}_{-0.1}$	$0.01^{+0.01}_{-0.00}$	...	0.00	$21^{+2}_{-1}$	7.8	0.00	0.00	$37^{+4}_{-4}$	$175^{+26}_{-23}$	...	
WR34	WN2–5w	CS	$7.3^{+0.8}_{-0.7}$	$4.4^{+0.5}_{-0.4}$	$5.59^{+0.20}_{-0.20}$	a	$-12.04^{+0.04}_{-0.05}$	1400	$8.4^{+5.6}_{-3.5}$	$0.55^{+0.17}_{-0.12}$	$0.64^{+0.09}_{-0.08}$	$0.24^{+0.02}_{-0.01}$	$0.26^{+0.02}_{-0.02}$	$0.22^{+0.01}_{-0.00}$	...	...	...	...	...	...
<b>WR35</b>	WN6–8	CS	$7.9^{+0.8}_{-0.6}$	$4.3 \pm 0.4$	$5.73^{+0.19}_{-0.19}$	a	$-11.93^{+0.04}_{-0.04}$	1000	$11.4^{+7.3}_{-4.6}$	$0.55^{+0.14}_{-0.11}$	$0.40^{+0.05}_{-0.05}$	$0.30^{+0.02}_{-0.02}$	$0.46^{+0.03}_{-0.03}$	$0.38^{+0.01}_{-0.00}$	$0.07^{+0.01}_{-0.00}$	$0.04^{+0.00}_{-0.01}$	$0.02^{+0.01}_{-0.00}$	$0.20^{+0.04}_{-0.03}$	...	
<b>WR36</b>	WN3–7s	CS	$6.7^{+0.6}_{-0.5}$	$3.8^{+0.3}_{-0.4}$	$5.39^{+0.17}_{-0.16}$	a	$-11.51^{+0.05}_{-0.04}$	2600	$11.4^{+6.2}_{-4.2}$	$1.20^{+0.27}_{-0.21}$	$0.58^{+0.07}_{-0.06}$	$0.10^{+0.01}_{-0.01}$	$0.19^{+0.01}_{-0.01}$	0.18	$0.11^{+0.01}_{-0.01}$	$0.07^{+0.01}_{-0.01}$	$0.07^{+0.00}_{-0.01}$	$0.12^{+0.01}_{-0.02}$	$0.18^{+0.03}_{-0.03}$	
<b>WR37</b>	WN3–7s	CS	$6.8^{+0.7}_{-0.6}$	$6.1 \pm 0.6$	$5.88^{+0.25}_{-0.26}$	a	$-12.24^{+0.05}_{-0.04}$	2800	$31.0^{+31.0}_{-16.0}$	$1.07^{+0.37}_{-0.26}$	$0.36^{+0.07}_{-0.06}$	0.03	$0.15^{+0.01}_{-0.02}$	0.17	$0.09^{+0.01}_{-0.01}$	$0.07^{+0.02}_{-0.01}$	0.02	$0.11^{+0.03}_{-0.03}$	...	
<b>WR40</b>	WN6–8	CS	$2.8^{+0.2}_{-0.1}$	$1.6^{+0.2}_{-0.1}$	$5.61^{+0.08}_{-0.07}$	a	$-9.74^{+0.04}_{-0.05}$	900	$10.7^{+2.5}_{-2.1}$	$0.68^{+0.07}_{-0.06}$	$0.33^{+0.01}_{-0.02}$	$0.11^{+0.00}_{-0.01}$	$0.76^{+0.02}_{-0.02}$	$0.99^{+0.01}_{-0.00}$	$0.08^{+0.01}_{-0.00}$	0.01	$0.48^{+0.02}_{-0.02}$	$0.71^{+0.05}_{-0.04}$	$0.28^{+0.02}_{-0.02}$	
WR43A	2×WN5–7h	HF	$7.3 \pm 0.4$	$3.9 \pm 0.4$	$6.56^{+0.17}_{-0.16}$	e	$-11.64^{+0.04}_{-0.04}$	1600	$11.7^{+6.6}_{-4.3}$	$0.08^{+0.02}_{-0.01}$	$0.19^{+0.03}_{-0.02}$	$0.31^{+0.02}_{-0.02}$	$0.47^{+0.03}_{-0.02}$	0.27	...	...	...	...	...	
WR43B	WN5–7h	HF	$7.3 \pm 0.4$	$3.9 \pm 0.4$	$6.43^{+0.16}_{-0.16}$	e	$-11.44^{+0.05}_{-0.04}$	1900	$18.1^{+10.0}_{-6.7}$	$0.18^{+0.03}_{-0.03}$	$0.26^{+0.03}_{-0.03}$	$0.25^{+0.01}_{-0.02}$	$0.46^{+0.03}_{-0.02}$	$0.37^{+0.00}_{-0.01}$	...	...	...	...	...	
<b>WR43C</b>	Of/WN	HF	$7.3 \pm 0.4$	$3.9 \pm 0.4$	$6.32^{+0.16}_{-0.17}$	e	$-12.07^{+0.04}_{-0.05}$	1900	$4.4^{+2.5}_{-1.6}$	$0.06^{+0.01}_{-0.01}$	$0.21^{+0.03}_{-0.02}$	$0.18^{+0.01}_{-0.01}$	$0.10^{+0.00}_{-0.01}$	$0.37^{+0.00}_{-0.01}$	...	...	...	...	...	
WR44	WN2–5w+O	CS	$8.5^{+0.9}_{-0.7}$	$2.7 \pm 0.3$	$5.84^{+0.14}_{-0.13}$	a	$-11.27^{+0.04}_{-0.05}$	1800	$9.0^{+3.3}_{-2.6}$	$0.33^{+0.07}_{-0.05}$	$0.83^{+0.06}_{-0.06}$	$0.11^{+0.00}_{-0.01}$	$0.15^{+0.01}_{-0.00}$	$0.16^{+0.00}_{-0.01}$	...	...	...	...	...	
<b>WR46</b>	WN2–5w	CS	$2.3^{+0.0}_{-0.1}$	$1.3 \pm 0.1$	$5.29^{+0.06}_{-0.06}$	a	$-10.68^{+0.04}_{-0.05}$	2500	$0.5^{+0.1}_{-0.1}$	$0.07^{+0.01}_{-0.00}$	...	...	...	$0.72^{+0.00}_{-0.01}$	0.11	0.01	0.00	$0.16^{+0.01}_{-0.00}$	...	
<b>WR47</b>	WN6–8+O	CS	$3.6 \pm 0.2$	$4.0^{+0.3}_{-0.4}$	...	b	$-11.03^{+0.04}_{-0.05}$	1400	$12.0^{+6.9}_{-4.5}$	...	...	$0.24^{+0.02}_{-0.01}$	$0.41^{+0.03}_{-0.02}$	$0.43^{+0.00}_{-0.01}$	$0.12^{+0.00}_{-0.01}$	$0.05^{+0.00}_{-0.01}$	$0.06^{+0.01}_{-0.00}$	$0.13^{+0.02}_{-0.02}$		
<b>WR47a</b>	WN6–8	AD	$8.1^{+1.0}_{-0.8}$	$7.6^{+0.8}_{-0.7}$	...	b	$-13.53^{+0.04}_{-0.04}$	900	$12.3^{+16.9}_{-7.3}$	...	...	$0.10^{+0.01}_{-0.01}$	$0.72^{+0.09}_{-0.08}$	$1.17^{+0.02}_{-0.02}$	$0.07^{+0.01}_{-0.01}$	$0.02^{+0.00}_{-0.01}$	$0.61^{+0.14}_{-0.12}$	$1.00^{+0.35}_{-0.26}$	$0.03^{+0.02}_{-0.01}$	
<b>WR49</b>	WN2–5w	CS	$8.4^{+0.9}_{-0.7}$	$3.0 \pm 0.3$	$5.25^{+0.15}_{-0.14}$	a	$-11.82^{+0.04}_{-0.04}$	1500	$3.8^{+1.6}_{-1.2}$	$0.55^{+0.12}_{-0.10}$	$0.66^{+0.07}_{-0.05}$	$0.29^{+0.01}_{-0.02}$	$0.27^{+0.01}_{-0.01}$	0.25	$0.11^{+0.01}_{-0.01}$	$0.04^{+0.00}_{-0.01}$	0.01	$0.22^{+0.03}_{-0.02}$	...	
<b>WR51</b>	WN2–5w																			

**Table A1.** continued

Star	Category	Data	$d$	$A_V$	log	Ref log	$F_{\text{HeII} 4686}$	$\text{HeII} 4686$	$L_{\text{HeII} 4686}$	$L_{\text{NIV} 3478,85}$	$L_{\text{NIV} 4058}$	$L_{4100}$	$L_{4630}$	$L_{\text{HeII} 5412}$	$L_{\text{CIV} 5801,12}$	$L_{\text{HeI} 5876}$	$L_{\text{H}\alpha}$	$L_{\text{NIV} 7103,29}$	$C_{\text{over}}^{\text{other}}$	
		ID	kpc	mag	$L_{\text{Bol}}/L_\odot$	erg s $^{-1}$ cm $^{-2}$	FWHM	10 $^{35}$ erg s $^{-1}$	10 $^{-3} L_{\text{Bol}}$	$L_{\text{HeII} 4686}$	$L_{\text{HeII} 4686}$	$L_{\text{HeII} 4686}$	$L_{\text{HeII} 4686}$	$L_{\text{HeII} 4686}$	$L_{\text{HeII} 4686}$	$L_{\text{HeII} 4686}$	$L_{\text{HeII} 4686}$	$L_{\text{HeII} 4686}$	$L_{\text{HeII} 4686}$	
<b>WR61</b>	WN2–5w	CS	$6.4 \pm 0.5$	$1.9 \pm 0.2$	$5.12 \pm 0.10$	a	$-11.13 \pm 0.05$	1600	$3.2 \pm 0.9$	$0.65 \pm 0.10$	$0.53 \pm 0.03$	$0.25 \pm 0.01$	$0.32 \pm 0.01$	$0.28 \pm 0.01$	$0.12 \pm 0.01$	$0.07 \pm 0.01$	$0.02 \pm 0.01$	$0.13 \pm 0.01$	...	
<b>WR67</b>	WN6–8	CS	$3.2 \pm 0.2$	$3.9 \pm 0.4$	$5.36 \pm 0.17$	a	$-11.23 \pm 0.05$	1300	$6.1 \pm 3.5$	$0.69 \pm 0.15$	$0.40 \pm 0.05$	$0.30 \pm 0.02$	$0.46 \pm 0.03$	0.48	$0.11 \pm 0.01$	$0.06 \pm 0.00$	0.04	$0.14 \pm 0.02$	...	
<b>WR71</b>	WN6–8	CS	$4.1 \pm 0.3$	$1.1 \pm 0.2$	$5.29 \pm 0.08$	a	$-10.23 \pm 0.04$	1400	$4.6 \pm 0.9$	$0.61 \pm 0.06$	$0.62 \pm 0.03$	$0.32 \pm 0.01$	$0.55 \pm 0.01$	0.52	$0.12 \pm 0.01$	0.04	0.04	$0.13 \pm 0.00$	...	
<b>WR74</b>	WN6–8	CS	$4.0 \pm 0.2$	$5.6 \pm 0.6$	$5.41 \pm 0.23$	a	$-12.40 \pm 0.04$	1100	$4.2 \pm 3.7$	$0.43 \pm 0.10$	...	$0.16 \pm 0.01$	$0.29 \pm 0.02$	$0.74 \pm 0.01$	$0.16 \pm 0.01$	$0.06 \pm 0.00$	$0.16 \pm 0.03$	$0.15 \pm 0.04$	$0.20 \pm 0.07$	
WR75	WN3–7s	CS	$3.5 \pm 0.3$	$3.5 \pm 0.3$	$5.61 \pm 0.15$	a	$-10.45 \pm 0.04$	2800	$26.6 \pm 13.2$	$1.71 \pm 0.32$	$0.72 \pm 0.08$	—	$0.77 \pm 0.03$	—	$0.39$	$0.12 \pm 0.01$	$0.03 \pm 0.00$	$0.08 \pm 0.01$	$0.11 \pm 0.01$	...
<b>WR78</b>	WN6–8	VU	$1.6 \pm 0.1$	$1.8 \pm 0.2$	$6.03 \pm 0.08$	a	$-9.37 \pm 0.04$	900	$10.0 \pm 2.5$	$0.24 \pm 0.03$	$0.05 \pm 0.01$	0.10	$0.47 \pm 0.01$	$0.61 \pm 0.00$	$0.11 \pm 0.00$	#0.03	$0.12 \pm 0.01$	$0.37 \pm 0.03$	$0.09 \pm 0.01$	
<b>WR82</b>	WN6–8	CS	$3.8 \pm 0.3$	$3.8 \pm 0.3$	$5.26 \pm 0.16$	a	$-11.58 \pm 0.04$	1000	$3.1 \pm 1.7$	$0.44 \pm 0.10$	$0.31 \pm 0.03$	$0.23 \pm 0.02$	$0.73 \pm 0.05$	$0.94 \pm 0.01$	$0.11 \pm 0.01$	0.01	$0.17 \pm 0.02$	$0.40 \pm 0.07$	...	
<b>WR83</b>	WN2–5w	CS	$4.6 \pm 0.4$	$4.0 \pm 0.4$	...	b	$-11.46 \pm 0.04$	1400	$7.6 \pm 4.4$	...	$0.75 \pm 0.09$	$0.37 \pm 0.03$	$0.50 \pm 0.03$	$0.47 \pm 0.00$	$0.10 \pm 0.00$	$0.04 \pm 0.00$	0.01	$0.19 \pm 0.03$	...	...
<b>WR84</b>	WN6–8	CS	$2.7 \pm 0.1$	$5.4 \pm 0.6$	$5.18 \pm 0.22$	a	$-11.94 \pm 0.04$	1100	$4.5 \pm 3.8$	$0.77 \pm 0.16$	$0.31 \pm 0.06$	$0.27 \pm 0.02$	$0.65 \pm 0.05$	$0.74 \pm 0.01$	$0.14 \pm 0.01$	$0.05 \pm 0.01$	$0.09 \pm 0.02$	$0.12 \pm 0.03$	...	
<b>WR85</b>	WN6–8	CS	$2.2 \pm 0.1$	$3.5 \pm 0.3$	$5.48 \pm 0.15$	a	$-10.75 \pm 0.04$	1100	$4.9 \pm 2.4$	$0.42 \pm 0.07$	$0.45 \pm 0.05$	$0.34 \pm 0.02$	$0.62 \pm 0.03$	$0.67 \pm 0.00$	$0.11 \pm 0.01$	0.03	$0.04 \pm 0.00$	$0.32 \pm 0.04$	...	
<b>WR87</b>	WN5–7h	CS	$3.0 \pm 0.1$	$6.4 \pm 0.6$	$6.11 \pm 0.26$	a	$-12.32 \pm 0.04$	1100	$6.5 \pm 6.8$	$0.13 \pm 0.03$	$0.57 \pm 0.12$	$0.14 \pm 0.01$	$0.70 \pm 0.07$	$1.04 \pm 0.01$	$0.06 \pm 0.01$	$0.06 \pm 0.01$	$0.06 \pm 0.01$	$0.77 \pm 0.22$	...	
<b>WR89</b>	WN5–7h	CS	$3.2 \pm 0.2$	$5.9 \pm 0.6$	$6.30 \pm 0.26$	a	$-11.95 \pm 0.04$	700	$10.9 \pm 10.4$	$0.14 \pm 0.03$	$1.07 \pm 0.21$	$0.16 \pm 0.01$	$0.95 \pm 0.09$	$1.01 \pm 0.01$	$0.03 \pm 0.01$	$0.01 \pm 0.01$	$0.07 \pm 0.01$	$0.73 \pm 0.19$	...	
WR91	WN3–7s	CS	$3.6 \pm 0.3$	$8.0 \pm 0.7$	$5.61 \pm 0.33$	a	$-12.68 \pm 0.04$	2000	$25.4 \pm 36.9$	$1.61 \pm 0.54$	...	...	...	$0.60 \pm 0.00$	$0.12 \pm 0.02$	$0.03 \pm 0.01$	$0.11 \pm 0.03$	$0.14 \pm 0.05$	...	
WR94	WN2–5w	CS	$1.1 \pm 0.0$	$6.1 \pm 0.6$	$5.65 \pm 0.25$	a	$-11.21 \pm 0.04$	1400	$8.1 \pm 7.9$	$0.47 \pm 0.08$	$1.04 \pm 0.19$	$0.41 \pm 0.04$	$0.54 \pm 0.05$	$0.38 \pm 0.00$	...	...	...	...	...	
<b>WR97</b>	WN3–7s+O	CS	$2.3 \pm 0.1$	$3.7 \pm 0.4$	...	b	$-11.53 \pm 0.05$	2000	$1.3 \pm 0.7$	...	$0.54 \pm 0.06$	$0.12 \pm 0.01$	0.07	0.42	$0.09 \pm 0.01$	$0.05 \pm 0.01$	0.00	$0.26 \pm 0.04$	...	
WR100	WN3–7s	CS	$2.5 \pm 0.2$	$5.6 \pm 0.6$	$5.38 \pm 0.23$	a	$-11.60 \pm 0.05$	1900	$11.0 \pm 9.8$	$1.19 \pm 0.31$	$0.37 \pm 0.07$	$0.26 \pm 0.02$	$0.59 \pm 0.05$	$0.55 \pm 0.01$	...	...	...	...	...	
<b>WR105</b>	WN9–11	II96	$3.5 \pm 0.6$	$7.7 \pm 0.7$	$6.28 \pm 0.33$	f	$-12.72 \pm 0.05$	500	$15.3 \pm 21.0$	$0.21 \pm 0.10$	...	0.00	$0.72 \pm 0.08$	$1.42 \pm 0.02$	0.02:	0.00	$0.82 \pm 0.19$	$1.6 \pm 0.5$	...	
<b>WR107</b>	WN6–8	II96	$1.8 \pm 0.3$	$6.3 \pm 0.6$	$4.85 \pm 0.30$	a	$-12.54 \pm 0.04$	1000	$1.1 \pm 1.0$	$0.38 \pm 0.17$	...	$0.22 \pm 0.02$	$0.87 \pm 0.07$	$1.36 \pm 0.01$	$0.17 \pm 0.02$	$0.05 \pm 0.01$	$0.49 \pm 0.07$	$0.17 \pm 0.04$	...	
<b>WR108</b>	WN9–11	II91	$3.1 \pm 0.2$	$3.7 \pm 0.3$	$5.42 \pm 0.15$	f	$-11.63 \pm 0.04$	400	$1.7 \pm 0.9$	$0.17 \pm 0.03$	...	0.00	$1.20 \pm 0.07$	$1.93 \pm 0.01$	0.02	0.02	$0.25 \pm 0.03$	$1.13 \pm 0.17$	0.01	
<b>WR110</b>	WN3–7s	AR	$1.8 \pm 0.1$	$3.8 \pm 0.4$	$5.61 \pm 0.16$	a	$-9.93 \pm 0.04$	3600	$29.8 \pm 15.8$	$1.88 \pm 0.27$	$0.57 \pm 0.07$	—	$0.47 \pm 0.02$	—	$0.20 \pm 0.01$	$0.11 \pm 0.01$	$0.03 \pm 0.01$	$0.07 \pm 0.01$	$0.13 \pm 0.02$	$0.17 \pm 0.02$
<b>WR116</b>	WN6–8	II96	$2.9 \pm 0.2$	$6.6 \pm 0.6$	$5.56 \pm 0.27$	a	$-12.49 \pm 0.04$	1100	$5.2 \pm 5.7$	$0.37 \pm 0.11$	...	$0.11 \pm 0.01$	$1.25 \pm 0.12$	$1.58 \pm 0.02$	$0.07 \pm 0.01$	0.01	$0.69 \pm 0.14$	$1.04 \pm 0.30$	...	
WR120	WN6–8	WI94	$2.7 \pm 0.5$	$4.7 \pm 0.5$	$5.39 \pm 0.23$	a	$-11.81 \pm 0.04$	1000	$2.7 \pm 1.9$	$0.28 \pm 0.10$	...	...	$0.89 \pm 0.01$	$0.24 \pm 0.02$	$0.08 \pm 0.01$	$0.41 \pm 0.06$	...	...	...	
<b>WR123</b>	WN6–8	AR+II91	$6.1 \pm 0.6$	$2.5 \pm 0.3$	$5.33 \pm 0.13$	a	$-11.41 \pm 0.04$	800	$3.2 \pm 1.2$	$0.38 \pm 0.08$	...	$0.12 \pm 0.00$	$1.15 \pm 0.05$	$1.54 \pm 0.00$	$0.17 \pm 0.01$	0.02	$0.68 \pm 0.06$	$0.15 \pm 0.02$	$\pm 0.08 \pm 0.01$	
WR124	WN6–8	II91	$5.4 \pm 0.5$	$3.8 \pm 0.4$	$5.62 \pm 0.17$	a	$-11.58 \pm 0.08$	800	$7.0 \pm 4.1$	$0.43 \pm 0.10$	...	...	...	$1.31 \pm 0.01$	$0.08 \pm 0.00$	0.02	$0.92 \pm 0.11$	$1.29 \pm 0.23$	...	
WR128	WN2–5w	II91	$3.3 \pm 0.3$	$1.4 \pm 0.1$	$5.34 \pm 0.08$	a	$-10.55 \pm 0.08$	1900	$1.7 \pm 0.5$	$0.20 \pm 0.02$	...	...	...	0.26	$0.11 \pm 0.00$	0.03	0.00	$0.23 \pm 0.02$	$0.13 \pm 0.01$	...
<b>WR131</b>	WN5–7h	II96+WI94	$8.2 \pm 1.0$	$4.3 \pm 0.4$	$6.17 \pm 0.19$	a	$-11.97 \pm 0.04$	800	$11.0 \pm 7.1$	$0.19 \pm 0.05$	...	$0.10 \pm 0.00$	$0.29 \pm 0.02$	0.35	$0.06 \pm 0.01$	0.03	$0.05 \pm 0.00$	...	...	...
WR133	WN2–5w+O	II91	$1.8 \pm 0.1$	$1.2 \pm 0.1$	...	b	$-9.66 \pm 0.08$	1700	$3.0 \pm 0.8$	...	...	0.14	$0.10 \pm 0.01$	0.12	0.00	$0.20 \pm 0.01$	$0.24 \pm 0.01$	...	...	
<b>WR134</b>	WN3–7s	II91	$1.9 \pm 0.0$	$1.9 \pm 0.2$	$5.67 \pm 0.09$	a	$-9.14 \pm 0.09$	2600	$25.9 \pm 8.1$	$1.43 \pm 0.14$	$0.55 \pm 0.03$	—	$0.43 \pm 0.02$	—	0.16	$0.13 \pm 0.01$	$0.06 \pm 0.00$	0.04	$0.16 \pm 0.01$	$0.20 \pm 0.02$
<b>WR136</b>	WN3–7s	II91	$1.7 \pm 0.0$	$1.7 \pm 0.2$	$5.68 \pm 0.07$	a	$-8.92 \pm 0.10$	1900	$27.2 \pm 7.9$	$1.49 \pm 0.12$	$0.33 \pm 0.02$	—	$0.56 \pm 0.02$	—	0.34	$0.15 \pm 0.00$	$0.05 \pm 0.00$	0.06	$0.24 \pm 0.01$	$0.18 \pm 0.02$
<b>WR138</b>	WN2–5w+O	II91	$2.2 \pm 0.1$	$1.9 \pm 0.2$	...	b	$-9.84 \pm 0.08$	1400	$7.2 \pm 2.3$	...	...	$0.19 \pm 0.01$	$0.21 \pm 0.01$	$0.28 \pm 0.01$	$0.15 \pm 0.01$	$0.07 \pm 0.01$	0.05	$0.29 \pm 0.02$	$0.28 \pm 0.02$	...
<b>WR138-1</b>	WN9–11	II13	$7.0 \pm 0.8$	$7.0 \pm 0.7$	...	b	$-13.68 \pm 0.08$	500	$3.3 \pm 4.0$	...	...	0.00	$1.25 \pm 0.14$	$1.17 \pm 0.02$	$0.07 \pm 0.01$	0.00	$1.04 \pm 0.22$	$1.59 \pm 0.40$	$0.01 \pm 0.01$	
WR139	WN2–5w+O	II91	$1.4 \pm 0.0$	$2.5 \pm 0.3$	...	b	$-9.93 \pm 0.08$	1600	$4.5 \pm 1.8$	...	...	...	...	0.25	$0.14 \pm 0.01$	$0.14 \pm 0.01$	0.05	$0.21 \pm 0.02$	$0.28 \pm 0.04$	...
WR141	WN2–5w+O	II91	$1.9 \pm 0.0$	$3.7 \pm 0.3$	...	b	$-10.27 \pm 0.08$	1700	$14.0 \pm 7.6$	...	...	...	...	0.25	$0.12 \pm 0.01$	$0.08 \pm 0.00$	0.04	$0.04 \pm 0.01$	$0.13 \pm 0.01$	$0.13 \pm 0.03$
<b>WR147</b>	WN6–8+B	II96	$1.7 \pm 0.1$	$10.7 \pm 1.1$	$6.58 \pm 0.43$	a	$-13.43 \pm 0.04$													

Table A1. continued

Star	Category	Data	$d$	$A_V$	$\log$	Ref	$\log F_{\text{HeII}} 4686$	$\text{HeII} 4686$	$L_{\text{HeII}} 4686$	$L_{\text{NIV}} 3478,85$	$L_{\text{NIV}} 4058$	$L_{4100}$	$L_{4630}$	$L_{\text{HeII}} 5412$	$L_{\text{CIV}} 5801,12$	$L_{\text{HeI}} 5876$	$L_{\text{H}\alpha}$	$L_{\text{NIV}} 7103,29$	
		ID	kpc	mag	$L_{\text{Bol}}/L_\odot$		$\text{erg s}^{-1} \text{cm}^{-2}$	FWHM	$10^{35} \text{erg s}^{-1}$	$10^{-3} L_{\text{Bol}}$	$L_{\text{HeII}} 4686$	$L_{\text{HeII}} 4686$	$L_{\text{HeII}} 4686$	$L_{\text{HeII}} 4686$	$L_{\text{HeII}} 4686$	$L_{\text{HeII}} 4686$	$L_{\text{HeII}} 4686$	$L_{\text{HeII}} 4686$	
WR149	WN2–5w	II13	5.3 $^{+0.4}_{-0.3}$	5.3 $^{+0.6}_{-0.5}$	5.48 $^{+0.22}_{-0.22}$	a	-12.20 $^{+0.08}_{-0.09}$	1300	8.5 $^{+7.2}_{-4.2}$	0.73 $^{+0.18}_{-0.15}$	...	0.20 $^{+0.01}_{-0.02}$	0.23 $^{+0.02}_{-0.02}$	0.21 $^{+0.00}_{-0.00}$	0.13 $^{+0.01}_{-0.02}$	0.09 $^{+0.01}_{-0.01}$	0.04 $^{+0.01}_{-0.00}$	0.13 $^{+0.02}_{-0.03}$	0.16 $^{+0.04}_{-0.04}$
WR152	WN2–5w	II91	3.5 $^{+0.3}_{-0.2}$	1.9 $\pm 0.2$	5.46 $^{+0.09}_{-0.09}$	a	-10.96 $^{+0.08}_{-0.10}$	2000	1.4 $^{+0.5}_{-0.4}$	0.13 $^{+0.02}_{-0.01}$	...	0.00	0.04	0.34	0.09	0.01	0.00	0.18 $^{+0.01}_{-0.01}$	0.04 $^{+0.00}_{-0.01}$
WR155	WN6–8+O	II91	2.7 $\pm 0.1$	2.2 $\pm 0.2$	...	b	-10.42 $^{+0.08}_{-0.10}$	1200	4.1 $^{+1.4}_{-1.2}$	...	...	...	...	0.44 $^{+0.00}_{-0.01}$	0.09 $^{+0.00}_{-0.01}$	0.05	0.06 $^{+0.01}_{-0.00}$	0.30 $^{+0.03}_{-0.02}$	0.13 $^{+0.01}_{-0.01}$
WR156	WN6–8	II91	3.3 $^{+0.2}_{-0.1}$	4.6 $^{+0.4}_{-0.5}$	5.81 $^{+0.19}_{-0.18}$	a	-11.61 $^{+0.07}_{-0.10}$	500	5.5 $^{+3.9}_{-2.5}$	0.22 $^{+0.04}_{-0.03}$	...	...	...	2.02 $^{+0.02}_{-0.02}$	0.05 $^{+0.01}_{-0.00}$	0.03 $^{+0.01}_{-0.00}$	0.45 $^{+0.06}_{-0.05}$	1.27 $^{+0.25}_{-0.21}$	...
WR157	WN2–5w	II91	2.8 $^{+0.2}_{-0.1}$	2.8 $\pm 0.3$	...	b	-10.53 $^{+0.08}_{-0.10}$	1300	6.6 $^{+2.8}_{-2.3}$	...	...	...	0.22	0.16 $^{+0.00}_{-0.01}$	...	...	...	...	
<b>BAT99-1</b>	WN3–7s	NE	49.6 $\pm 1.0$	0.5 $^{+0.1}_{-0.0}$	5.29 $^{+0.03}_{-0.02}$	g	-12.19 $^{+0.04}_{-0.04}$	2000	3.4 $^{+0.4}_{-0.4}$	0.45 $^{+0.02}_{-0.01}$	$\pm 0.13$	0.00	0.05	0.18	0.14	0.01	0.00	0.19	0.00
<b>BAT99-3</b>	WN3–7s	NE	49.6 $\pm 1.0$	0.5 $^{+0.0}_{-0.1}$	5.50 $^{+0.03}_{-0.02}$	g	-11.77 $^{+0.04}_{-0.05}$	2000	8.2 $^{+0.9}_{-0.9}$	0.67 $^{+0.02}_{-0.02}$	$\pm 0.66^{+0.01}_{-0.02}$	0.03	0.08	0.17	0.14	0.05	0.02	0.16 $^{+0.00}_{-0.01}$	0.08 $^{+0.00}_{-0.01}$
<b>BAT99-5</b>	WN2–5w	NE	49.6 $\pm 1.0$	1.0 $\pm 0.1$	5.44 $^{+0.05}_{-0.04}$	g	-12.72 $^{+0.04}_{-0.05}$	2400	1.7 $^{+0.3}_{-0.2}$	0.16 $^{+0.01}_{-0.01}$	...	0.00	0.04 $^{+0.01}_{-0.00}$	0.04	0.15 $^{+0.00}_{-0.01}$	0.00	0.00	0.17 $^{+0.01}_{-0.00}$	0.00
<b>BAT99-7</b>	WN3–7s	NE	49.6 $\pm 1.0$	0.3 $\pm 0.0$	5.83 $^{+0.02}_{-0.02}$	g	-11.11 $^{+0.04}_{-0.05}$	3800	31.7 $^{+3.4}_{-3.4}$	1.21 $^{+0.03}_{-0.03}$	$\pm 0.30^{+0.00}_{-0.01}$	0.00	0.05 $^{+0.00}_{-0.01}$	0.09	0.11	0.03	0.00	0.15 $^{+0.00}_{-0.01}$	0.02
<b>BAT99-13</b>	WN9–11	AR+SC	49.6 $\pm 1.0$	0.8 $^{+0.0}_{-0.1}$	5.55 $^{+0.04}_{-0.03}$	g	-12.98 $^{+0.04}_{-0.05}$	200	0.7 $^{+0.1}_{-0.1}$	0.05 $^{+0.00}_{-0.00}$	...	0.00	3.7 $^{+0.0}_{-0.1}$	2.4	0.01	0.00	3.3 $^{+0.0}_{-0.0}$	11.1 $^{+0.3}_{-0.3}$	...
<b>BAT99-15</b>	WN3–7s	NE	49.6 $\pm 1.0$	0.3 $\pm 0.0$	5.56 $^{+0.02}_{-0.02}$	g	-11.53 $^{+0.04}_{-0.04}$	2200	12.2 $^{+1.3}_{-1.3}$	0.87 $^{+0.02}_{-0.02}$	$\pm 0.55^{+0.01}_{-0.01}$	0.04	0.12	0.16	0.13	0.07	0.03	0.16 $^{+0.00}_{-0.01}$	0.07
<b>BAT99-16</b>	WN6–8	AR+SC	49.6 $\pm 1.0$	0.3 $^{+0.1}_{-0.0}$	5.79 $^{+0.02}_{-0.02}$	g	-11.61 $^{+0.05}_{-0.04}$	700	10.6 $^{+1.2}_{-1.1}$	0.44 $^{+0.02}_{-0.01}$	$\pm 0.16^{+0.01}_{-0.00}$	0.23	0.50 $^{+0.01}_{-0.00}$	0.54	0.10	0.04	0.19 $^{+0.00}_{-0.01}$	0.51 $^{+0.01}_{-0.00}$	...
<b>BAT99-17</b>	WN2–5w+B	NE	49.6 $\pm 1.0$	0.4 $^{+0.0}_{-0.1}$	5.63 $^{+0.03}_{-0.02}$	h	-11.78 $^{+0.04}_{-0.04}$	1800	7.4 $^{+0.8}_{-0.8}$	0.45 $^{+0.01}_{-0.01}$	$\pm 0.75^{+0.02}_{-0.01}$	0.08	0.10	0.18	0.13	0.07	0.01	0.15 $^{+0.01}_{-0.00}$	0.10
<b>BAT99-18</b>	WN2–5w	NE	49.6 $\pm 1.0$	0.4 $^{+0.0}_{-0.1}$	5.62 $^{+0.03}_{-0.02}$	g	-12.00 $^{+0.04}_{-0.05}$	1800	4.5 $^{+0.5}_{-0.5}$	0.28 $^{+0.00}_{-0.01}$	$\pm 0.80^{+0.01}_{-0.02}$	0.09	0.11	0.18	0.10 $^{+0.01}_{-0.00}$	0.03	0.00	0.20	0.07
<b>BAT99-22</b>	WN9–11	AR+SC	49.6 $\pm 1.0$	0.5 $^{+0.0}_{-0.1}$	5.74 $^{+0.03}_{-0.02}$	g	-12.17 $^{+0.04}_{-0.05}$	300	3.4 $^{+0.4}_{-0.4}$	0.16 $^{+0.01}_{-0.01}$	$\pm 0.00$	0.00	1.18 $^{+0.01}_{-0.01}$	1.52	0.00	0.03	0.77 $^{+0.01}_{-0.01}$	3.27 $^{+0.06}_{-0.06}$	...
<b>BAT99-23</b>	WN2–5w	NE	49.6 $\pm 1.0$	2.3 $^{+0.2}_{-0.3}$	5.54 $^{+0.09}_{-0.09}$	g	-13.20 $^{+0.04}_{-0.05}$	1800	2.2 $^{+0.7}_{-0.5}$	0.17 $^{+0.01}_{-0.02}$	...	0.08 $^{+0.00}_{-0.01}$	0.19 $^{+0.01}_{-0.01}$	0.25	0.10	0.00	0.00	0.26 $^{+0.02}_{-0.02}$	0.04 $^{+0.00}_{-0.01}$
<b>BAT99-24</b>	WN3–7s	NE	49.6 $\pm 1.0$	0.4 $^{+0.0}_{-0.1}$	5.53 $^{+0.03}_{-0.02}$	g	-11.51 $^{+0.04}_{-0.05}$	2600	13.7 $^{+1.5}_{-1.5}$	1.04 $^{+0.03}_{-0.03}$	$\pm 0.54^{+0.01}_{-0.01}$	0.04	0.11	0.14	0.13	0.04	0.02	0.15 $^{+0.01}_{-0.00}$	0.09
<b>BAT99-25</b>	WN2–5w	NE	49.6 $\pm 1.0$	0.6 $^{+0.0}_{-0.1}$	5.54 $^{+0.03}_{-0.03}$	g	-12.71 $^{+0.05}_{-0.04}$	1700	1.1 $^{+0.1}_{-0.1}$	0.08 $^{+0.00}_{-0.00}$	...	0.07	0.00	0.11	0.08	0.01	0.00	0.30 $^{+0.00}_{-0.01}$	0.06
<b>BAT99-26</b>	WN3–7s	NE	49.6 $\pm 1.0$	0.5 $^{+0.1}_{-0.0}$	5.61 $^{+0.03}_{-0.02}$	g	-11.78 $^{+0.04}_{-0.05}$	1800	8.7 $^{+1.0}_{-1.0}$	0.55 $^{+0.02}_{-0.02}$	$\pm 0.83^{+0.02}_{-0.02}$	0.07	0.11	0.18	0.13	0.09 $^{+0.00}_{-0.01}$	0.01	0.13	0.10 $^{+0.01}_{-0.00}$
<b>BAT99-30</b>	WN6–8	AR	49.6 $\pm 1.0$	0.3 $^{+0.0}_{-0.1}$	5.64 $^{+0.02}_{-0.02}$	g	-11.76 $^{+0.04}_{-0.05}$	1000	6.8 $^{+0.7}_{-0.7}$	0.40 $^{+0.01}_{-0.01}$	$\pm 0.29^{+0.00}_{-0.01}$	0.20	0.39	0.28	0.10	0.05	0.05	$\pm 0.50^{+0.01}_{-0.00}$	...
<b>BAT99-31</b>	WN3–7s	NE	49.6 $\pm 1.0$	0.6 $^{+0.1}_{-0.0}$	5.32 $^{+0.03}_{-0.03}$	g	-12.08 $^{+0.04}_{-0.05}$	2000	4.9 $^{+0.6}_{-0.6}$	0.61 $^{+0.02}_{-0.02}$	$\pm 0.57^{+0.02}_{-0.01}$	0.05	0.10	0.19	0.13 $^{+0.00}_{-0.01}$	0.07 $^{+0.00}_{-0.01}$	0.01	0.27 $^{+0.01}_{-0.01}$	0.08
<b>BAT99-32</b>	WN6–8+O	AR+SC	49.6 $\pm 1.0$	0.3 $\pm 0.0$	5.93 $^{+0.02}_{-0.02}$	g	-11.36 $^{+0.04}_{-0.05}$	1400	17.9 $^{+1.9}_{-1.9}$	0.54 $^{+0.01}_{-0.01}$	$\pm 0.36$	0.19	0.26	0.14	0.12	0.03	0.04	0.24 $^{+0.01}_{-0.00}$	...
<b>BAT99-35</b>	WN2–5w	NE	49.6 $\pm 1.0$	0.4 $^{+0.1}_{-0.0}$	5.59 $^{+0.03}_{-0.02}$	g	-11.97 $^{+0.04}_{-0.05}$	1800	4.9 $^{+0.6}_{-0.5}$	0.33 $^{+0.01}_{-0.01}$	$\pm 0.80^{+0.02}_{-0.01}$	0.03	0.07	0.23	0.13	0.01	0.00	0.19	0.06
<b>BAT99-37</b>	WN2–5w	NE	49.6 $\pm 1.0$	1.9 $\pm 0.2$	5.64 $^{+0.08}_{-0.07}$	g	-12.62 $^{+0.04}_{-0.05}$	2000	5.6 $^{+1.4}_{-1.2}$	0.33 $^{+0.03}_{-0.02}$	...	0.04 $^{+0.00}_{-0.01}$	0.09 $^{+0.01}_{-0.00}$	0.25	0.12 $^{+0.00}_{-0.01}$	0.02	0.00	0.14 $^{+0.02}_{-0.00}$	0.03
<b>BAT99-40</b>	WN2–5w+O	NE	49.6 $\pm 1.0$	0.6 $^{+0.0}_{-0.1}$	5.61 $^{+0.03}_{-0.03}$	g	-12.34 $^{+0.04}_{-0.05}$	1600	2.5 $^{+0.3}_{-0.3}$	0.16 $^{+0.01}_{-0.01}$	$\pm 0.63^{+0.02}_{-0.02}$	0.06	0.12	0.08	0.08	0.08 $^{+0.00}_{-0.00}$	0.00	0.23 $^{+0.00}_{-0.01}$	0.07
<b>BAT99-41</b>	WN3–7s	NE	49.6 $\pm 1.0$	0.5 $^{+0.0}_{-0.1}$	5.59 $^{+0.03}_{-0.02}$	g	-11.82 $^{+0.04}_{-0.05}$	1600	7.3 $^{+0.8}_{-0.8}$	0.48 $^{+0.02}_{-0.02}$	$\pm 0.07$	0.04	0.10 $^{+0.01}_{-0.00}$	0.18	0.13 $^{+0.01}_{-0.00}$	0.08	0.01	0.14	0.10
<b>BAT99-44</b>	WN6–8	AR	49.6 $\pm 1.0$	0.5 $^{+0.0}_{-0.1}$	5.65 $^{+0.03}_{-0.02}$	g	-12.13 $^{+0.04}_{-0.05}$	900	3.6 $^{+0.4}_{-0.4}$	0.21 $^{+0.00}_{-0.01}$	$\pm 0.15^{+0.01}_{-0.00}$	0.18	0.63 $^{+0.01}_{-0.01}$	0.74	0.08	0.04	0.19	$\pm 1.01^{+0.02}_{-0.02}$	...
<b>BAT99-45</b>	WN9–11	AR+SC	49.6 $\pm 1.0$	0.3 $^{+0.0}_{-0.0}$	5.75 $^{+0.02}_{-0.02}$	1	-12.40 $^{+0.05}_{-0.05}$	200	1.6 $^{+0.2}_{-0.2}$	0.07 $^{+0.01}_{-0.00}$	...	0.03	2.2 $^{+0.0}_{-0.0}$	2.3	0.05	0.00	2.8	6.8 $^{+0.0}_{-0.1}$	...
<b>BAT99-46</b>	WN2–5w	NE	49.6 $\pm 1.0$	0.8 $\pm 0.1$	5.43 $^{+0.04}_{-0.03}$	g	-12.27 $^{+0.04}_{-0.05}$	1700	3.8 $^{+0.5}_{-0.5}$	0.36 $^{+0.02}_{-0.01}$	$\pm 0.78^{+0.03}_{-0.03}$	0.05	0.11 $^{+0.00}_{-0.01}$	0.16	0.12 $^{+0.01}_{-0.00}$	0.03	0.01	0.17 $^{+0.00}_{-0.01}$	0.10
<b>BAT99-47</b>	WN3–7s	NE	49.6 $\pm 1.0$	0.8 $^{+0.0}_{-0.1}$	5.58 $^{+0.04}_{-0.03}$	g	-12.00 $^{+0.04}_{-0.05}$	1600	6.8 $^{+0.9}_{-0.9}$	0.46 $^{+0.02}_{-0.02}$	...	0.01	0.07	0.19 $^{+0.01}_{-0.00}$	0.13	0.02	0.00	0.13 $^{+0.01}_{-0.00}$	0.02
<b>BAT99-48</b>	WN3–7s	NE	49.6 $\pm 1.0$	0.4 $^{+0.0}_{-0.1}$	5.39 $^{+0.03}_{-0.02}$	g	-11.74 $^{+0.05}_{-0.05}$	2000	8.0 $^{+0.9}_{-0.9}$	0.84 $^{+0.03}_{-0.02}$	$\pm 0.70^{+0.01}_{-0.01}$	0.03	0.09	0.19	0.13	0.08 $^{+0.00}_{-0.01}$	0.02	0.14 $^{+0.00}_{-0.01}$	0.08
<b>BAT99-50</b>	WN2–5w	NE	49.6 $\pm 1.0$	0.7 $^{+0.0}_{-0.1}$	5.64 $^{+0.03}_{-0.03}$	g	-12.54 $^{+0.04}_{-0.04}$	1200	1.8 $^{+0.2}_{-0.2}$	0.11 $^{+0.00}_{-0.01}$	...	0.27	0.20	0.05	0.07	0.03	0		

**Table A1.** continued

Table A1. continued

Star	Category	Data	$d$	$A_V$	log	Ref	$\log F_{\text{HeII} 4686}$	$\text{HeII} 4686$	$L_{\text{HeII} 4686}$	$L_{\text{NIV} 3478,85}$	$L_{\text{NIV} 4058}$	$L_{4100}$	$L_{4630}$	$L_{\text{HeII} 5412}$	$L_{\text{CIV} 5801,12}$	$L_{\text{HeI} 5876}$	$L_{\text{H}\alpha}$	$L_{\text{NIV} 7103,29}$	
		ID	kpc	mag	$L_{\text{Bol}}/L_\odot$		$\text{erg s}^{-1} \text{cm}^{-2}$	FWHM	$10^{35} \text{ erg s}^{-1} 10^{-3} L_{\text{Bol}}$	$\bar{L}_{\text{HeII} 4686}$	$\bar{L}_{\text{HeII} 4686}$	$\bar{L}_{\text{HeII} 4686}$	$\bar{L}_{\text{HeII} 4686}$	$\bar{L}_{\text{HeII} 4686}$	$\bar{L}_{\text{HeII} 4686}$	$\bar{L}_{\text{HeII} 4686}$	$\bar{L}_{\text{HeII} 4686}$		
<b>BAT99-116</b>	2×WN5–7h	VM	49.6±1.0	2.0±0.2	6.70 <sup>+0.08</sup> <sub>-0.09</sub>	k	−11.87 <sup>+0.08</sup> <sub>-0.10</sub>	1800	33.3 <sup>+10.4</sup> <sub>-9.3</sub>	0.17 <sup>+0.01</sup> <sub>-0.01</sub>	...	...	...	0.05	0.07	0.04 <sup>+0.00</sup> <sub>-0.01</sub>	0.03 <sup>+0.01</sup> <sub>-0.00</sub>	0.39 <sup>+0.03</sup> <sub>-0.02</sub>	0.11 <sup>+0.01</sup> <sub>-0.01</sub>
<b>BAT99-117</b>	WN5–7h	NE	49.6±1.0	0.7±0.1	6.39 <sup>+0.04</sup> <sub>-0.03</sub>	g	−11.82 <sup>+0.05</sup> <sub>-0.05</sub>	2000	9.9 <sup>+1.3</sup> <sub>-1.2</sub>	0.10 <sup>+0.01</sup> <sub>-0.02</sub>	‡0.68 <sup>+0.02</sup> <sub>-0.02</sub>	0.09 <sup>+0.01</sup> <sub>-0.00</sub>	0.03	0.00	0.07 <sup>+0.01</sup> <sub>-0.00</sub>	0.01	0.00	0.24 <sup>+0.01</sup> <sub>-0.01</sub>	0.11
<b>BAT99-118</b>	2×WN6–8	AR+SC	49.6±1.0	0.6 <sup>+0.1</sup> <sub>-0.0</sub>	6.71 <sup>+0.03</sup> <sub>-0.03</sub>	l	−10.86 <sup>+0.04</sup> <sub>-0.05</sub>	1400	80.1 <sup>+10.0</sup> <sub>-9.7</sub>	0.41 <sup>+0.01</sup> <sub>-0.02</sub>	...	0.15	0.26 <sup>+0.00</sup> <sub>-0.01</sub>	0.15	0.09	0.04	0.04	0.41 <sup>+0.00</sup> <sub>-0.01</sub>	...
<b>BAT99-119</b>	WN6–8+O	AR+SC	49.6±1.0	1.1 <sup>+0.1</sup> <sub>-0.2</sub>	6.63 <sup>+0.05</sup> <sub>-0.04</sub>	h	−11.34 <sup>+0.04</sup> <sub>-0.04</sub>	1100	43.3 <sup>+7.0</sup> <sub>-6.5</sub>	0.26 <sup>+0.01</sup> <sub>-0.01</sub>	0.17 <sup>+0.01</sup> <sub>-0.01</sub>	0.17	0.23 <sup>+0.01</sup> <sub>-0.00</sub>	0.17	0.10 <sup>+0.01</sup> <sub>-0.00</sub>	0.05	0.03	0.32 <sup>+0.02</sup> <sub>-0.01</sub>	...
<b>BAT99-120</b>	WN9–11	AR+SC	49.6±1.0	0.6 <sup>+0.0</sup> <sub>-0.1</sub>	5.57 <sup>+0.03</sup> <sub>-0.03</sub>	g	−12.30 <sup>+0.04</sup> <sub>-0.05</sub>	300	2.7 <sup>+0.4</sup> <sub>-0.3</sub>	0.19 <sup>+0.01</sup> <sub>-0.01</sub>	...	0.03	0.86 <sup>+0.01</sup> <sub>-0.01</sub>	1.34 <sup>+0.01</sup> <sub>-0.00</sub>	0.02	0.01	0.45 <sup>+0.00</sup> <sub>-0.01</sub>	1.54 <sup>+0.03</sup> <sub>-0.03</sub>	...
<b>BAT99-122</b>	WN5–7h	NE	49.6±1.0	1.1 <sup>+0.1</sup> <sub>-0.2</sub>	6.22 <sup>+0.05</sup> <sub>-0.04</sub>	g	−11.50 <sup>+0.04</sup> <sub>-0.05</sub>	1300	29.5 <sup>+4.7</sup> <sub>-4.4</sub>	0.46 <sup>+0.02</sup> <sub>-0.02</sub>	‡0.23 <sup>+0.01</sup> <sub>-0.01</sub>	0.25 <sup>+0.00</sup> <sub>-0.01</sub>	0.35 <sup>+0.01</sup> <sub>-0.01</sub>	0.10 <sup>+0.00</sup> <sub>-0.01</sub>	0.11	0.04	0.02	0.31 <sup>+0.01</sup> <sub>-0.02</sub>	0.11 <sup>+0.01</sup> <sub>-0.00</sub>
BAT99-128	WN3–7s	NE	49.6±1.0	0.6 <sup>+0.1</sup> <sub>-0.0</sub>	5.43 <sup>+0.03</sup> <sub>-0.03</sub>	g	−12.00 <sup>+0.05</sup> <sub>-0.04</sub>	1800	6.0 <sup>+0.8</sup> <sub>-0.7</sub>	0.58 <sup>+0.02</sup> <sub>-0.02</sub>	...	0.01	0.06	0.18	0.15 <sup>+0.00</sup> <sub>-0.01</sub>	0.01	0.08	0.17 <sup>+0.01</sup> <sub>-0.00</sub>	0.01
<b>BAT99-130</b>	WN9–11	AR+SC	49.6±1.0	0.9 <sup>+0.1</sup> <sub>-0.1</sub>	5.67 <sup>+0.04</sup> <sub>-0.04</sub>	g	−13.42 <sup>+0.04</sup> <sub>-0.05</sub>	200	0.3 <sup>+0.1</sup> <sub>-0.0</sub>	0.02 <sup>+0.00</sup> <sub>-0.00</sub>	...	0.00	2.2 <sup>+0.1</sup> <sub>-0.0</sub>	4.2 <sup>+0.0</sup> <sub>-0.0</sub>	0.00	0.00	3.3 <sup>+0.1</sup> <sub>-0.1</sub>	12 <sup>+0</sup> <sub>-0</sub>	...
BAT99-131	WN3–7s	NE	49.6±1.0	0.5 <sup>+0.0</sup> <sub>-0.1</sub>	5.66 <sup>+0.03</sup> <sub>-0.02</sub>	g	−11.65 <sup>+0.04</sup> <sub>-0.04</sub>	1600	11.4 <sup>+1.3</sup> <sub>-1.3</sub>	0.64 <sup>+0.02</sup> <sub>-0.02</sub>	...	0.06	0.10 <sup>+0.00</sup> <sub>-0.01</sub>	0.19	0.14	0.04	0.01	0.14 <sup>+0.01</sup> <sub>-0.00</sub>	0.09 <sup>+0.01</sup> <sub>-0.00</sub>
<b>BAT99-132</b>	WN3–7s	NE	49.6±1.0	0.9 <sup>+0.0</sup> <sub>-0.1</sub>	5.57 <sup>+0.04</sup> <sub>-0.04</sub>	g	−11.69 <sup>+0.05</sup> <sub>-0.04</sub>	1900	15.8 <sup>+2.2</sup> <sub>-2.2</sub>	1.10 <sup>+0.05</sup> <sub>-0.06</sub>	‡0.64 <sup>+0.03</sup> <sub>-0.02</sub>	0.06	0.11 <sup>+0.01</sup> <sub>-0.00</sub>	0.16	0.14	0.04	0.01	0.18 <sup>+0.01</sup> <sub>-0.01</sub>	0.11 <sup>+0.01</sup> <sub>-0.00</sub>
BAT99-133	WN9–11	AR+SC	49.6±1.0	0.4 <sup>+0.1</sup> <sub>-0.0</sub>	5.68 <sup>+0.02</sup> <sub>-0.02</sub>	g	−12.98 <sup>+0.04</sup> <sub>-0.05</sub>	200	0.5 <sup>+0.0</sup> <sub>-0.1</sub>	0.03 <sup>+0.00</sup> <sub>-0.01</sub>	...	0.00	1.5 <sup>+0.0</sup> <sub>-0.1</sub>	1.7 <sup>+0.0</sup> <sub>-0.0</sub>	0.00	0.00	2.2 <sup>+0.0</sup> <sub>-0.1</sub>	5.4 <sup>+0.1</sup> <sub>-0.1</sub>	...
<b>BAT99-134</b>	WN3–7s	NE	49.6±1.0	0.2±0.0	5.50 <sup>+0.02</sup> <sub>-0.02</sub>	g	−11.62 <sup>+0.04</sup> <sub>-0.05</sub>	2100	9.0 <sup>+0.9</sup> <sub>-0.9</sub>	0.73 <sup>+0.02</sup> <sub>-0.01</sub>	‡0.57 <sup>+0.01</sup> <sub>-0.01</sub>	0.04	0.08	0.17	0.12 <sup>+0.01</sup> <sub>-0.00</sub>	0.06	0.02	0.15 <sup>+0.01</sup> <sub>-0.00</sub>	0.05 <sup>+0.01</sup> <sub>-0.00</sub>
<b>LMC 170–2</b>	WN2–5w	MM	49.6±1.0	0.4±0.0	5.68 <sup>+0.03</sup> <sub>-0.02</sub>	n	−13.45 <sup>+0.04</sup> <sub>-0.05</sub>	1900	0.16 <sup>+0.02</sup> <sub>-0.02</sub>	0.01 <sup>+0.00</sup> <sub>-0.00</sub>	0.00	0.01	0.00	0.38	0.04	0.01	0.00	0.19	0.00
<b>VFTS 682</b>	WN5–7h	VX	49.6±1.0	4.6±0.5	6.46 <sup>+0.19</sup> <sub>-0.18</sub>	m	−13.21 <sup>+0.04</sup> <sub>-0.05</sub>	1800	22.2 <sup>+14.0</sup> <sub>-8.8</sub>	0.20 <sup>+0.02</sup> <sub>-0.02</sub>	0.50 <sup>+0.07</sup> <sub>-0.06</sub>	0.18 <sup>+0.01</sup> <sub>-0.02</sub>	0.17 <sup>+0.01</sup> <sub>-0.01</sub>	0.10	0.08	0.04	0.00	0.46 <sup>+0.06</sup> <sub>-0.05</sub>	0.17 <sup>+0.02</sup> <sub>-0.02</sub>
<b>AB1</b>	WN2–5w	NE	61.2±1.2	0.8±0.1	6.08 <sup>+0.04</sup> <sub>-0.03</sub>	o	−12.92 <sup>+0.04</sup> <sub>-0.04</sub>	1500	1.4 <sup>+0.2</sup> <sub>-0.2</sub>	0.03 <sup>+0.00</sup> <sub>-0.00</sub>	...	0.06	0.00	0.26	0.10	0.00	0.00	0.38 <sup>+0.01</sup> <sub>-0.01</sub>	0.00
<b>AB2</b>	WN2–5w	NE	61.2±1.2	0.4 <sup>+0.0</sup> <sub>-0.1</sub>	5.58 <sup>+0.03</sup> <sub>-0.02</sub>	o	−12.76 <sup>+0.04</sup> <sub>-0.05</sub>	1000	1.2 <sup>+0.1</sup> <sub>-0.2</sub>	0.08 <sup>+0.00</sup> <sub>-0.00</sub>	...	0.25	0.00	0.00	0.05	0.05	0.00	0.46 <sup>+0.01</sup> <sub>-0.00</sub>	0.22
AB3	WN2–5w+O	CS	61.2±1.2	0.6 <sup>+0.0</sup> <sub>-0.1</sub>	5.94 <sup>+0.03</sup> <sub>-0.02</sub>	p	−12.36 <sup>+0.04</sup> <sub>-0.04</sub>	1600	3.6 <sup>+0.5</sup> <sub>-0.4</sub>	0.11 <sup>+0.00</sup> <sub>-0.01</sub>	0.58 <sup>+0.02</sup> <sub>-0.01</sub>	0.05	0.03	0.23	...	...	...	...	...
<b>AB4</b>	WN6–8	AR	61.2±1.2	0.3 <sup>+0.1</sup> <sub>-0.0</sub>	5.79 <sup>+0.03</sup> <sub>-0.02</sub>	o	−11.94 <sup>+0.04</sup> <sub>-0.05</sub>	900	7.4 <sup>+0.8</sup> <sub>-0.8</sub>	0.31 <sup>+0.01</sup> <sub>-0.01</sub>	‡0.28 <sup>+0.00</sup> <sub>-0.01</sub>	0.13	0.12	0.06	0.10	0.02	0.00	0.24	0.07
<b>AB5</b>	2×WN6–8	HS	61.2±1.2	0.2 <sup>+0.1</sup> <sub>-0.0</sub>	6.49 <sup>+0.02</sup> <sub>-0.02</sub>	q,r	−11.09 <sup>+0.04</sup> <sub>-0.05</sub>	1300	47.0 <sup>+5.0</sup> <sub>-4.9</sub>	0.39 <sup>+0.01</sup> <sub>-0.01</sub>	0.18 <sup>+0.01</sup> <sub>-0.00</sub>	0.04	0.08	0.01	0.10	0.04	0.04	0.22 <sup>+0.00</sup> <sub>-0.01</sub>	0.06
AB6	WN2–5w+O	AR+CS	61.2±1.2	0.2±0.0	6.29 <sup>+0.02</sup> <sub>-0.02</sub>	p	−12.35 <sup>+0.04</sup> <sub>-0.05</sub>	1900	2.5 <sup>+0.3</sup> <sub>-0.3</sub>	0.03 <sup>+0.00</sup> <sub>-0.00</sub>	...	0.00	0.00	0.21	...	...	...	...	...
<b>AB7</b>	WN2–5w+O	AR	61.2±1.2	0.2 <sup>+0.1</sup> <sub>-0.0</sub>	6.11 <sup>+0.02</sup> <sub>-0.02</sub>	p	−12.20 <sup>+0.04</sup> <sub>-0.05</sub>	1700	3.7 <sup>+0.4</sup> <sub>-0.4</sub>	0.07 <sup>+0.01</sup> <sub>-0.00</sub>	...	0.00	0.00	0.05	0.00	0.00	0.00	0.13 <sup>+0.01</sup> <sub>-0.00</sub>	0.00
<b>AB9</b>	WN2–5w	NE	61.2±1.2	0.3 <sup>+0.1</sup> <sub>-0.0</sub>	6.06 <sup>+0.03</sup> <sub>-0.02</sub>	o	−12.96 <sup>+0.04</sup> <sub>-0.05</sub>	1700	0.7 <sup>+0.1</sup> <sub>-0.1</sub>	0.02 <sup>+0.00</sup> <sub>-0.00</sub>	...	0.00	0.00	0.19	0.07	0.00	0.00	0.18	0.00
<b>AB10</b>	WN2–5w	NE	61.2±1.2	0.5 <sup>+0.0</sup> <sub>-0.1</sub>	5.66 <sup>+0.03</sup> <sub>-0.02</sub>	o	−13.02 <sup>+0.04</sup> <sub>-0.04</sub>	1900	0.7 <sup>+0.1</sup> <sub>-0.1</sub>	0.04 <sup>+0.00</sup> <sub>-0.00</sub>	...	0.02	0.00	0.35	0.06	0.00	0.00	0.00	0.00
<b>AB11</b>	WN2–5w	NE	61.2±1.2	0.4 <sup>+0.1</sup> <sub>-0.0</sub>	5.86 <sup>+0.03</sup> <sub>-0.02</sub>	o	−13.15 <sup>+0.04</sup> <sub>-0.04</sub>	1700	0.5 <sup>+0.1</sup> <sub>-0.1</sub>	0.02 <sup>+0.00</sup> <sub>-0.00</sub>	...	0.00	0.00	0.36	0.02	0.03	0.00	0.20 <sup>+0.01</sup> <sub>-0.00</sub>	0.00
<b>AB12</b>	WN2–5w	NE	61.2±1.2	0.5 <sup>+0.1</sup> <sub>-0.0</sub>	5.91 <sup>+0.03</sup> <sub>-0.02</sub>	o	−13.06 <sup>+0.04</sup> <sub>-0.05</sub>	1700	0.7 <sup>+0.1</sup> <sub>-0.1</sub>	0.02 <sup>+0.00</sup> <sub>-0.00</sub>	...	0.00	0.00	0.13	0.05	0.00	0.00	0.14 <sup>+0.00</sup> <sub>-0.01</sub>	0.00

Line luminosities of Wolf-Rayet stars

a: Hamann et al. (2006); b: Crowther & Hadfield (2006); c: Crowther et al. (1995a); d: Smith et al. (1994); e: Crowther et al. (2010); f: Bohannan & Crowther (1999) g: Hainich et al. (2014); h: Shenar et al. (2019); i: Crowther & Smith (1997); j: Brands et al. (2022); k: Tehrani et al. (2019); l: Shenar et al. (2021) m: Rubio-Diez et al. (in prep); n: Neugent et al. (2017); o: Hainich et al. (2015); p: Shenar et al. (2016); q: Koenigsberger et al. (2014); r: Hillier et al. (2019)

Note: # CASPEC observations (Schmutz 1997); ‡: SIT observations (Torres-Dodgen & Massey 1988); †: MUSE/NFM observations (Castro et al. 2021); ◊: CTIO/R-C spectrograph observations (Foellmi et al. 2003)

**Table A2.** Luminosities of prominent optical emission lines of Galactic(WR) and LMC (BAT99) WN/C, categorised as either strong-lined (WN3–7s/C) or early/late weak-lined (WN2–5w/C or WN6–8/C) for consistency with WN stars. He II  $\lambda\lambda 4686$  FWHM are also provided in  $\text{km s}^{-1}$  ( $\pm 100 \text{ km s}^{-1}$ ). The feature at  $\lambda\lambda 4100$  involves N III  $\lambda\lambda 4097, 4103$ , Si IV  $\lambda\lambda 4088, 4116$ , He II  $\lambda 4100 + \text{H}\delta$ , while the feature at  $\lambda\lambda 4630$  involves N V  $\lambda\lambda 4603, 20$ , N III  $\lambda\lambda 4634, 41$  and C III  $\lambda\lambda 4647, 51$ . Stars included in spectral templates are indicated in bold.

Star	Category	Data	$d$	$A_V$	log	Ref	$F_{\text{HeII} 4686}$	$\text{HeII} 4686$	$L_{\text{HeII} 4686}$	$L_{\text{NIV} 3478, 85}$	$L_{\text{NIV} 4058}$	$L_{4100}$	$L_{4630}$	$L_{\text{HeII} 5412}$	$L_{\text{CIII} 5696}$	$L_{\text{CIV} 5801, 12}$	$L_{\text{HeII} 6560}$	$L_{\text{NIV} 7105, 9}$		
		ID	kpc	mag	$L_{\text{Bol}}/L_\odot$		$\text{erg s}^{-1} \text{cm}^{-2}$	FWHM	$10^{35} \text{ erg s}^{-1}$	$10^{-3} L_{\text{Bol}}$	$L_{\text{HeII} 4686}$	$L_{\text{HeII} 4686}$	$L_{\text{HeII} 4686}$	$L_{\text{HeII} 4686}$	$L_{\text{HeII} 4686}$	$L_{\text{HeII} 4686}$	$L_{\text{HeII} 4686}$	$L_{\text{HeII} 4686}$		
<b>WR8</b>	WN6–8/C	CS	$3.5 \pm 0.2$	$2.7 \pm 0.3$	$5.61^{+0.11}_{-0.12}$	a	$-10.64^{+0.04}_{-0.05}$	1300	$6.9^{+2.6}_{-2.0}$	$0.45^{+0.06}_{-0.06}$	$0.82^{+0.07}_{-0.06}$	$0.91^{+0.04}_{-0.04}$	$0.87^{+0.04}_{-0.03}$	$3.36^{+0.01}_{-0.01}$	$0.13^{+0.01}_{-0.00}$	$0.03^{+0.01}_{-0.00}$	$0.67^{+0.06}_{-0.04}$	$0.15^{+0.02}_{-0.01}$	...	
<b>WR26</b>	WN3–7s/C	CS	$6.6^{+0.8}_{-0.6}$	$4.7 \pm 0.5$	$5.72^{+0.21}_{-0.21}$	a	$-12.07^{+0.04}_{-0.04}$	2400	$8.8^{+6.3}_{-3.8}$	$0.44^{+0.13}_{-0.10}$	$0.64^{+0.09}_{-0.08}$	—	$0.68^{+0.04}_{-0.05}$	—	$3.09^{+0.01}_{-0.01}$	$0.21^{+0.02}_{-0.02}$	0.00	$2.28^{+0.32}_{-0.27}$	$0.17^{+0.04}_{-0.03}$	...
<b>WR58</b>	WN3–7s/C	CS	$6.7^{+0.5}_{-0.4}$	$1.9 \pm 0.2$	$5.01^{+0.10}_{-0.11}$	a	$-11.13^{+0.04}_{-0.04}$	2200	$3.6^{+1.0}_{-0.8}$	$0.93^{+0.14}_{-0.12}$	$0.67^{+0.04}_{-0.04}$	$0.17^{+0.01}_{-0.00}$	$0.21^{+0.01}_{-0.01}$	0.28	$0.15^{+0.01}_{-0.00}$	0.00	$0.26^{+0.02}_{-0.01}$	$0.21^{+0.02}_{-0.02}$	...	
<b>WR98</b>	WN6–8/C	CS	$2.2 \pm 0.1$	$5.0 \pm 0.5$	$5.69^{+0.20}_{-0.21}$	a	$-11.80^{+0.04}_{-0.04}$	1100	$3.1^{+2.5}_{-1.4}$	$0.17^{+0.04}_{-0.03}$	...	...	...	...	$2.29^{+0.01}_{-0.01}$	$0.12^{+0.01}_{-0.01}$	$0.18^{+0.03}_{-0.03}$	$0.30^{+0.06}_{-0.04}$	$0.11^{+0.04}_{-0.02}$	...
<b>WR126</b>	WN2–5w/C	KI	$11.3^{+1.1}_{-1.0}$	$3.6^{+0.3}_{-0.4}$	$6.25^{+0.16}_{-0.17}$	a	$-12.20^{+0.04}_{-0.05}$	1700	$5.2^{+2.7}_{-1.9}$	$0.08^{+0.02}_{-0.02}$	...	—	$0.73^{+0.04}_{-0.04}$	—	$3.93^{+0.01}_{-0.02}$	$0.30^{+0.02}_{-0.02}$	0.00	$3.97^{+0.41}_{-0.38}$	$0.33^{+0.05}_{-0.05}$	$0.34^{+0.06}_{-0.06}$
<b>WR145</b>	WN6–8/C+O	WI94	$1.6 \pm 0.0$	$7.0 \pm 0.7$	$5.71^{+0.28}_{-0.28}$	a	$-11.94^{+0.04}_{-0.05}$	1300	$9.5^{+11.4}_{-5.3}$	$0.48^{+0.10}_{-0.09}$	...	...	...	...	$0.82^{+0.01}_{-0.00}$	$0.13^{+0.02}_{-0.02}$	0.01	$0.63^{+0.14}_{-0.11}$	...	...
<b>WR153</b>	WN6–8/C+O	II91	$4.5 \pm 0.3$	$2.1^{+0.3}_{-0.2}$	...	b	$-10.45^{+0.08}_{-0.09}$	1400	$9.7^{+3.4}_{-2.9}$	...	...	...	...	...	0.52	$0.22^{+0.01}_{-0.01}$	0.00	$0.53^{+0.03}_{-0.03}$	$0.28^{+0.02}_{-0.02}$	$0.20^{+0.02}_{-0.02}$
<b>BAT99-36</b>	WN3–7s/C	AR	$49.6 \pm 1.0$	$0.5^{+0.0}_{-0.1}$	$5.70^{+0.03}_{-0.02}$	c	$-11.73^{+0.05}_{-0.04}$	2100	$9.5^{+1.1}_{-1.1}$	$0.49^{+0.02}_{-0.02}$	$\ddagger 0.60^{+0.01}_{-0.01}$	0.03	0.08	0.24	0.12	0.00	$1.17^{+0.02}_{-0.01}$	...	...	
<b>BAT99-88</b>	WN3–7s/C	NE	$49.6 \pm 1.0$	$3.2^{+0.3}_{-0.4}$	$5.79^{+0.13}_{-0.12}$	c	$-12.97^{+0.04}_{-0.05}$	2900	$10.3^{+4.5}_{-3.2}$	$0.43^{+0.05}_{-0.04}$	...	0.00	$0.09^{+0.00}_{-0.01}$	0.17	$0.11^{+0.01}_{-0.01}$	0.00	$1.52^{+0.12}_{-0.12}$	$0.15^{+0.02}_{-0.02}$	$0.05^{+0.01}_{-0.01}$	

a: Sander et al. (2012), b: Crowther & Hadfield (2006), c: Hainich et al. (2014)

Note:  $\ddagger$ : SIT observations (Torres-Dodgen & Massey 1988)

**Table A3.** Luminosities of prominent optical emission lines of Galactic (WR) and LMC (BAT99) WC stars, categorised as early-type (WC4–5), mid-type (WC6–7) or late-type (WC8–9) stars. C IV  $\lambda\lambda$ 5801,12 FWHM are also provided in  $\text{km s}^{-1}$  ( $\pm 100 \text{ km s}^{-1}$ ). The feature at 6559–81 involves He II 6560 and C II  $\lambda\lambda$ 6559,81. Stars included in spectral templates are indicated in bold (the remainder are excluded owing to limited spectral coverage)

WR	Category	Data	$d$	$A_V$	log	Ref	$F_{\text{CIV}} \text{ 5801,12}$	CIV 5801,12	$L_{\text{CIV}} \text{ 5801,12}$	$L_{\text{OIV}} \text{ 3403,13}$	$L_{\text{CIII}} \text{ 4647,51}$	$L_{\text{HeII}} \text{ 4686}$	$L_{\text{CIII}} \text{ 5696}$	$L_{\text{HeI}} \text{ 5876}$	$L_{\text{6559–81}}$	$L_{\text{CIII}} \text{ 6727,73}$	$L_{\text{CIV}} \text{ 7725}$	$L_{\text{CIII}} \text{ 9701,19}$		
		ID	kpc	mag	$L_{\text{Bol}}/L_\odot$		$\text{erg s}^{-1} \text{ cm}^{-2}$	FWHM	$10^{35} \text{ erg s}^{-1}$	$10^{-3} L_{\text{Bol}}$	$L_{\text{5801,12}}$	$L_{\text{5801,12}}$	$L_{\text{5801,12}}$	$L_{\text{5801–12}}$	$L_{\text{5801,12}}$	$L_{\text{5801,12}}$	$L_{\text{5801,12}}$	$L_{\text{5801,12}}$		
<b>WR4</b>	WC4–5	WI02	$2.6_{-0.1}^{+0.2}$	$2.3_{-0.3}^{+0.2}$	$5.41_{-0.10}^{+0.10}$	a	$-9.72_{-0.05}^{+0.04}$	2200	$10.9_{-2.3}^{+2.6}$	$1.10_{-0.08}^{+0.08}$	$1.01_{-0.13}^{+0.14}$	—	$2.60_{-0.16}^{+0.16}$	—	0.07	0.06	0.06	$0.11_{-0.00}^{+0.01}$	$0.10_{-0.01}^{+0.00}$	
<b>WR5</b>	WC6–7	WI02	$2.8_{-0.1}^{+0.2}$	$3.2_{-0.3}^{+0.2}$	$5.49_{-0.13}^{+0.14}$	a	$-9.95_{-0.04}^{+0.04}$	1900	$16.9_{-4.5}^{+5.7}$	$1.41_{-0.09}^{+0.11}$	$0.87_{-0.15}^{+0.18}$	$2.58_{-0.22}^{+0.23}$	$0.38_{-0.03}^{+0.04}$	$0.09_{-0.00}^{+0.01}$	0.08	0.08	$0.13_{-0.01}^{+0.01}$	$0.08_{-0.00}^{+0.01}$	$\dagger 0.17_{-0.02}^{+0.03}$	
<b>WR9</b>	WC4–5+O	CS	$3.5_{\pm 0.2}$	$3.9_{-0.4}^{+0.4}$	...	b	$-10.19_{-0.05}^{+0.04}$	3200	$27.0_{-8.2}^{+11.2}$	...	...	—	$2.70_{-0.27}^{+0.31}$	—	0.00	0.00	$0.10_{-0.00}^{+0.01}$	$0.15_{-0.01}^{+0.00}$		
<b>WR13</b>	WC6–7	CS	$4.3_{-0.2}^{+0.3}$	$4.5_{-0.4}^{+0.5}$	$5.45_{-0.18}^{+0.19}$	a	$-10.92_{-0.05}^{+0.04}$	2000	$13.1_{-4.5}^{+6.4}$	$1.20_{-0.07}^{+0.09}$	...	—	$2.49_{-0.29}^{+0.34}$	—	0.08	0.08	$0.10_{-0.01}^{+0.01}$	$0.15_{-0.01}^{+0.01}$		
<b>WR14</b>	WC6–7	AD	$1.7_{-0.0}^{+0.1}$	$2.4_{-0.2}^{+0.3}$	$5.56_{-0.10}^{+0.10}$	a	$-9.46_{-0.04}^{+0.05}$	1900	$10.3_{-2.2}^{+2.6}$	$0.73_{-0.03}^{+0.03}$	$0.75_{-0.10}^{+0.12}$	$2.73_{-0.18}^{+0.19}$	$0.66_{-0.05}^{+0.04}$	0.32	0.12	$0.16_{-0.01}^{+0.00}$	$0.19_{-0.01}^{+0.00}$	$0.12_{-0.01}^{+0.00}$	$0.33_{-0.03}^{+0.04}$	
<b>WR15</b>	WC6–7	CS	$2.5_{\pm 0.1}$	$4.6_{-0.4}^{+0.5}$	$5.83_{-0.18}^{+0.19}$	a	$-10.07_{-0.04}^{+0.04}$	2900	$33.4_{-11.5}^{+16.6}$	$1.27_{-0.05}^{+0.05}$	...	—	$2.37_{-0.27}^{+0.33}$	—	0.17	0.18	$0.10_{-0.00}^{+0.01}$	$0.12_{-0.01}^{+0.01}$		
<b>WR17</b>	WC4–5	AD	$5.0_{-0.4}^{+0.5}$	$1.2_{-0.2}^{+0.1}$	$5.30_{-0.09}^{+0.09}$	a	$-9.97_{-0.05}^{+0.04}$	1900	$8.6_{-1.4}^{+1.5}$	$1.12_{-0.08}^{+0.08}$	$0.36_{-0.02}^{+0.03}$	$2.03_{-0.07}^{+0.06}$	$0.51_{-0.01}^{+0.02}$	0.03	0.07	$0.08_{-0.01}^{+0.00}$	0.11	0.08	$0.13_{-0.01}^{+0.00}$	
<b>WR19</b>	WC4–5+O	AD	$4.7 \pm 0.3$	$5.1_{-0.5}^{+0.5}$	...	b	$-11.11_{-0.04}^{+0.04}$	4000	$16.3_{-6.1}^{+9.2}$	...	$0.74_{-0.19}^{+0.26}$	—	$1.98_{-0.26}^{+0.30}$	—	0.00	0.00	0.03	$0.08_{-0.01}^{+0.01}$	$0.08_{-0.01}^{+0.01}$	$0.18_{-0.04}^{+0.05}$
<b>WR23</b>	WC6–7	AD	$2.3 \pm 0.1$	$2.3_{-0.2}^{+0.3}$	$5.51_{-0.10}^{+0.09}$	a	$-9.49_{-0.05}^{+0.04}$	2100	$15.4_{-3.2}^{+3.8}$	$1.24_{-0.05}^{+0.06}$	$0.79_{-0.09}^{+0.11}$	$2.50_{-0.14}^{+0.15}$	$0.65_{-0.03}^{+0.04}$	0.23	0.13	$0.13_{-0.01}^{+0.00}$	$0.17_{-0.00}^{+0.01}$	$0.12_{-0.01}^{+0.01}$	$0.29_{-0.03}^{+0.03}$	
<b>WR27</b>	WC6–7	CS	$2.3_{-0.0}^{+0.1}$	$6.3_{-0.7}^{+0.6}$	$5.17_{-0.26}^{+0.25}$	a	$-11.29_{-0.04}^{+0.04}$	2200	$7.8_{-3.4}^{+5.8}$	$1.39_{-0.05}^{+0.05}$	$0.71_{-0.11}^{+0.26}$	$2.63_{-0.36}^{+0.40}$	$0.45_{-0.06}^{+0.06}$	$0.14_{-0.01}^{+0.00}$	0.07	$0.11_{-0.00}^{+0.01}$	$0.19_{-0.01}^{+0.02}$	...	...	
<b>WR30</b>	WC6–7+O	CS	$5.9 \pm 0.5$	$2.1_{-0.2}^{+0.3}$	...	b	$-10.48_{-0.04}^{+0.04}$	2100	$8.8_{-1.9}^{+2.1}$	...	$0.28_{-0.03}^{+0.04}$	$1.84_{-0.10}^{+0.12}$	$0.78_{-0.04}^{+0.04}$	0.07	0.08	$0.13_{-0.01}^{+0.00}$	$0.13_{-0.01}^{+0.00}$	...	...	
<b>WR33</b>	WC4–5	CS	$6.6_{-0.7}^{+0.9}$	$2.3_{-0.3}^{+0.2}$	$5.31_{-0.13}^{+0.14}$	a	$-10.34_{-0.05}^{+0.04}$	3400	$16.4_{-3.7}^{+4.4}$	$2.08_{-0.22}^{+0.25}$	...	—	$2.50_{-0.15}^{+0.16}$	—	0.00	0.00	0.10	0.13	...	...
<b>WR38</b>	WC4–5	AD	$6.3_{-0.7}^{+0.9}$	$4.2_{-0.5}^{+0.4}$	$5.14_{-0.20}^{+0.20}$	a	$-11.32_{-0.04}^{+0.05}$	3300	$8.6_{-2.9}^{+4.0}$	$1.62_{-0.22}^{+0.27}$	$0.38_{-0.08}^{+0.11}$	—	$1.70_{-0.19}^{+0.20}$	—	0.00	0.00	0.02	0.05	$0.06_{-0.01}^{+0.01}$	$0.04_{-0.00}^{+0.01}$
<b>WR39</b>	WC6–7+O	CS	$4.4_{-1.0}^{+1.4}$	$6.4_{-0.7}^{+0.6}$	$6.12_{-0.33}^{+0.35}$	a	$-12.05_{-0.05}^{+0.04}$	2900	$5.1_{-2.5}^{+4.1}$	$0.10_{-0.02}^{+0.04}$	...	—	$3.61_{-0.58}^{+0.69}$	—	$0.42_{-0.01}^{+0.00}$	0.25	$0.32_{-0.03}^{+0.02}$	$0.21_{-0.02}^{+0.02}$	...	...
<b>WR50</b>	WC6–7+O	CS	$3.4 \pm 0.2$	$3.9_{-0.4}^{+0.4}$	$5.39_{-0.16}^{+0.16}$	a	$-10.82_{-0.04}^{+0.04}$	2400	$6.1_{-1.9}^{+2.6}$	$0.65_{-0.05}^{+0.05}$	$0.91_{-0.18}^{+0.21}$	—	$2.98_{-0.28}^{+0.32}$	—	0.43	0.09	$0.19_{-0.00}^{+0.01}$	$0.16_{-0.00}^{+0.01}$	...	...
<b>WR53</b>	WC8–9	AD	$2.9 \pm 0.1$	$2.8_{-0.3}^{+0.3}$	$5.14_{-0.12}^{+0.12}$	a	$-10.64_{-0.05}^{+0.04}$	1500	$2.5_{-0.6}^{+0.7}$	$0.47_{-0.03}^{+0.03}$	$0.84_{-0.12}^{+0.15}$	$3.43_{-0.26}^{+0.27}$	$1.10_{-0.08}^{+0.09}$	$2.60_{-0.02}^{+0.01}$	0.29	$0.62_{-0.02}^{+0.02}$	$0.44_{-0.02}^{+0.02}$	$0.14_{-0.01}^{+0.02}$	$0.88_{-0.11}^{+0.12}$	
<b>WR56</b>	WC6–7	CS	$7.5 \pm 0.7$	$2.6_{-0.2}^{+0.3}$	$5.00_{-0.14}^{+0.13}$	a	$-11.42_{-0.05}^{+0.04}$	1700	$2.4_{-0.8}^{+1.0}$	$0.63_{-0.07}^{+0.07}$	$1.08_{-0.16}^{+0.18}$	$2.95_{-0.21}^{+0.22}$	$0.81_{-0.06}^{+0.06}$	0.56	0.15	$0.20_{-0.01}^{+0.01}$	$0.18_{-0.01}^{+0.01}$	...	...	
<b>WR57</b>	WC8–9	CS	$3.0_{-0.1}^{+0.2}$	$1.7_{-0.2}^{+0.1}$	$5.16_{-0.07}^{+0.08}$	a	$-10.06_{-0.05}^{+0.04}$	1700	$3.9_{-0.7}^{+0.7}$	$0.69_{-0.04}^{+0.05}$	$3.21_{-0.26}^{+0.28}$	$3.37_{-0.13}^{+0.13}$	$0.93_{-0.03}^{+0.04}$	$1.14_{-0.01}^{+0.00}$	0.18	$0.32_{-0.01}^{+0.01}$	$0.25_{-0.01}^{+0.00}$	...	...	
<b>WR59</b>	WC8–9	CS	$3.4 \pm 0.2$	$7.6_{-0.7}^{+0.8}$	$5.67_{-0.30}^{+0.31}$	a	$-12.28_{-0.04}^{+0.04}$	1400	$5.1_{-2.5}^{+4.9}$	$0.28_{-0.01}^{+0.02}$	...	$5.55_{-1.04}^{+1.27}$	$1.54_{-0.28}^{+0.34}$	$3.68_{-0.06}^{+0.05}$	$0.57_{-0.00}^{+0.01}$	$1.21_{-0.11}^{+0.12}$	$1.01_{-0.11}^{+0.12}$	...	...	
<b>WR60</b>	WC8–9	CS	$3.4 \pm 0.3$	$5.4_{-0.5}^{+0.6}$	$5.73_{-0.22}^{+0.23}$	a	$-11.03_{-0.05}^{+0.04}$	1800	$13.4_{-5.3}^{+8.2}$	$0.64_{-0.06}^{+0.08}$	$1.57_{-0.43}^{+0.59}$	$2.40_{-0.34}^{+0.38}$	$1.26_{-0.17}^{+0.20}$	$1.87_{-0.02}^{+0.02}$	0.39	$0.42_{-0.03}^{+0.02}$	$0.28_{-0.02}^{+0.02}$	...	...	
<b>WR65</b>	WC8–9+B	CS	$2.8 \pm 0.2$	$7.5_{-0.7}^{+0.8}$	$5.71_{-0.33}^{+0.34}$	a	$-12.46_{-0.04}^{+0.04}$	1400	$2.0_{-1.0}^{+1.8}$	$0.10_{-0.00}^{+0.01}$	...	$5.56_{-1.04}^{+1.28}$	$1.32_{-0.24}^{+0.29}$	$4.14_{-0.07}^{+0.06}$	$0.86_{-0.01}^{+0.01}$	$1.51_{-0.14}^{+0.15}$	$0.86_{-0.09}^{+0.11}$	...	...	
<b>WR68</b>	WC6–7	CS	$5.9_{-0.5}^{+0.6}$	$5.3_{-0.6}^{+0.5}$	$5.87_{-0.22}^{+0.22}$	a	$-11.31_{-0.04}^{+0.05}$	1900	$19.0_{-7.3}^{+11.1}$	$0.67_{-0.07}^{+0.08}$	...	$2.55_{-0.35}^{+0.39}$	$0.81_{-0.11}^{+0.12}$	$0.51_{-0.00}^{+0.01}$	0.26	$0.20_{-0.01}^{+0.01}$	$0.17_{-0.01}^{+0.02}$	...	...	
<b>WR69</b>	WC8–9	CS	$2.6 \pm 0.1$	$2.0 \pm 0.2$	$5.06_{-0.09}^{+0.10}$	a	$-10.63_{-0.05}^{+0.04}$	1500	$1.1_{-0.2}^{+0.2}$	$0.24_{-0.02}^{+0.02}$	...	$4.33_{-0.24}^{+0.26}$	$1.18_{-0.06}^{+0.07}$	$4.48_{-0.02}^{+0.01}$	0.70	$1.70_{-0.05}^{+0.04}$	...	...		
<b>WR70</b>	WC8–9+B	CS	$3.1_{-0.2}^{+0.1}$	$4.7_{-0.4}^{+0.5}$	...	b	$-11.41_{-0.04}^{+0.04}$	1200	$2.6_{-1.3}^{+1.3}$	...	...	$3.44_{-0.42}^{+0.48}$	$1.19_{-0.14}^{+0.16}$	$3.52_{-0.04}^{+0.03}$	$0.35_{-0.01}^{+0.00}$	$1.65_{-0.09}^{+0.10}$	...	...		
<b>WR73</b>	WC8–9	CS	$6.9_{-0.8}^{+1.0}$	$5.7_{-0.5}^{+0.6}$	...	b	$-12.20_{-0.05}^{+0.04}$	1600	$4.9_{-2.0}^{+3.3}$	...	...	$3.36_{-0.49}^{+0.57}$	$0.99_{-0.14}^{+0.16}$	$3.20_{-0.03}^{+0.04}$	$0.36_{-0.01}^{+0.00}$	$1.10_{-0.07}^{+0.09}$	$0.49_{-0.04}^{+0.04}$	...	...	
<b>WR77</b>	WC8–9+O	CS	$3.1 \pm 0.2$	$3.4_{-0.3}^{+0.4}$	...	b	$-11.49_{-0.05}^{+0.04}$	1600	$0.7_{-0.2}^{+0.3}$	...	...	$1.81_{-0.17}^{+0.17}$	$0.87_{-0.07}^{+0.09}$	$2.15_{-0.01}^{+0.01}$	0.25	$0.60_{-0.02}^{+0.03}$	$0.47_{-0.02}^{+0.02}$	...	...	
<b>WR80</b>	WC8–9+O	CS	$3.8 \pm 0.3$	$7.0_{-0.7}^{+0.7}$	$5.23_{-0.29}^{+0.29}$	a	$-12.19_{-0.05}^{+0.04}$	1500	$4.4_{-2.1}^{+3.7}$	$0.68_{-0.06}^{+0.07}$	...	$3.58_{-0.61}^{+0.73}$	$1.06_{-0.18}^{+0.20}$	$3.77_{-0.05}^{+0.06}$	$0.49_{-0.01}^{+0.00}$	$1.31_{-0.11}^{+0.12}$	$1.00_{-0.09}^{+0.11}$	...	...	
<b>WR81</b>	WC8–9	CS	$2.5 \pm 0.1$	$6.0_{-0.6}^{+0.6}$	$5.38_{-0.24}^{+0.24}$	a	$-11.56_{-0.05}^{+0.04}$	1500	$3.5_{-1.5}^{+2.4}$	$0.38_{-0.02}^{+0.02}$	...	$3.48_{-0.50}^{+0.59}$	$1.30_{-0.18}^{+0.21}$	$3.90_{-0.04}^{+0.05}$	$0.91_{-0.00}^{+0.01}$	$1.37_{-0.10}^{+0.10}$	$0.51_{-0.04}^{+0.05}$	...	...	
<b>WR88</b>	WC8–9	CS	$2.7_{-0.1}^{+0.2}$	$5.9_{-0.6}^{+0.6}$	$5.27_{-0.24}^{+0.24}$	a	$-11.86_{-0.04}^{+0.04}$	1400	$2.1_{-0.9}^{+1.5}$	$0.30_{-0.02}^{+0.02}$	...	$5.32_{-0.72}^{+0.72}$ </								

**Table A3.** continued

WR	Category	Data	<i>d</i>	$A_V$	log	Ref log	$F_{\text{CIV}} \text{ 5801,12}$	$\text{CIV} \text{ 5801,12}$	$L_{\text{CIV}} \text{ 5801,2}$	$L_{\text{OIV}} \text{ 3403,13}$	$L_{\text{CIII}} \text{ 4647,51}$	$L_{\text{HeII}} \text{ 4686}$	$L_{\text{CIII}} \text{ 5696}$	$L_{\text{HeI}} \text{ 5876}$	$L_{\text{6559–81}}$	$L_{\text{CIII}} \text{ 6727,73}$	$L_{\text{CIV}} \text{ 7725}$	$L_{\text{CIII}} \text{ 9719}$	$C_{\text{EW}}$		
		ID	kpc	mag	$L_{\text{Bol}}/L_\odot$	erg s $^{-1}$ cm $^{-2}$	FWHM	10 $^{35}$ erg s $^{-1}$	10 $^{-3}$ $L_{\text{Bol}}$	$L_{\text{5801,12}}$	$L_{\text{5801,12}}$	$L_{\text{5801,12}}$	$L_{\text{5801,12}}$	$L_{\text{5801,12}}$	$L_{\text{5801,12}}$	$L_{\text{5801,12}}$	$L_{\text{5801,12}}$	$L_{\text{5801,12}}$	$L_{\text{5801,12}}$		
<b>WR111</b>	WC4–5	WI02	1.3 $^{+0.1}_{-0.0}$	1.3 $^{+0.1}_{-0.2}$	5.20 $^{+0.07}_{-0.07}$	a	–8.86 $^{+0.04}_{-0.08}$	2200	8.7 $^{+1.4}_{-1.3}$	1.44 $^{+0.09}_{-0.08}$	0.69 $^{+0.05}_{-0.05}$	—	2.64 $^{+0.10}_{-0.08}$	—	0.06	0.08	0.08	0.14 $^{+0.00}_{-0.01}$	0.10 $^{+0.00}_{-0.01}$	$\dagger$ 0.18 $^{+0.01}_{-0.01}$	
<b>WR113</b>	WC8–9+O	KI	1.9 $^{+0.1}_{-0.0}$	4.1 $^{+0.5}_{-0.4}$	6.01 $^{+0.16}_{-0.20}$	a	–10.47 $^{+0.04}_{-0.05}$	1500	5.5 $^{+2.5}_{-1.8}$	0.14 $^{+0.01}_{-0.00}$	1.11 $^{+0.24}_{-0.20}$	4.05 $^{+0.39}_{-0.36}$	0.87 $^{+0.08}_{-0.07}$	2.20 $^{+0.02}_{-0.01}$	0.29	0.75 $^{+0.04}_{-0.03}$	0.60 $^{+0.03}_{-0.03}$	...	...	<i>Crowther et al.</i>	
<b>WR114</b>	WC4–5	KI	1.9 $\pm 0.1$	5.1 $^{+0.5}_{-0.5}$	5.29 $^{+0.21}_{-0.20}$	a	–10.54 $^{+0.04}_{-0.05}$	2100	9.4 $^{+5.2}_{-3.5}$	1.25 $^{+0.07}_{-0.07}$	0.59 $^{+0.20}_{-0.15}$	2.41 $^{+0.36}_{-0.32}$	0.49 $^{+0.07}_{-0.06}$	0.07	0.09	0.08 $^{+0.00}_{-0.01}$	0.14 $^{+0.01}_{-0.01}$	...	...		
<b>WR117</b>	WC8–9	WI02	5.0 $^{+0.6}_{-0.5}$	5.9 $^{+0.5}_{-0.6}$	5.57 $^{+0.25}_{-0.25}$	a	–11.57 $^{+0.04}_{-0.05}$	1700	12.2 $^{+8.2}_{-5.1}$	0.85 $^{+0.14}_{-0.10}$	0.72 $^{+0.29}_{-0.21}$	2.95 $^{+0.51}_{-0.44}$	0.87 $^{+0.14}_{-0.13}$	2.90 $^{+0.03}_{-0.04}$	0.38 $^{+0.00}_{-0.01}$	0.99 $^{+0.07}_{-0.07}$	0.48 $^{+0.05}_{-0.04}$	0.14 $^{+0.03}_{-0.02}$	...		
<b>WR119</b>	WC8–9	KI	4.1 $^{+0.3}_{-0.2}$	3.4 $^{+0.3}_{-0.4}$	4.85 $^{+0.14}_{-0.15}$	a	–11.65 $^{+0.04}_{-0.05}$	1300	0.8 $^{+0.3}_{-0.2}$	0.31 $^{+0.02}_{-0.03}$	...	3.31 $^{+0.32}_{-0.30}$	1.03 $^{+0.09}_{-0.09}$	4.14 $^{+0.03}_{-0.02}$	0.73 $^{+0.00}_{-0.01}$	1.56 $^{+0.07}_{-0.07}$	0.64 $^{+0.04}_{-0.03}$	...	$\dagger$ 1.26 $^{+0.21}_{-0.19}$		
<b>WR121</b>	WC8–9	WI02	3.4 $\pm 0.2$	5.3 $^{+0.5}_{-0.6}$	5.51 $^{+0.22}_{-0.21}$	a	–11.55 $^{+0.04}_{-0.05}$	1400	3.4 $^{+2.0}_{-1.1}$	0.27 $^{+0.02}_{-0.01}$	...	3.29 $^{+0.51}_{-0.45}$	0.99 $^{+0.15}_{-0.13}$	3.64 $^{+0.03}_{-0.04}$	0.91 $^{+0.01}_{-0.00}$	1.24 $^{+0.09}_{-0.07}$	0.65 $^{+0.06}_{-0.05}$	0.06 $^{+0.01}_{-0.01}$	0.96 $^{+0.26}_{-0.21}$		
WR125	WC6–7+O	KI	5.9 $^{+0.7}_{-0.6}$	6.0 $^{+0.6}_{-0.6}$	6.28 $^{+0.26}_{-0.25}$	a	–11.38 $^{+0.04}_{-0.05}$	2800	29.7 $^{+20.5}_{-12.7}$	0.40 $^{+0.07}_{-0.05}$	...	—	2.98 $^{+0.52}_{-0.46}$	—	1.03 $^{+0.01}_{-0.01}$	0.29	0.21 $^{+0.02}_{-0.01}$	0.23 $^{+0.02}_{-0.02}$	...	...	
<b>WR132</b>	WC6–7	KI	4.2 $^{+0.3}_{-0.2}$	4.3 $^{+0.4}_{-0.4}$	5.34 $^{+0.18}_{-0.18}$	a	–10.87 $^{+0.04}_{-0.04}$	2000	11.8 $^{+5.5}_{-3.9}$	1.41 $^{+0.10}_{-0.09}$	0.80 $^{+0.23}_{-0.18}$	2.56 $^{+0.22}_{-0.29}$	0.64 $^{+0.08}_{-0.07}$	0.19	0.10	0.11 $^{+0.00}_{-0.01}$	0.16 $^{+0.01}_{-0.01}$	...	...		
<b>WR135</b>	WC8–9	WI02	2.4 $^{+0.1}_{-0.2}$	1.5 $^{+0.2}_{-0.1}$	5.54 $^{+0.08}_{-0.07}$	a	–9.45 $^{+0.04}_{-0.04}$	1400	8.6 $^{+1.5}_{-1.4}$	0.64 $^{+0.04}_{-0.04}$	1.35 $^{+0.13}_{-0.09}$	3.34 $^{+0.14}_{-0.14}$	0.85 $^{+0.03}_{-0.03}$	1.06	0.23	0.31 $^{+0.00}_{-0.01}$	0.28 $^{+0.00}_{-0.01}$	0.13 $^{+0.00}_{-0.01}$	0.59 $^{+0.04}_{-0.04}$		
<b>WR137</b>	WC6–7+O	KI	2.0 $\pm 0.1$	2.4 $^{+0.3}_{-0.2}$	5.89 $^{+0.10}_{-0.10}$	a	–9.54 $^{+0.04}_{-0.05}$	1700	11.1 $^{+2.9}_{-2.4}$	0.37 $^{+0.02}_{-0.01}$	0.98 $^{+0.15}_{-0.13}$	3.38 $^{+0.24}_{-0.22}$	0.75 $^{+0.05}_{-0.04}$	0.59	0.13	0.26 $^{+0.01}_{-0.01}$	0.22 $^{+0.01}_{-0.00}$	...	$\dagger$ 0.36 $^{+0.05}_{-0.03}$		
<b>WR140</b>	WC6–7+O	II13	1.8 $^{+0.0}_{-0.1}$	2.1 $^{+0.3}_{-0.2}$	...	b	–8.90 $^{+0.08}_{-0.09}$	2900	29.3 $^{+8.4}_{-7.7}$	...	0.36 $^{+0.05}_{-0.04}$	—	2.24 $^{+0.13}_{-0.12}$	—	0.34	0.08	0.11 $^{+0.01}_{-0.00}$	0.12 $^{+0.00}_{-0.01}$	0.10 $^{+0.01}_{-0.01}$	0.30 $^{+0.04}_{-0.02}$	
<b>WR143</b>	WC4–5+O	KI	1.8 $\pm 0.1$	4.4 $^{+0.4}_{-0.5}$	5.45 $^{+0.18}_{-0.18}$	a	–10.31 $^{+0.04}_{-0.04}$	2900	7.3 $^{+3.3}_{-2.4}$	0.66 $^{+0.04}_{-0.03}$	0.37 $^{+0.16}_{-0.09}$	—	2.36 $^{+0.41}_{-0.35}$	—	0.00	0.00	0.04	0.08 $^{+0.01}_{-0.01}$	...	...	
<b>WR144</b>	WC4–5	WI02	1.7 $^{+0.0}_{-0.1}$	7.0 $^{+0.7}_{-0.7}$	5.15 $^{+0.28}_{-0.28}$	a	–11.14 $^{+0.04}_{-0.04}$	2800	10.3 $^{+8.6}_{-4.8}$	1.89 $^{+0.06}_{-0.05}$	...	—	1.13 $^{+0.21}_{-0.17}$	—	0.00	0.00	0.05 $^{+0.00}_{-0.01}$	0.12 $^{+0.01}_{-0.01}$	0.12 $^{+0.03}_{-0.01}$	...	
WR150	WC4–5	KI	6.8 $^{+0.8}_{-0.6}$	3.5 $^{+0.3}_{-0.4}$	5.54 $^{+0.17}_{-0.16}$	a	–10.70 $^{+0.04}_{-0.04}$	2900	23.1 $^{+8.9}_{-6.9}$	1.73 $^{+0.24}_{-0.20}$	0.28 $^{+0.05}_{-0.04}$	—	2.29 $^{+0.20}_{-0.19}$	—	0.00	0.09	0.11 $^{+0.00}_{-0.01}$	0.14 $^{+0.01}_{-0.01}$	...	...	
<b>WR154</b>	WC6–7	WI02	4.7 $\pm 0.3$	2.9 $^{+0.3}_{-0.3}$	5.76 $^{+0.13}_{-0.14}$	a	–10.18 $^{+0.05}_{-0.04}$	2100	25.9 $^{+8.6}_{-6.8}$	1.17 $^{+0.10}_{-0.08}$	0.70 $^{+0.13}_{-0.11}$	2.37 $^{+0.20}_{-0.18}$	0.64 $^{+0.05}_{-0.05}$	0.18	0.12	0.10 $^{+0.01}_{-0.00}$	0.16 $^{+0.01}_{-0.00}$	0.11 $^{+0.01}_{-0.01}$	0.22 $^{+0.04}_{-0.02}$		
<b>BAT99-8</b>	WC4–5	MM	49.6 $\pm 1.0$	0.4 $^{+0.0}_{-0.0}$	5.47 $^{+0.03}_{-0.02}$	c	–11.31 $^{+0.04}_{-0.05}$	2600	20.2 $^{+2.2}_{-2.2}$	1.76 $^{+0.04}_{-0.03}$	0.52 $^{+0.02}_{-0.01}$	—	1.71 $^{+0.02}_{-0.01}$	—	0.03	0.08	0.04	0.07	0.08	0.07	
<b>BAT99-9</b>	WC4–5	MM	49.6 $\pm 1.0$	0.5 $^{+0.0}_{-0.1}$	5.47 $^{+0.03}_{-0.02}$	c	–11.20 $^{+0.05}_{-0.04}$	2600	28.7 $^{+3.2}_{-3.2}$	2.51 $^{+0.06}_{-0.05}$	0.25 $^{+0.01}_{-0.00}$	—	1.05 $^{+0.01}_{-0.02}$	—	0.01	0.06	0.04	0.03	0.05	0.02	
<b>BAT99-10</b>	WC4–5+O	AD	49.6 $\pm 1.0$	0.1 $^{+0.0}_{-0.0}$	...	b	–11.09 $^{+0.04}_{-0.05}$	3200	25.4 $^{+2.6}_{-2.6}$	...	...	—	1.26	—	0.00	0.00	...	0.09	0.06	...	
<b>BAT99-11</b>	WC4–5	MM	49.6 $\pm 1.0$	0.4 $^{+0.1}_{-0.0}$	5.85 $^{+0.03}_{-0.02}$	c	–10.81 $^{+0.04}_{-0.04}$	3500	66.7 $^{+7.2}_{-7.2}$	2.43 $^{+0.05}_{-0.05}$	0.40 $^{+0.01}_{-0.02}$	—	1.73 $^{+0.02}_{-0.02}$	—	0.01	0.10	0.05	0.08	0.06	0.06	
<b>BAT99-20</b>	WC4–5+O	AD	49.6 $\pm 1.0$	1.2 $^{+0.1}_{-0.2}$	...	b	–11.72 $^{+0.04}_{-0.05}$	3900	15.2 $^{+2.2}_{-2.1}$	...	...	—	1.81 $^{+0.05}_{-0.06}$	—	0.00	0.00	...	0.05	0.05	...	
<b>BAT99-28</b>	WC4–5+O	AD	49.6 $\pm 1.0$	0.2 $^{+0.0}_{-0.1}$	...	b	–11.10 $^{+0.04}_{-0.04}$	3400	26.8 $^{+2.7}_{-2.8}$	...	...	—	2.20 $^{+0.00}_{-0.01}$	—	0.13	0.00	0.09	0.09	0.07	...	
<b>BAT99-34</b>	WC4–5+O	AD	49.6 $\pm 1.0$	0.1 $^{+0.0}_{-0.0}$	...	b	–11.19 $^{+0.04}_{-0.04}$	2700	20.4 $^{+2.1}_{-2.1}$	...	...	—	1.41 $^{+0.01}_{-0.00}$	—	0.01	0.00	0.05	0.05	0.05	...	
<b>BAT99-38</b>	WC4–5+O	AD	49.6 $\pm 1.0$	0.2 $^{+0.0}_{-0.1}$	...	b	–11.14 $^{+0.04}_{-0.04}$	3600	24.4 $^{+2.6}_{-2.5}$	...	...	—	1.26 $^{+0.00}_{-0.01}$	—	0.01	0.00	...	0.03	0.06	...	
<b>BAT99-39</b>	WC4–5+O	AD	49.6 $\pm 1.0$	0.1 $^{+0.0}_{-0.0}$	...	b	–11.18 $^{+0.04}_{-0.05}$	3900	21.4 $^{+2.3}_{-2.2}$	...	...	—	1.45 $^{+0.00}_{-0.01}$	—	0.02	0.00	...	0.04	0.05	...	
<b>BAT99-52</b>	WC4–5	MM	49.6 $\pm 1.0$	0.3 $^{+0.1}_{-0.0}$	5.64 $^{+0.02}_{-0.02}$	c	–11.06 $^{+0.04}_{-0.05}$	3000	34.3 $^{+3.7}_{-3.6}$	2.03 $^{+0.04}_{-0.04}$	0.68 $^{+0.02}_{-0.02}$	—	2.05 $^{+0.01}_{-0.02}$	—	0.03	0.09	0.04	0.08	0.07	0.07	
<b>BAT99-53</b>	WC4–5+O	AD	49.6 $\pm 1.0$	0.4 $^{+0.1}_{-0.0}$	...	b	–11.07 $^{+0.04}_{-0.05}$	3700	35.7 $^{+3.8}_{-3.9}$	...	...	—	1.60 $^{+0.01}_{-0.02}$	—	0.00	0.00	...	0.05	0.06	...	
<b>BAT99-61</b>	WC4–5	MM	49.6 $\pm 1.0$	0.5 $^{+0.0}_{-0.1}$	5.87 $^{+0.03}_{-0.02}$	d	–10.85 $^{+0.04}_{-0.05}$	3400	63.5 $^{+7.1}_{-7.0}$	2.21 $^{+0.05}_{-0.05}$	0.31 $^{+0.01}_{-0.01}$	—	1.68 $^{+0.02}_{-0.02}$	—	0.01	0.14	0.06	0.07	0.05	0.06	
<b>BAT99-70</b>	WC4–5+O	AD	49.6 $\pm 1.0$	1.5 $^{+0.2}_{-0.1}$	...	b	–11.09 $^{+0.04}_{-0.05}$	4300	89.4 $^{+15.6}_{-14.3}$	...	...	—	1.03 $^{+0.04}_{-0.04}$	—	0.00	0.00	0.05	0.03	0.04	...	
<b>BAT99-84</b>	WC4–5+O	AD	49.6 $\pm 1.0$	0.5 $^{+0.0}_{-0.1}$	...	b	–11.09 $^{+0.05}_{-0.04}$	3200	36.7 $^{+4.0}_{-4.0}$	...	...	—	1.96 $^{+0.03}_{-0.02}$	—	0.01	0.00	0.05	0.09	0.07	...	
<b>BAT99-85</b>	WC4–5+O	AD	49.6 $\pm 1.0$	1.1 $^{+0.1}_{-0.1}$	...	b	–11.34 $^{+0.04}_{-0.04}$	3700	35.6 $^{+5.1}_{-4.9}$	...	...	—	1.25 $^{+0.04}_{-0.04}$	—	0.00	0.00	...	0.10	0.06	...	
<b>BAT99-90</b>	WC4–5	MM	49.6 $\pm 1.0$	1.1 $^{+0.1}_{-0.1}$	5.48 $^{+0.05}_{-0.04}$	d	–1														

**Table A4.** Luminosities of prominent optical emission lines of Galactic (WR), LMC (BAT99, LMC, LH) and SMC (AB) WO stars. CIV  $\lambda\lambda 5801,12$  FWHM are also provided in  $\text{km s}^{-1}$  ( $\pm 200 \text{ km s}^{-1}$ ). Stars included in spectral templates are indicated in bold (the remainder are excluded owing to limited spectral coverage)

Star	Category	Data	<i>d</i>	Av	log	Ref	log $F_{\text{CIV}} 5801,12$	CIV 5801,12	$L_{\text{CIV}} 5801,12$	$L_{\text{OIV}} 3403,13$	$L_{\text{OVI}} 3811,34$	$L_{\text{CIV}} 4658+\text{HeII} 4686$	$L_{\text{OV}} 5572,5607$	$L_{\text{HeII}} 6560$	$L_{\text{CIV}} 7725$	
		ID	kpc	mag	$L_{\text{Bol}}/L_{\odot}$		$\text{erg s}^{-1} \text{cm}^{-2}$	FWHM	$10^{35} \text{ erg s}^{-1} 10^{-3} L_{\text{Bol}}$	$L_{\text{CIV}} 5801,12$	$L_{\text{CIV}} 5801,12$	$L_{\text{CIV}} 5801,12$	$L_{\text{CIV}} 5801,12$	$L_{\text{CIV}} 5801,12$	$L_{\text{CIV}} 5801,12$	
<b>WR30a</b>	WO+O	AD	$8.0^{+0.7}_{-0.5}$	$4.1 \pm 0.4$	...	a	$-11.47^{+0.04}_{-0.05}$	5200	$8.7^{+3.8}_{-2.8}$	...	$0.66^{+0.18}_{-0.14}$	$0.35^{+0.08}_{-0.06}$	$0.81^{+0.09}_{-0.09}$	0.14	...	$0.05^{+0.00}_{-0.01}$
<b>WR93b</b>	WO	VX	$2.1^{+0.1}_{-0.1}$	$6.3 \pm 0.6$	$4.88^{+0.26}_{-0.26}$	b	$-11.90^{+0.05}_{-0.04}$	8400	$1.5^{+1.1}_{-0.6}$	$0.52^{+0.04}_{-0.03}$	$1.6^{+0.6}_{-0.5}$	$1.7^{+0.5}_{-0.4}$	$0.71^{+0.13}_{-0.10}$	$0.12^{+0.01}_{-0.00}$	0.06	$0.14^{+0.02}_{-0.02}$
<b>WR102</b>	WO	WI02	$2.6^{+0.1}_{-0.1}$	$3.9 \pm 0.4$	$4.95^{+0.17}_{-0.16}$	b	$-12.10^{+0.04}_{-0.04}$	6600	$0.2^{+0.1}_{-0.1}$	$0.05^{+0.01}_{-0.00}$	$3.1^{+0.8}_{-0.6}$	$25^{+5}_{-4}$	$3.2^{+0.3}_{-0.3}$	$1.31^{+0.02}_{-0.02}$	$0.38^{+0.02}_{-0.02}$	$1.10^{+0.13}_{-0.09}$
<b>WR142</b>	WO	WI02	$1.6^{+0.1}_{-0.0}$	$4.9 \pm 0.5$	$5.33^{+0.20}_{-0.20}$	b	$-11.16^{+0.04}_{-0.04}$	7000	$1.5^{+0.7}_{-0.6}$	$0.18^{+0.00}_{-0.00}$	$2.0^{+0.7}_{-0.5}$	$7.1^{+2.1}_{-1.6}$	$2.2^{+0.3}_{-0.3}$	$0.43^{+0.01}_{-0.01}$	$0.22^{+0.01}_{-0.02}$	$0.53^{+0.09}_{-0.07}$
<b>LH41-1042</b>	WO	VX	$49.6 \pm 1.0$	$0.4 \pm 0.0$	$5.25^{+0.02}_{-0.02}$	b	$-11.52^{+0.04}_{-0.04}$	5600	$12.7^{+1.3}_{-1.4}$	$1.85^{+0.03}_{-0.04}$	$0.78^{+0.02}_{-0.02}$	$0.33^{+0.00}_{-0.01}$	$0.78^{+0.01}_{-0.01}$	0.10	0.03	0.06
<b>LMC195-1</b>	WO	MM	$49.6 \pm 1.0$	$0.4 \pm 0.0$	$5.40^{+0.03}_{-0.02}$	c	$-12.26^{+0.04}_{-0.04}$	4900	$2.3^{+0.2}_{-0.2}$	$0.24^{+0.0}_{-0.1}$	$4.3^{+0.1}_{-0.2}$	$5.8^{+0.1}_{-0.1}$	$1.5^{+0.1}_{-0.0}$	0.32	0.17	0.29
<b>BAT99-123</b>	WO	MM	$49.6 \pm 1.0$	$0.5^{+0.0}_{-0.1}$	$5.40^{+0.03}_{-0.02}$	c	$-11.50^{+0.04}_{-0.05}$	5400	$14.2^{+1.6}_{-1.5}$	$1.46^{+0.04}_{-0.03}$	$0.64^{+0.03}_{-0.02}$	$0.40^{+0.02}_{-0.01}$	$0.45^{+0.00}_{-0.01}$	0.05	$0.02^{+0.01}_{-0.00}$	0.06
<b>AB 8</b>	WO+O	AD	$61.2 \pm 1.2$	$0.2 \pm 0.0$	$6.16^{+0.02}_{-0.02}$	d	$-11.22^{+0.05}_{-0.04}$	5300	$32.9^{+3.4}_{-3.4}$	$0.59^{+0.01}_{-0.01}$	$0.96^{+0.01}_{-0.02}$	$0.70^{+0.01}_{-0.01}$	$0.65^{+0.01}_{-0.00}$	0.16	0.04	0.19

a: Rate & Crowther (2020) b: Tramper et al. (2015); c: Aadland et al. (2022b), d: Shenar et al. (2016)

## APPENDIX B: TEMPLATES

Continuum subtracted WR emission line templates are provided for the Milky Way, LMC and SMC in Figs. B1–B6. Templates are degraded to a uniform spectra resolution of 10Å, and are provided from single and single+binary WR stars, since the latter are often contaminated by (Balmer) absorption lines from companion OB stars. Average velocity corrections of 284 km s<sup>-1</sup> and 162 km s<sup>-1</sup> have been applied for the LMC and SMC, respectively (Tully et al. 2016).

This paper has been typeset from a TeX/LaTeX file prepared by the author.

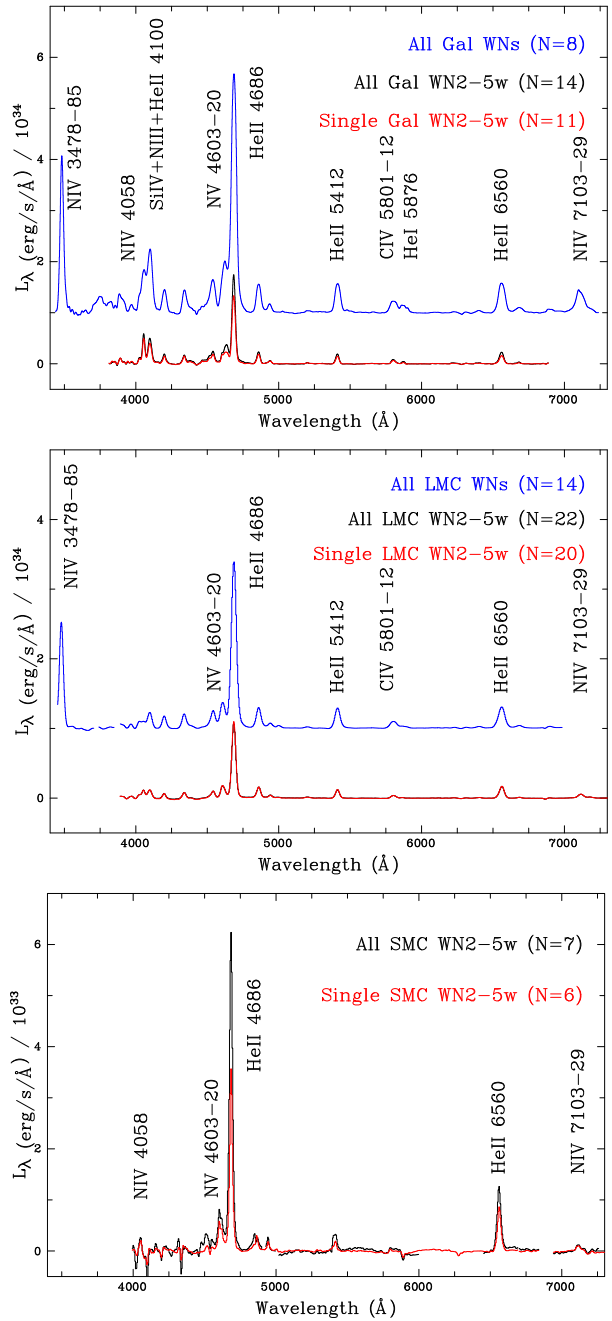


**Figure B1.** Upper panel: Galactic WN2–5w emission line templates based on single (red) and all (black) stars, plus WN3–7s templates (blue, offset by  $10^{34}$  erg s<sup>-1</sup> Å<sup>-1</sup>); Middle panel: LMC emission line templates; Lower panel: SMC emission line templates (no strong-lined WN stars are known).

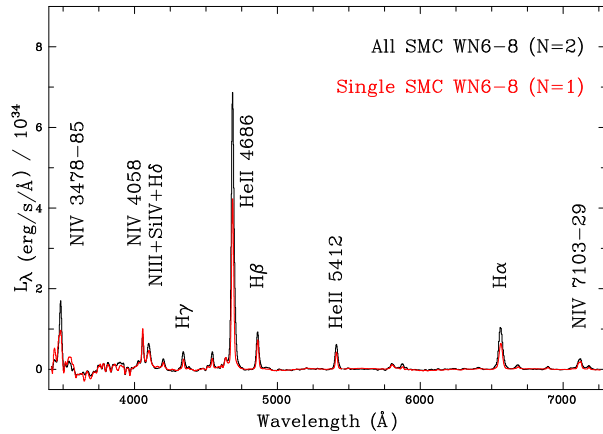
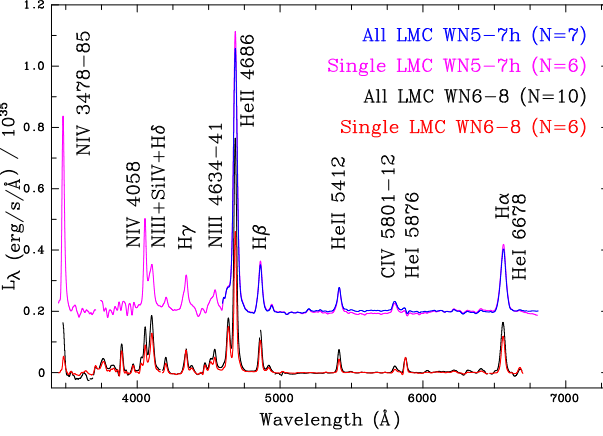
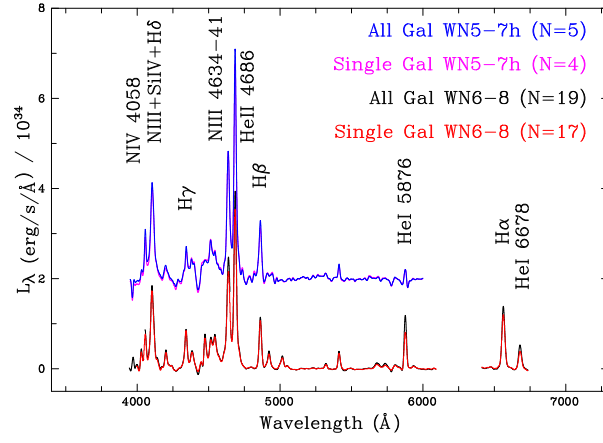


**Figure B2.** Upper panel: Galactic WN6–8 emission line templates based on single (red) and all (black) stars, plus WN5–7h templates (pink and blue, offset by  $2 \times 10^{34} \text{ erg s}^{-1} \text{ Å}^{-1}$ ); Middle panel: LMC WN6–8 and WN5–7h emission line templates; Lower panel: SMC WN6–8 emission line templates. LMC WN5–7h templates exclude the region shortward of  $\lambda 4600$  owing to the use of VLT/MUSE datasets (Castro et al. 2018).

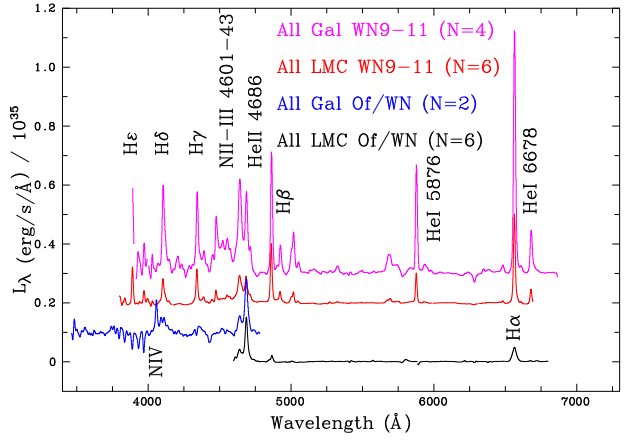


**Figure B3.** Emission line templates for LMC (black) and Milky Way (blue, offset by  $10^{34} \text{ erg/s/Å}$ ) Of/WN stars, plus LMC (red, offset by  $2 \times 10^{34} \text{ erg s}^{-1} \text{ Å}^{-1}$ ) and Milky Way (pink, offset by  $3 \times 10^{34} \text{ erg/s/Å}$ ) WN9–11 stars. LMC Of/WN templates exclude the region shortward of  $\lambda 4600$  owing to the use of VLT/MUSE datasets (Castro et al. 2018)

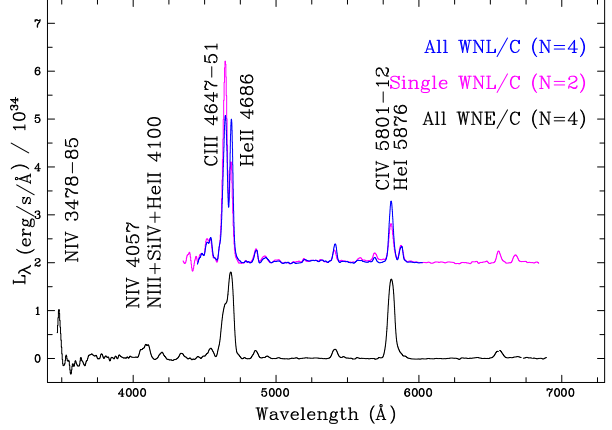


**Figure B4.** WN/C emission line templates for single WNE/C (black, 3 Milky Way and 2 LMC), single WNL/C (2 Milky Way, pink) and all WNL/C (4 Milky Way, blue) the latter group offset by  $2 \times 10^{34} \text{ erg s}^{-1} \text{ Å}^{-1}$ .

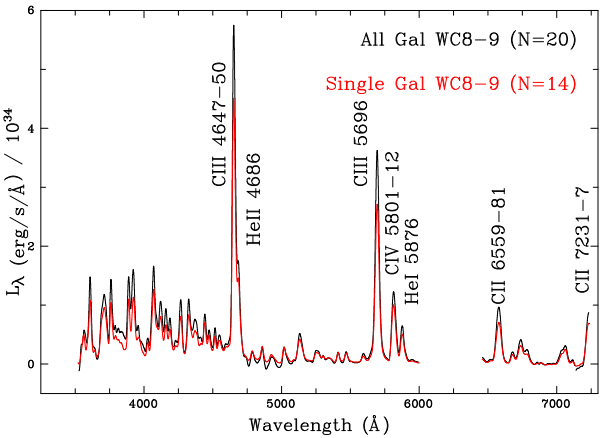
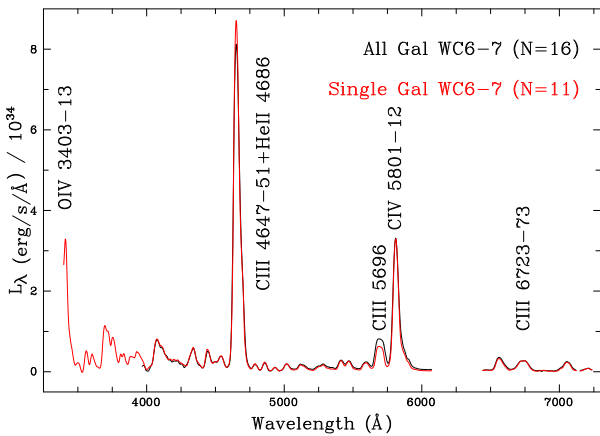
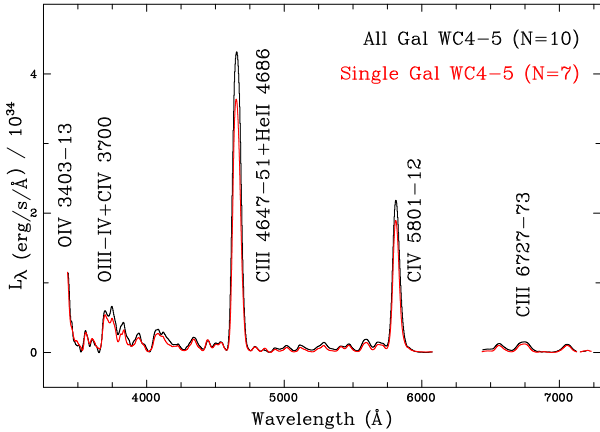


**Figure B5.** Upper panel: Galactic WC4–5 emission line templates based on single (red) and all (black) stars; Middle panel: Galactic WC6–7 emission line templates; Lower panel: Galactic WC8–9 emission line templates. The forest of blue features in WC8–9 stars primarily involve C II–III (Crowther et al. 2006b).

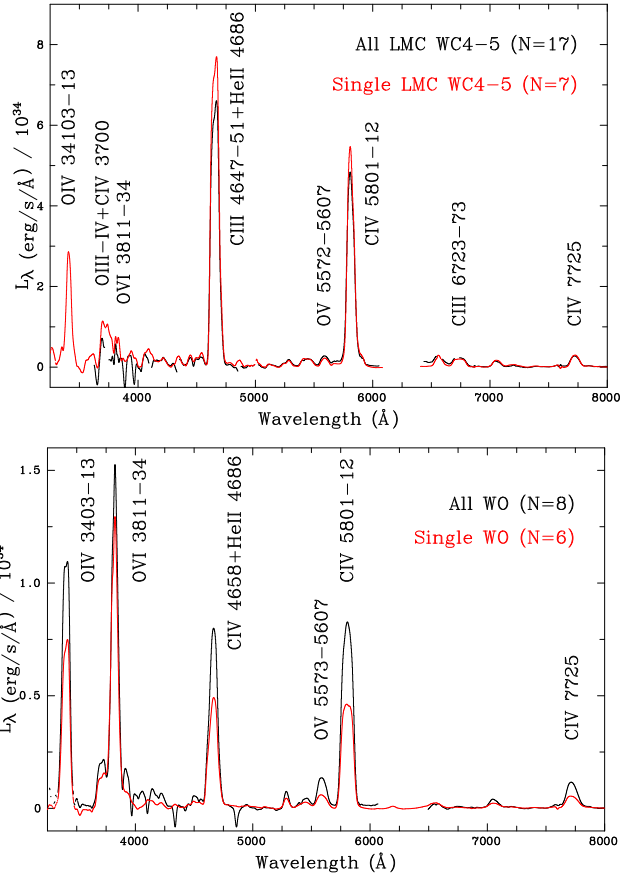


**Figure B6.** Upper panel: LMC WC4–5 emission line templates based on single (red) and all (black) stars; Lower panel: WO emission line templates based on single (red) and all (black) stars, incorporating all Milky Way (4), LMC (3) and SMC (1) stars.